Processing and characterisation of nano carbon doped MgB2 form of wire and bulk

Wai Kong Yeoh
University of Wollongong

Processing and Characterisation of Nano Carbon Doped MgB_2 in Form of Wire and Bulk

A thesis submitted in fulfillment of the requirements for the award of the degree of

DOCTOR OF PHILOSOPHY

From

UNIVERSITY OF WOLLONGONG

By

Wai Kong Yeoh

Institute for Superconducting and Electronic Materials

2006

DECLARATION

This is to certify that the work presented in this thesis was carried out by the candidate in the laboratories of the Institute for Superconducting and Electronic Materials (ISEM), at the University of Wollongong, NSW, Australia, and has not been submitted for a degree to any other institution for higher education.

Wai Kong Yeoh

2006

ACKNOWLEDGMENTS

I would like to express my since appreciate and thankfulness to my supervisors Prof. S. X. Dou and Dr. J. Horvat for their continuos academic guidance, encouragement and support during my three years PhD study in Institute for Superconducting and Electronic Materials at University of Wollongong.

I would also like to express my gratitude to Prof. H. K. Liu, Dr. X. L. Wang, Dr. M. Ionescu, Dr. K. Konstantinov Dr M. J. Qin and Dr J. H. Kim for their contribution in measurements, the useful discussion and suggestions.

This work wont be completed without the help of Prof. P. R. Munroe from University of New South Wales, Dr Vicki J Keast and Mr. S. Bulcock from University of Sydney, Dr D. Wexler and Dr Z. Chen from Materials Engineering, University of Wollongong, Mr. M. Tomsic from Hyper Tech, USA, Dr. H. Kumakura from NIMS and Mr. S. K. Chen and Dr. K. S. Tan from University of Cambridge for their great collaboration.

My special thanks to all my colleagues at ISEM including Dr. S. Soltanian, Dr. S. Zhou, X. Xu, M. S. Park, S. H. Ng, S. Y. Chew and friends at Richard Johnson College and back home, and all the members and technicians at the Faculty of Engineering especially Mrs. B. M. Allen, Mrs. J. Bistro, Mr. R. Kinnell, Mr. G. Tillman and Mr. N. Mackie for their friendly help and assistance in using the facilities.

I would also like to acknowledge the Department of Education, Science and Training, Australia for providing my PhD scholarship and Miss Cynthia Grant who is my scholarship coordinator for her enthusiastic support.

Finally I wish to thank my parents, my elder brother, my sister in law and my nephew for their patience and support.

Table of Content

List of Figures

List of Tables

ABSTRACT

The objective of this work is to further enhance the critical current density of the MgB_2 superconductor by doping with the two carbon sources: multiwalled carbon nanotube (CNT) and nano carbon. The work in this thesis concentrates on the fabrication and characterization on the CNT and nano C doped MgB_2 with main objective being the enhancement of the critical current density in the high magnetic field. Consequently, introducing effective pinning centres in the form of dopants to enhance the flux pinning will be the main task of this project.

In this project, the effect of carbon doping MgB_2 with carbon nanotubes and nano C on transition temperature, lattice parameters, critical current density and flux pinning for $MgB_{2-x}C_x$ with x = 0, 0.05, 0.1, 0.2 and 0.3 under the various condition was studied. Both types of doping showed excellent J_c compared to the pure MgB_2, with significant enhancement observed at higher temperature. Magnetic $J_c(H)$ was enhanced by a factor of 72 at 5K for a field 8T and a factor of 33 at 20K for a field of 5T for nano C bulk samples, respectively. On the other hand, $J_c(H)$ of CNT samples was enhanced by a factor of 26 and 13 under the equivalent conditions. In high field, transport J_c of magnitude 2122 A/cm^2 and 3821 A/cm^2 was observed at 4.2K and 12T for CNT and nano C doped MgB_2. These results indicate that flux pinning was enhanced by the boron substitution for carbon with increasing processing temperature. However, it was found that the lattice distortion and optimum doping level is different in the CNT and nano C samples which is due to the reactivity of the carbon source, resulting in different carbon substitution rate. Due to better reactivity and homogenous mixing of nano C, nano C doped MgB_2 resulted in better improvement in magnetic and transport $J_c(H)$, as

compared to CNT doped MgB_2. This is mainly because CNT fibres with high aspect ratio tend to entangle, which suppressed the reactivity.

The depression of T_c, which is caused by the boron substitution for carbon, increases with increasing the doping level, processing temperature and duration for both types of carbon doping. By controlling the extent of the substitution and inclusion of carbon, we can achieve the optimal improvement of critical current density and flux pinning in magnetic fields while maintaining the minimum reduction in T_c. In addition, the values of H_{c2} and H_{irr} are higher for CNT doped samples than for the pure MgB_2 at the same value of T/T_c. The morphology of the CNT doped MgB_2 is similar to that of nano C doped MgB_2, but different from the pure MgB_2. The microstructure exhibits noticeable nanoparticles with size around 10-20nm, which are believed to be MgO and MgB_2.

Magnetization measurements indicate a change in the critical current density with the length of nanotube and not with its outside diameter. This is due to longer nanotubes tending to entangle with each other, preventing their homogenous mixing with MgB_2 and dispersion. Low intensity ultrasonication, as a method of dispersion of CNT's into precursor magnesium and boron powder, was introduced to improve homogeneity of mixing of CNT's with the MgB_2 matrix. Ultrasonication of CNT doped MgB_2 resulted in a significant enhancement in the field dependence of critical current density, while avoiding the side-effects that would occur at higher processing temperatures.

Carbon nanotubes (CNT's) have unusual electrical, mechanical and thermal properties. The elongated CNT's induce anisotropy in J_c in relation to the direction of applied field

in MgB_2/Fe wires and the value of J_c for the carbon nanotube-doped wires is insensitive to heating rates. We believe that by taking the extraordinary electrical, mechanical and thermal properties of CNT's, the mechanical properties and thermal stability of CNT doped wire will be substantially improved. Studies on these properties are underway.

Chapter 1 Introduction

1.1 Introduction

Superconductors are materials that lose their resistance to electrical current flow below a certain critical temperature (T_c), a certain critical current density (J_c) and certain critical field (H_c). Superconductors have generated great interest for power applications including loss-free electric transmission cables, motors, generators, transformers, energy storages, levitation trains, ultra-fast computers etc. Besides that, the superconductivity phenomenon also opens the challenges to modern physics of superconductors. Many materials become superconducting when they are cooled to near absolute zero temperature (-273^{o}C) including the C_{60} [1] and the DNA [2]. Figure 1 showed the history of superconductor development with time. Up to recent date the highest superconducting temperature (T_c) is still held by the Hg-based superconductor (153K) that was found in 1993. There are a total of 13 Nobel laureates, from H.K. Onnes (1913) to the recent one P. C. Lauterbur and Sir P. Mansfield (2003) on their contributions for theory, experimental results and application of superconductivity.

Critical transition temperature (T_c) is the temperature above which a superconductor loses its superconductivity. The maximum current density that a superconductor can carry under superconducting state is called critical current density (J_c). Superconductors can be divided into two classes according to their response to magnetic field. When a type I superconductor is placed in a weak external magnetic field, the field penetrates the superconductor for only a short distance λ, called the London penetration depth, over which it decays to zero. This is called the Meissner effect, and is a defining

characteristic of superconductivity. For most superconductors, the penetration depth is on the order of 100 nm.

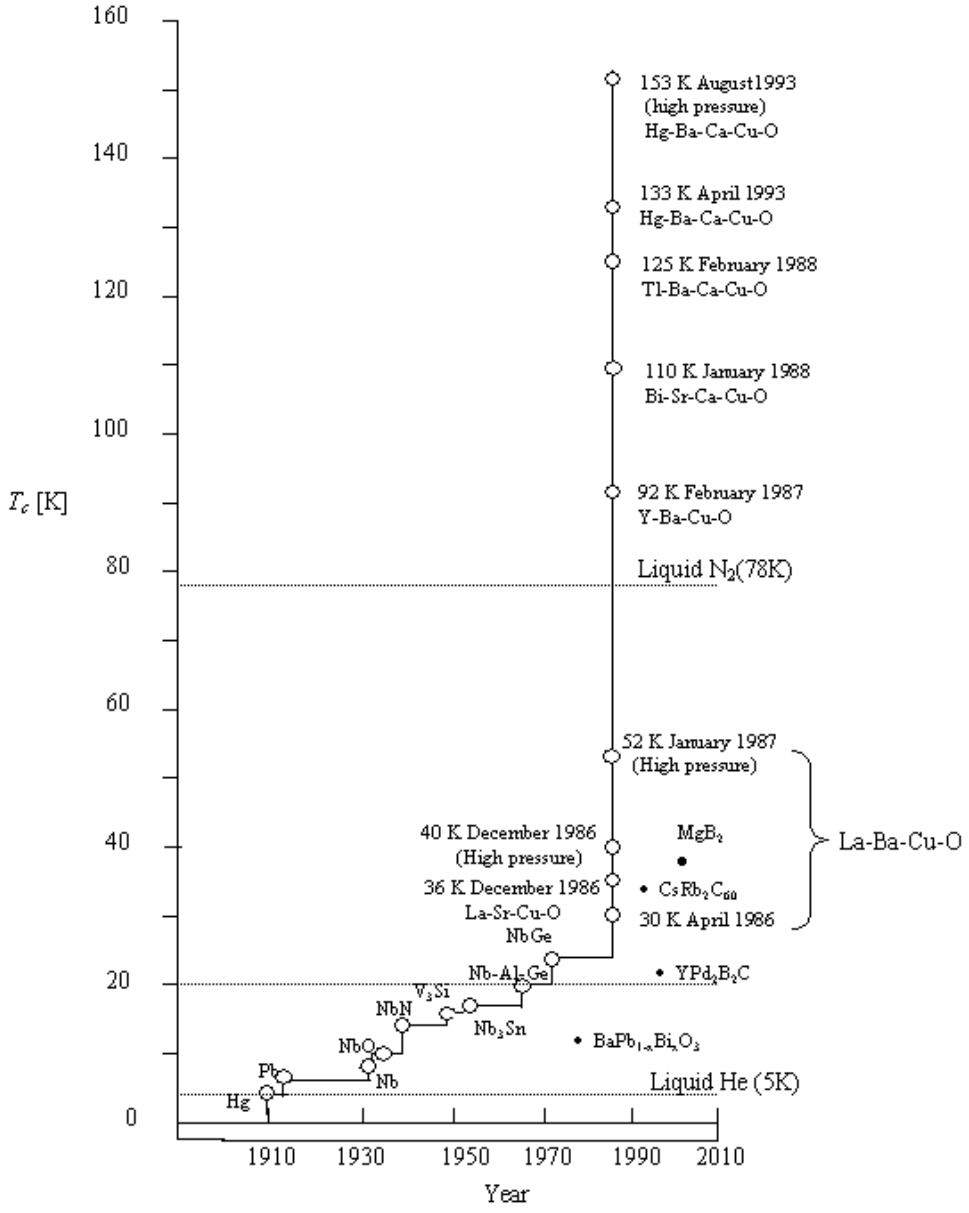

Figure 1.1 Evolution of T_c with time

In Type II superconductors, the field penetrates in the same way as in type I superconductors, up to the first critical field H_{c1}. Raising the applied field above H_{c1} leads to a mixed state in which magnetic field additionally penetrates the

superconductor in form of thin filaments. These filaments are called magnetic vortices and each of them carries one magnetic flux quantum (Φ_0= 2.067 x 10^{-15} Tm^2). Increasing field further above H_{c1}, an increasing amount of magnetic vortices penetrates the material, but there remains no resistance to the flow of electrical current as long as the magnetic vortices do not move under the influence of electrical current and magnetic field. The diameter of the vortices is of the order of coherence length of the superconductor, ξ, i.e. typically nanometers (coherence length of MgB_2 ~ $\xi_{ab}(0)$ = 3.7–12 nm, $\xi_c(0)$ = 1.6–3.6 nm) [3]). At the upper critical field H_{c2}, superconductivity is destroyed..

It is very important that these vortices do not move in response to magnetic fields and currents if superconductors are to carry large currents. Vortex movement results in resistivity. Magnetic vortices can be effectively pinned at sites of atomic defects, such as inclusions, impurities, and grain boundaries. These defects are the most effective pinning centres when their size roughly matches the size of the vortices, i.e. coherence length. Practical performance of the superconductors is greatly affected by the effectiveness of vortex pinning and therefore by the type, density and extent of the defects, T_c, ξ, λ.

LTS stands for "low temperature superconductors", which typically refers to the Nb based alloys (most commonly Nb-47wt. %Ti) and A15 (Nb_3Sn and Nb_3Al). LTS have T_c well below 20 K (-253 °C). Nb-47wt. %Ti alloy has become the dominant commercial superconductor because it can be economically manufactured in a ductile form with the prerequisite nano-structure needed for high critical current. Similarly,

Nb_3Sn based strand, although based on a brittle A15 superconducting phase, can be manufactured into strong composites in km lengths and microstructures that promote high critical current densities. These superconductors are often termed "technical superconductors" because of their applicability to engineering tasks. All these conductors require cooling to 4 K (liquid He is the most common coolant). In fact, the well established Nb-based low temperature superconductors represent 99.99% of world production of superconducting materials.

In 1986, the discovery of new class of superconductor namely high temperature cuprate superconductors (HTS) by K.A. Műller and J. G. Bednorz [4] was marked as the breakthrough of superconductivity. Although the HTS have relatively high critical temperature compared to the LTS and can be made superconducting by immersion in liquid nitrogen with a boiling temperature of 77K (–196^{o}C), most of them are unsuitable for practical applications because of the weak link effect [5] or the toxicity of the starting materials, like thallium and mercury based superconductors. The most promising HTS for application are the bismuth-based and the yttrium based superconductors, where development on Bi2223/Ag tapes and YBCO coated conductor attracted attention due to potentially high J_c and T_c of these superconductors.

Today's MRI machines use more expensive niobium-alloy wires and require costly liquid helium refrigeration to maintain superconducting properties. The price of pre-reacted MgB_2 is about US$750/kg to US$300/kg depending on the volume demand. This results in the cost of production (CP) for MgB_2 wire in the range of US$0.16 to US$0.88 per kA per metre of wire, at 25 K, 1 T. When we compare this result with CP

of niobium–titanium (NbTi) and niobium–tin (Nb_3Sn), which is roughly \$1/kA·m at 4.2 K and 2 T, and \$10/kA·m at 4.2 K and 10 T, respectively, we could predict that MgB_2 wire could potentially replace NbTi for power devices such as transformers and MRI [6]. With a smaller conductor, the cost of wire used in MRI magnets could be reduced from US \$3-10 per kiloampere of current per meter of wire to only US \$1-2. The development of less expensive wires by the private sector could put an MRI machine in every doctor's office and even in veterinary hospitals.

Recent improvements in cryocooler design have resulted in a threefold to fourfold increase in cooling power. The application of MgB_2 depends closely on the development of the cryoooler. Cryogenic refrigeration systems required for operation at temperatures near 25 K are much less complex and less energy-hungry than those operating at temperatures near 4 K. For example, one-stage cryocoolers normally can reach temperatures near 40 K, while two-stage coolers can simply reach temperatures as low as 10-15 K. However, a three-stage cryocooler is needed to get down to temperatures below 10 K.

The superconductivity of MgB_2 has been hidden for nearly 50 years [7] although it has the highest T_c among the intermetallic superconductors. The discovery of superconductivity in MgB_2 [8] has also changed our approaches to theory of superconductivity. The limit of T_c in metallic superconductors had been believed to be ~ 30K, as predicted by the BCS theory. The recent discovery also showed that we still have not come close to discovering all the materials that exhibit superconductivity and it is quite likely that new superconducting materials will be found in the future. Up to

the time this introduction was written, the first paper on MgB_2 by J. Akitmitsu in Nature has been cited for 1617 times and this is just a conservative estimate.

The discovery also prompted a new wave of investigation on high T_c materials in similar systems. Large number of experimental and theoretical work has been carried out in a short time [9-13] because of its unexpectedly high T_c. Beside the high T_c, simple crystal structure, large coherence length, high critical field, transparency of grain boundaries to supercurrent and low normal state resistivity are all fascinating topics to study for both large scale application and electronic devices. Moreover, the presence of two gap superconductivity (π and σ bands) [14] has been theoretically and experimentally established. Despite all this, MgB_2 shows a significant isotope effect, the same as for low temperature superconductor.

However, critical current density of pristine MgB_2 drops rapidly in the high magnetic field due to the weak pinning centres and low upper critical field. During the past three years, novel techniques for enhancing the useability of MgB_2 have been reported, including chemical alloying, irradiation, thermo-mechanical processing techniques and magnetic shielding to improve the critical density, upper critical field and the irreversibility field. Although many difficulties need to be overcome, rapid progress in the fabrication of various forms of MgB_2 in single crystals, bulk samples, tapes, wires and thin films is quite promising for the realization of practical applications in the near future.

Among the studies, atomic substitution, especially using nano-particles, may help in clarification of the superconductivity mechanism thus making it appropriate for

practical application. Mostly negative results were obtained from the early studies on the effect of elemental doping on the MgB_2. On the other hand, the momentum of enhancing flux pinning using chemical doping is moving to a positive side. Nano-SiC powder is well known for effective improvement of the critical current density, besides C, B_4C etc. Chemical doping is expected to have a secondary effect on the H_{c2} and $H_{irr.}$ Although partial substitution has been attempted with many elements, only two elements doping procedures are widely recognized: substitution of B for C and Mg for Al. With different kinds of precursor powder, fabrication technique and the processing condition, C doped MgB_2 has significantly enhanced J_c and H_{c2}. By taking the advantage of the two bands superconductivity [14], partial substitution by a small amount of dopants will increase the impurity scattering due to the chemical disorder. Among various carbon precursors, carbon nanotubes (CNT) are particularly interesting as their high aspect ratio and nanometer diameter may make them more effective pinning centers compared to the ordinary carbon.

The superconductivity of MgB_2-carbon nanotube composites was first studied by Wei et al. [16]. However, the effect of carbon nanotube doping on critical current density and flux pinning has not been reported. In this project, we will study the effect of the CNT doping of MgB_2 on the superconducting properties interesting for practical applications. We will show that CNT doping improves both vortex pinning and H_{c2} despite some degradation on T_c by doping with C extracted from CNT. The improvement of H_{c2} was predicted by the theory of two-band scattering [15], where homogeneously distributed impurities in the crystal lattice are expected to increase H_{c2}. An enhancement of critical current density and flux pinning by two orders of magnitude in magnetic fields was

obtained by controlling the extent of carbon nanotube substitution and inclusion (depending on processing time and temperature). The substitution effect can be achieved when the C out of CNT replaces the B site in the MgB_2 while the inclusion effect is incorporation of whole of CNT into the MgB_2 matrix, as indicated by the, SEM and TEM results.

An important issue of nanotube dispersion will be systematically studied, namely the effect of CNT dimension (length and diameter) on the doped MgB_2. In this case the low intensity ultra-sonication was introduced to prevent agglomeration of CNT and obtained more homogenous mixing. The magnetization measurement indicates that shorter length of CNT will result in a higher critical density of CNT in the MgB_2, because longer CNT tend to agglomerate and entangle with each other.

We will also report a systematic study of the influence of heating rates of sample production on the superconducting properties of *in situ* MgB_2 -CNT/Fe wires, compared to the undoped MgB_2/Fe wires. The elongated CNT's in the MgB_2 wire induce anisotropy in J_c in relation to the direction of applied field.

Experimental results indicate that carbon from CNT is doped into MgB_2, changing its T_c, H_{c2} and J_c. To clarify this effect of carbon substitution using CNT, the effects on transition critical temperature, lattice parameters, critical current density, and flux pinning were studied by doping MgB_2 with carbon nano particles for bulk and wire samples, under a wide range of processing conditions. Nano-carbon doped MgB_2 resulted in a significant improvement in $J_c(H)$ at higher processing temperatures, where substantial substitution of boron for carbon occurred similar to the CNT doped MgB_2.

B substitution for C is proposed to be responsible for the enhancement of vortex pinning.

Finally, effect of carbon substitution of both nano-C and CNT was studied with main focus on the optimum doping level and effect of carbon substitution on the J_c and the phase formation. It was found that the lattice distortion and optimum doping level is different in the CNT and nano C samples. This indicates that under the same doping level and processing conditions, carbon substitution is more effective for the nano C samples than the CNT samples. Since the carbon in the CNT needs to break out from the atomic carbon sheet of CNT before it can take part in the carbon substitution, the carbon substitution in the CNT consumed more energy compared to the nano C and indirectly reduced the opportunity of carbon substitution under the same condition.

References

[1] J. H. Schon, C. Kloc, B. Batlogg, *Nature* **408**,549-552 (2000)

[2] A. Y. Kasumov, M. Kociak, S. Guěron, B. Reulet, V. T. Volkov, D. V. Klinov, and H. Bouchiat, *Science* **291**, 280 (2001).

[3] C. Buzea and T. Yamashita, *Supercond. Sci. Technol*. **14**, R115 (2001)

[4] G. Bednorz and K.A. Müller, *Z. Phys. B*, **64**, 189 (1986).

[5] J. W. Ekin, A. I. Braginski, A. J. Panson, M. A. Janocko, D. W. Capone II, N. J. Zaluzec, B. Flandermeyer, O. F. de Lima, M. Hong, J. Kwo, and S. H. Liou, J. of Appl. Phys. **62**, 4821-4828 (1987).

[6] P. M. Grant, *Industrial Physicist*, **7**, 22 (2001)

[7] M. Jones, R. Marsh, *J. Am. Chem. Soc*., **76**, 1434 (1954).

[8] J. Nagamatsu, N. Nakagawa, T. Muranaka, Y. Zenitani and J. Akimitsu, *Nature*, **410**, 63 (2001)

[9] J. Kortus, I. I. Mazin, K. D. Belashchenko, V. P. Antropov and L. L. Boyer, *Phys. Rev. B* **86**, 4656 (2001)

[10] J. M. An and W. E. Pickett, *Phys. Rev. Lett*. **86**, 4366 (2001)

[11] S. L. Bud'ko, G. Lapertot, C. Petrovic, C. E. Cunningham, N. Anderson and P. C. Canfield, *Phys. Rev. Lett.* **86**, 1877 (2001)

[12] A. Sharoni, I. Felner, O. Millo, *Phys. Rev. B* **63**, 2205081 (2001).

[13] H. Kotegawa, K. Ishida, Y. Kitaoka, T. Muranaka, J. Akimitsu, *Phys. Rev. Lett.* **87**, 127001 (2001)

[14] A. Gurevich, *Phys. Rev. B* **67**, 184515 (2003).

[15] H. J. Choi, D. Roundy, H. Sun, M. L. Cohen and S. G. Louie, *Nature* **418**, 758 (2002)

[16] J. Wei, Y Li, C. Xu, B. Wei, and D. Wu, *Mater. Chem. Phys*. **78**, 785 (2003).

Chapter 2: Literature review of MgB_2 superconductor

2.1 Introduction

In the past five years, MgB_2 has been fabricated in the following forms: bulks, single crystals, thin films, tapes and wires. In addition to the relatively high T_c and simple crystal structure, MgB_2 possesses large coherent length, high critical current densities and transparency of grain boundaries to current flow. In this chapter, we will review the basic electronic and magnetic properties of the MgB_2 as well as its crystal structure. We will also discuss the preparation method that has been well developed for experimentation on MgB_2. In addition, introduction to the future prospect of MgB_2 and the development for the application in the market of superconductor today will be given.

2.2 The Discovery of MgB_2

In January 2001, Prof. J. Akimitsu announced the discovery of superconductivity in magnesium diboride with feasible superconductivity observed up to 39K (-234^{o}C). The discovery has generated enormous interest and excitement in the superconductivity community and the world in general. Many newspapers and news channels such as the New York Times, the Washington Post, the Chicago Tribune, CNN, etc., have reported on it. The UK based journal Nature published Akimitsu group's paper in 2001 and revived the interest of superconductivity in non-oxides and boron related compounds.

Boron atoms have a suitable size and electronic structure for forming direct B-B bonds than can form various kinds of boron networks. Higher dimensionality of networks is formed with increasing the boron content [1]. There are more than 50 boride compounds with different structures reported to be superconductors. The details can be found in the review paper [2]. However, the most outstanding discovery is that of B, which will exhibit superconductivity under high pressure with the transition temperature of 11.2K [3]. All the AlB_2 type borides are listed in the table 1 with their transition temperatures. Among all of these compounds some were discovered before the discovery of the superconductivity in MgB_2 and some after. A more systematic investigations and studies of the relationship between stoichiometry and crystal structure needs to be carried out since there were some contradictory results in some compounds like TaB_2 and ZrB_2. The fact that some borides have the controversial results on the critical temperature, suggests that non-stociometry may be an important factor in the superconductivity of this family.

Table 2.1: Superconducting transition temperatures of Al-B_2 type boride superconductors

Formula	Transition temperature (K)	Reference
NbB_2	0.62	[4]
$NbB_{2.5}$	6.4	[5]
$Nb_{0.76}B_2$	9.2	[6]
$MoB_{2.5}$	8.1	[5]
BeB_2	0.72-0.79	[7]
ZrB_2	5.5	[8]
TaB_2	9.5	[9]

2.3 Crystal and Electronic structure of MgB_2

MgB_2 possesses an AlB_2-type hexagonal structure (space group P6/mmm) with alternating boron honeycomb planes and magnesium triangular planes, as shown in the

Fig 2.1. Each Mg atom is located at the centre of a hexagon formed by boron and it donates its electron to the boron planes; hence the B-B bonding is strongly anisotropic. With the structure of MgB_2 similar to the graphite, the distance between the boron planes is significantly longer than the distance between the boron atoms in the planes. He et al. [10] analysed the crystal structure of MgB_2 using the Rietveld method and found that the compound has the unit cell parameters: a = 0.3081361(14) nm and c = 0.351782(17) nm at room temperature. The same conclusions on the crystal structure have been made on the basis of studies of high resolution transmission electron microscopy (HRTEM) [11], high resolution powder diffraction [12] electron energy loss spectroscopy [13]. This value of lattice parameters for MgB_2 is in the middle of the values of lattice parameters of AlB_2-type compounds. There is no sign of structural transition for MgB_2 down to 2K or under high pressure of 40GPa.

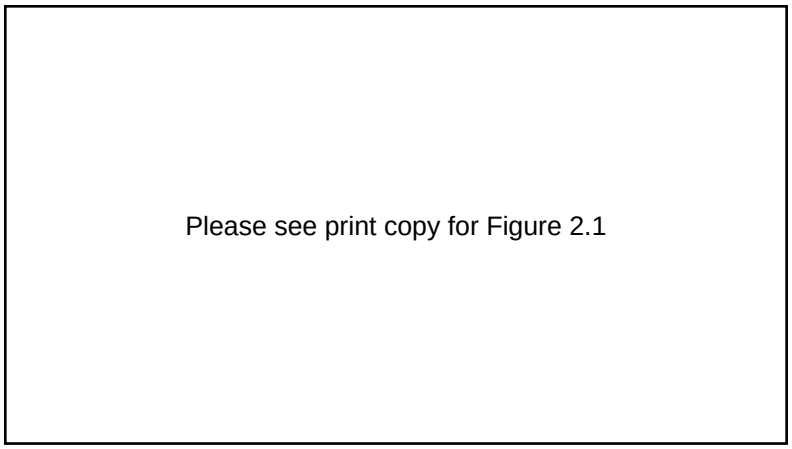

Figure 2.1 : Crystal structure of MgB_2 [14].

The band structure of MgB_2 has been long reported before and after the discovery of the superconductivity of MgB_2 [15-22] and it is now known in detail. Despite its crystal structure being similar to graphite intercalated compounds, the band structures are more

similar to those of graphite, with three incompletely filled σ bands (in-plane sp_xp_y hybridization) and two π bands (bonding and antibonding) corresponding to the sp^2-hybrid bonding.

In MgB_2, the sp^2 boron orbitals overlap, creating σ bonds within the neighbouring atoms in the plane while the reaming p orbitals extend above and below the plane and create the π bonds. These bonds are responsible for the corresponding σ and π energy bands, each of them contributing to superconductivity in MgB_2. As shown in the figure 2.2a the golden hexagonal network is associated with the σ bands, whereas the six green lobes above and below the boron plate are associated with the π bands. These 2D and 3D metallic-type states contribute almost equally to the state of the Fermi level and the electrons are delocalized through out the honeycomb. Unlike conventional metallic bands, the σ band has charge concentrated along the B-B axes, rather spread through the unit cell (figure 2.2b). In the Fermi surface of the MgB_2 superconductor, the green and blue surface comes from the bonding $p_{x,y}$ bands, the blue tubular network from the bonding p_z bands, and the red tubular network from the antibonding p_z band. However, the complexity of the electronic structure of MgB_2 especially coexistence of both quasi-2D covalent cylindrical network and a 3-D metallic type interlayer conducting network raise the possibility of having two distinct superconducting energy gaps.

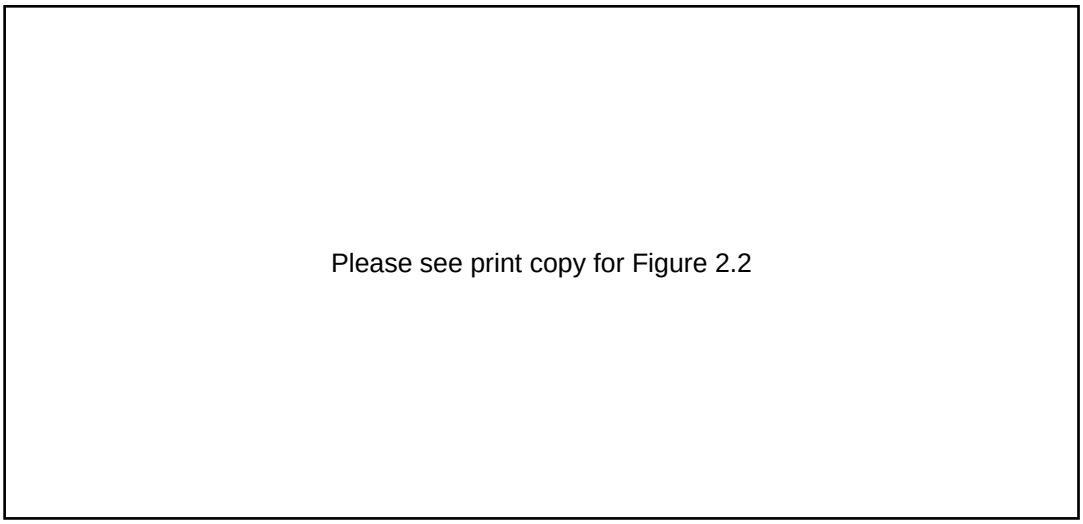

Figure2.2 Electronic structure of MgB_2 (a) the 2-D network of σ bands and 3-D network of π bands [23] (b) Fermi surface of MgB_2. The vertical sections of cylinders at the corners are associated with the σ bands; the more 3 D network of tunnels and caves in the centres of the zone is associated with π bands [19].

Historically, two-band superconductivity was proposed right after the formulation of the BCS theory as the extension of the BCS theory by Suhl et al. [24]. In the early 1960s, experimental claims of two-band superconductivity in some transition metals like V, Nb and Ta [25, 26] and later in $SrTiO_3$ [27] and borocarbide [28] were published.

MgB_2 appears to be the first system for which multiband superconductivity has been identified by several experimental techniques: heat capacity, tunnelling spectroscopy, Raman spectroscopy, penetration depth measurements and angle-resolved photoemission spectroscopy using polycrystalline samples or the single crystals. The strong electron coupling in the 2-D σ bands and weak coupling in the 3D π bands lead to existence of two superconducting energy gaps in this material. The two bands interact with each other and manifest the unique properties of MgB_2 with different degree of interaction. There are three different impurity scattering channels in MgB_2 alloys: intraband scattering within each σ and π band and interband scattering between

them. As a result, by tuning the rate of interactions, the upper critical field can be significantly enhanced [29, 30].

In most of the experimental reports, the σ gap was observed to decreases with the decreasing of T_c while the π gap remained constant and independent of the T_c. The reports from Gonnelli et al. [31, 32] demonstrated a different behaviour of the superconducting gaps, depending on the type of dopant. E. Ohimichi suggested that the two-gap superconductivity concept is still valid in carbon-substituted samples, and that the smaller π-band gap is robust against carbon substitution in contrast to an appreciable decrease in the larger σ-band gap [33]. The interband impurity scattering between σ and π bands is exceptionally small, due to the particular electronic structure of MgB_2, so that in the superconducting state the two gaps in the σ and π bands are preserved even in ‘‘dirty’’ samples with a considerably reduced T_c and a broad range of normal state resistivities. However, a recent point contact study on MgB_2 crystals containing high C substitution levels showed a merging of the σ and π gaps for the first time as expected from the theoretical prediction that the σ and π band gaps merge into a single gap giving T_c =25 K [34].

2.4 Electron Phonon Coupling in Superconductivity of MgB_2

MgB_2 with the reported T_c of 39K seems to be at the upper limit that can be explained by the phonon-mediated BCS superconductivity. BCS predicted that high frequency phonons in the low atomic mass compounds produce a high T_c. Superconductivity in MgB_2 is interested from the fundamental point of view raising questions whether it can

be understood within the conventional electron-phonon (EP) mechanism or, the high transition temperature might imply an exotic coupling mechanism.

According to initial findings, MgB_2 seems to be a conventional BCS type superconductor. The measurements of the isotope effect revealed the importance of the electron-phonon interaction for the Cooper pairing mechanism in MgB_2: T_c shifted by 1K when ^{11}B was substituted for the ^{10}B [35, 36] as shown in figure 2.3.

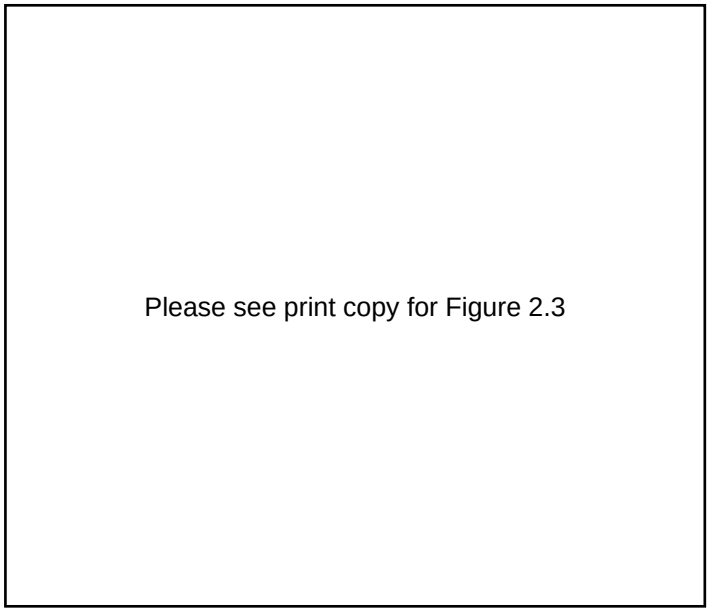

Figure 2.3 Boron Isotope Effect in Superconducting MgB_2 [37].

Besides that, most of the experimental results like linear T-dependence of the H_{c2} with a positive curvature near T_c [38], shift of the T_c to a lower temperature with the increasing of magnetic field in the resistivity measurements [39, 40] were reported to be similar to the low temperature superconductor.

On the other hand, some reports indicated unconventional superconductivity similar to cuprates, like quadratic T-dependence of the penetration depth λ(T) [41-43] and reversal of the sign of the Hall coefficient near T_c [44]. More recently, optical studies in *c*-axis oriented superconducting MgB_2 films indicate that the electron-phonon coupling is very weak and insufficient to produce the high T_c in the MgB_2 [45]. The value of the isotope-effect exponent of MgB_2 (0.32) is much lower than the expected value of 0.5 for BSC superconductor [35].

Nevertheless, majority of theorists support the BSC mechanism, *i.e.*, an electron-phonon driven *s*-wave mechanism of the superconductivity in MgB_2. There are a few fundamental ideas, which use the hole superconductivity to explain the paring mechanism in the MgB_2. In this case, the planes of B atoms are proposed to be akin to the Cu-O planes in the cuprates and the high temperature superconductivity in MgB_2 arises from the boron $p_{x,y}$ orbitals in the negatively charges B-planes [46, 47].

2.5 Preparation Method

The low cost and simple preparation methods of MgB_2 promise the important large-scale and electronic device application. In this section we will concentrate on the fabrication of bulk pellet and wires and some of the important synthesis issues of MgB_2. Although magnesium diboride is available from chemical suppliers as commercial powder, the critical properties like critical current density and upper critical field of this commercial powder are not good enough for practical applications .

2.5.1 Bulk MgB_2 superconductor

2.5.1.1 In-situ Reaction

MgB_2 can be synthesized by a simple route: reaction of B with Mg vapor, generally at temperatures above 650^{o}C which is the melting point of the Mg. Up to date this method has been used to form MgB_2 powder, sintered pellets, wires and films. The binary diagram for Mg-B is shown in the figure 2.4 [48]. MgB_2 is known as a line compound that decomposes above 1500^{o}C when it is in equilibrium with Mg vapor. As from the phase diagram, the liquid phase of MgB_2 varies from around 650^{o}C to 1000^{o}C which also indicates a big variation of processing temperature to form MgB_2. Prolonged liquid phase is necessary to yield a homogenous MgB_2 with a better superconducting properties. Yamamoto et. al reported that a formation of MgB_2 below the melting point of magnesium is possible under many hours of processing, which is also known as solid-solid reaction of magnesium and boron [49]. Kumakura et al. succeeded in synthesis of high J_c in situ MgB_2 tapes by low temperature reaction for 1 h below 650^{o}C, using ultrafine magnesium or MgH_2 and high purity boron powders as starting materials [50, 51]. GaN, which has low melting point, has been used to promote the liquid phase processing in MgB_2 and thus the J_c was enhanced by a factor of 2 and 10, for temperatures of, 5 K and 20 K, respectively [52].

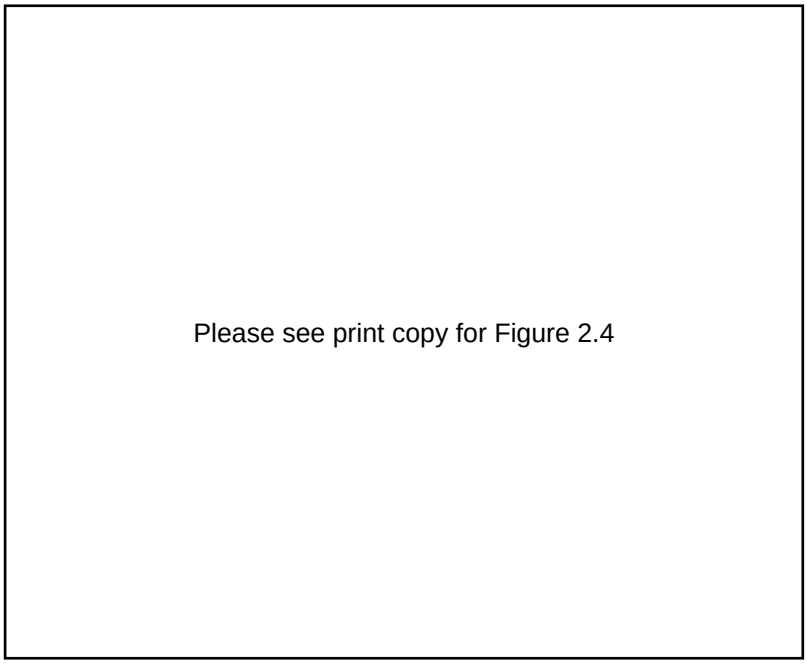

Figure 2.4 Phase Diagram of Mg+B [48].

2.5.1.2 Hot Isostatic Pressing (HIP)

HIP process for MgB_2 is promising as it can produce highly-dense, low-porosity, crack-free samples which allow improvement of mechanical properties of MgB_2. HIP has been reported to improve superconducting properties in bulks and wires samples [53-56].

In particular, a hot isostatic pressed (HIPed) MgB_2 pellet was found to have significantly increased J_c at high fields as compared to its non-HIPed counterpart as shown in the figure 2.5. The improvement is attributed to elimination of porosity present in the MgB_2 pellets, resulting in an improved connectivity of the material between the pores as shown in figure 2.6. The HIP process was also found to induce

high density of structural defects like small angle twisting, tilting, and bending boundaries resulting in the formation of subgrains within MgB_2 crystallites [55].

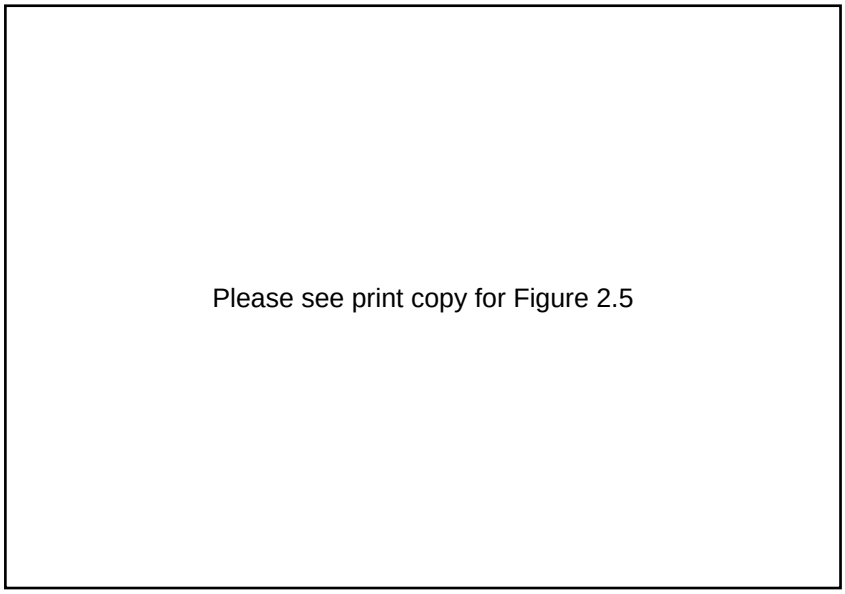

Figure 2.5 Magnetic critical current density J_c as a function of magnetic field H for the non-HIPed and HIPed samples at 5 and 30 K. The J_c at 0 field is nearly the same for both samples, but the differences between the samples increases with field, and the drop in J_c at higher fields is remarkably faster in the non-HIPed sample than in the HIPed one [55]

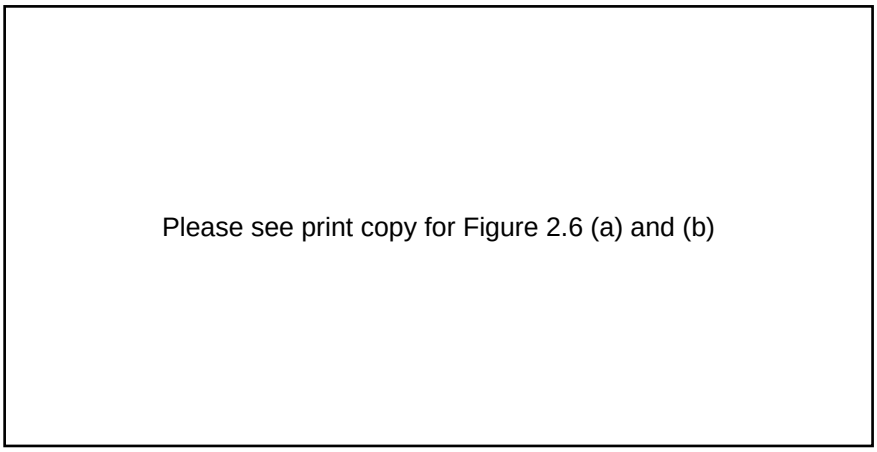

Figure 2.6 SEM micrographs of MgB_2 samples (a) surface of the non-HIPed and (b) surface of HIPed sample [55].

2.5.1.3 Mechanical alloying

It is a well known fact that, mechanical alloying is a non-equilibrium processing technique to prepare metastable amorphous, quasi crystalline, and nanocrystalline materials [57]. The use of mechanical alloying (MA) for the preparation of nanocrystalline MgB_2 superconductors was shown to be an appropriate technique that yields a highly pure, homogeneous, nanocrystalline structure and refined particle size, thus, enhancing flux pinning ability of the grain boundaries [57-65].

Starting materials and milling balls are placed together in a milling vial, which is exposed to a strong vibration or rotational acceleration causing impacts of milling balls leading to repeated fractioning and cold welding of powder particles. The milling conditions can be adjusted so the desired phase forms via solid-state reaction at moderate temperatures. Normally the milling process will be performed in the Ar atmosphere in the sealed tungsten carbide vial on a planetary or SPEX ball mill. However, long time of milling will expose the final product to impurities contamination from the vial. Using mechanically alloyed elemental Mg and B with subsequent hot pressing, J_c and the irreversibility line have been substantially improved [58]. The increment in J_c was ascribed to the large number of grain boundary pinning contributed by nanoparticles. Meanwhile, mechanical milling on the commercially available MgB_2 powder has led to deterioration of T_c and superconductivity was totally lost after 20 h of milling. However, T_c was subsequently restored upon annealing [66]. More recently, it was demonstrated for MgB_2 with carbon doping under high-energy mechanical milling combined with HIP that substantial enhancement of the critical current density and the upper critical field can be obtained [67].

2.5.2 MgB_2 Superconductor Tape and Wire

2.5.2.1 Powder in Tube (PIT)

It has been mentioned that MgB_2 is not significantly affected by weak links, and thus high transport critical current densities of the order of 10^6 A/cm^2 have been reported in the temperature range between 4.2 and 25 K in tape and wire samples [68-70]. This has important consequences for the application of MgB_2 wires and tapes for cable and magnet industries to be competitive with low T_c superconductors, like NbTi and Nb_3Sn for operation at temperatures around 20K.

The general process of tape and wire fabrication is the powder-in-tube (PIT) process, [70-76] which is characterized by filling metallic tubes with powder and then drawing and rolling into tapes (figure 2.7) . Two methods have been reported in the literature so far for wire application. One is the in situ PIT technique, which consists of filling of the metallic tubes with elemental Mg and B powders and subsequent deformation and heat treatment [71, 72, 77].

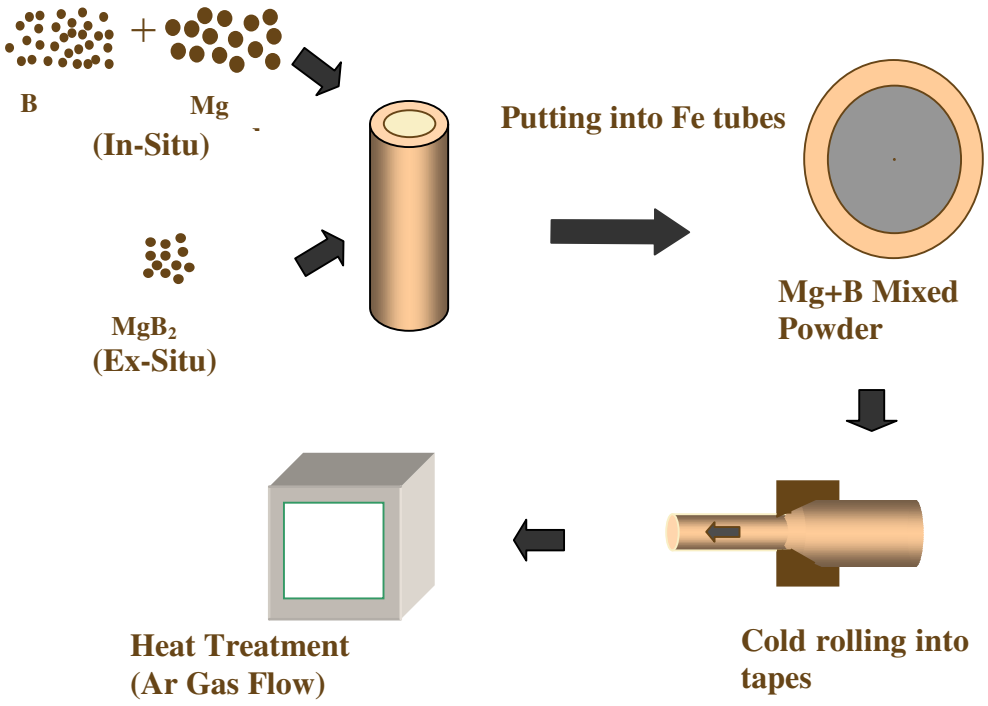

Figure 2.7 Process of Powder In Tube (PIT) for in-situ and ex-site method.

Another is the ex situ PIT technique, which consists of direct filling of the metallic tubes with reacted MgB_2 powder, followed by deformation [74, 75]. Heat treatment at 600-1000 °C is usually applied to the cold-worked tape or wire to obtain superconductivity. Although the fabrication of ex-situ method is cheaper and simpler, the in-situ method holds significant advantages that make it worth further exploring. For example, it is easy to carry out impurity doping [78-80]. Already, long mono core wires over 100 m in length have been successfully developed by the PIT method [81, 82].

Generally, normal metal cladding provides parallel electrical conduction, thermal stabilization, and mechanical protection for the superconductor cores. In particular, MgB_2 is mechanically hard and brittle and therefore difficult to draw into the desired

wire geometry. Sheath materials which are applied to MgB_2 core were stainless Steel (SS) [75, 83-86], Cu [71, 74, 87], Ag [71, 74], Ni [74, 77], Cu–Ni [86], and Fe [72, 77, 88-90]. The selection of sheath materials is limited due to reactivity of Mg for the *in situ* process. Mg tends to react and combine with many metals such as Cu or Ag to form solid solutions or intermetallics with lowered melting points [91] which make the metal cladding not suitable during processing of MgB_2 at around 900 to 1,000^{o}C.

The sheath material's toughness and chemical compatibility with MgB_2 are crucial for fabricating long-length MgB_2 tapes or wires with high critical current. Sheath materials with high mechanical strength, such as stainless steel (SS) and carbon steel (CS), can achieve high J_c values for tapes prepared by the ex situ process [75, 92]. However, sheath materials with high mechanical strength usually show poor ductility. Others, such as Nb and Ta, increase the fabrication cost and weight and reduce the merits of using MgB_2. Among these metals, Fe is one of the most promising materials due to its ductility, low cost and light weight as well as the suitability of this technique for large-scale industrial production.

Besides that, it was shown that field dependence of J_c is strongly improved by the presence of the iron sheath, which suggests that interaction between ferromagnet and superconductor can be used to substantially improve the field performance of MgB_2/Fe wires at relatively low fields [93, 94]. The improvement of $J_c(H)$ by the iron sheath was expected because the ferromagnetic sheath would shield the superconducting core from the external field. Therefore, up to a certain value of external field, the field inside the sheath would be zero. This would provide an almost constant value of J_c up to that

particular field, which depends on the permeability and thickness of the iron sheath. This would be followed by a decrease of J_c with H for higher fields in the same manner as if there was no iron sheath. However, improvement of J_c was observed to extend to much higher fields than expected from a mere magnetic shielding, which was attributed to an interaction between iron and superconductor. This can be very effectively employed for decoupling the superconducting filaments in multifilamentary MgB_2/Fe wires to substantially lower the AC loss in the wires [95]. An overview of the current state of development of MgB_2 wires and tapes can be found in the review paper [96].

2.5.3 Alternative Preparation Routes

The very first superconducting MgB_2 wires were prepared by the diffusion of Mg into commercially available B whiskers of 200 μm diameters or exposure of boron filaments to Mg vapour [97]. The wires obtained by this method exhibit very low residual resistivity values, ρ_o of the order of 0.6 μΩ cm and have better than 80% the theoretical density of MgB_2.

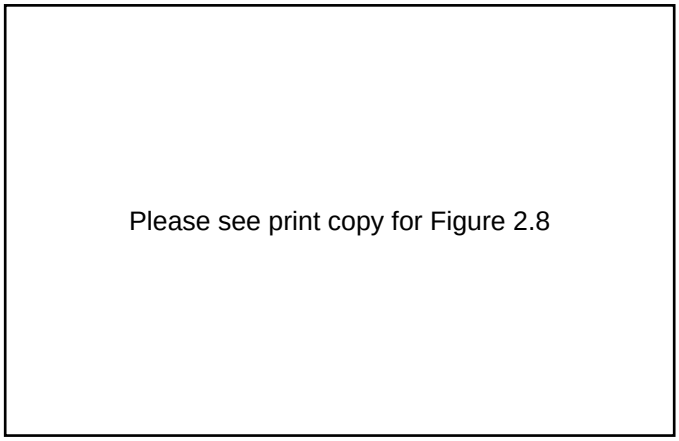

Figure 2.8 MgB_2 wire segments made from 100 μm diameter boron filaments [97].

Another technique was so-called continuous tube filling/forming (CTFF) process [98]. In the CTFF process, powder is dispensed onto a strip of metal as it is being continuously formed into a tube. High purity long Fe strips (23 mm wide, 0.20 mm thick) are formed continuously into a tube with an overlap-closed tube process and powder being enclosed in a sheath. After that, the closed tube can be inserted into a seamless Monel or Cu–30Ni tube and deformed to the round wire. In fact, this technique has been used to prepare commercial MgB_2 wires and tapes by the Hyper Tech Research, Incorporated, Columbus, USA.

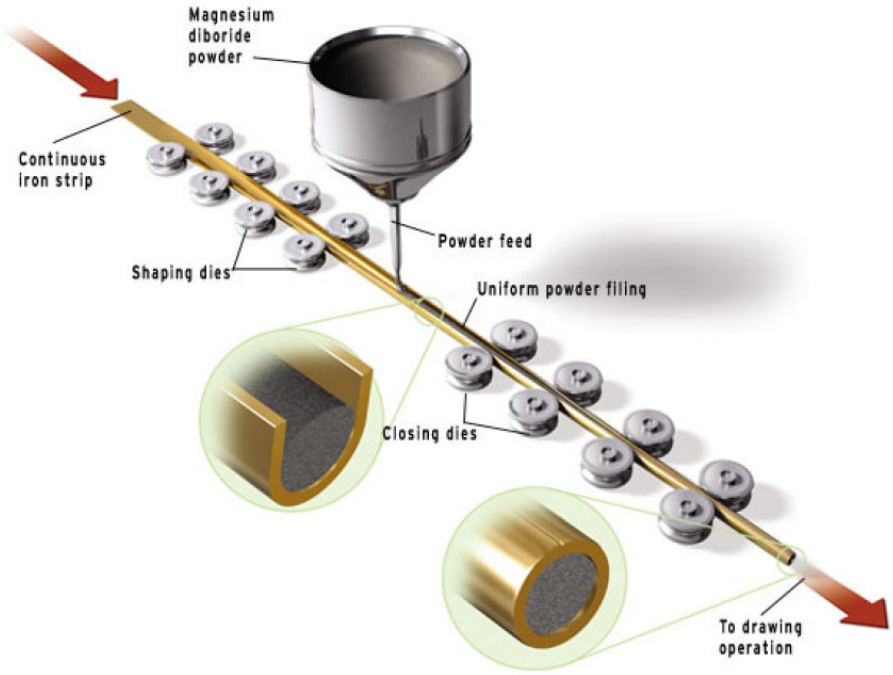

Figure 2.9 Schematic of the continuous tube filling/forming (CTFF) process.

A variation of the PIT preparation route was reactive liquid infiltration [99]. This technique has been successfully applied to the manufacture of both monofilamentary and multifilamentary wires of several tens of meters in length. The process starts with a

steel clad thin Niobium (Nb) tube filled with cylindrical magnesium rod and fine boron powder. The MgB_2 composites were formed inside the Nd tube upon heat treatment, resulting in a very compact, dense and finely grained MgB_2. Using Mg infiltration to react with B, Mg was not mixed with B at the initial stage like the PIT method.

More recently, Togano et al. proposed a new approach for the fabrication of MgB_2 tape utilizing an interface diffusion reaction between a Fe–Mg alloy substrate and a boron layer [100]. In this process, the Fe-Mg alloy will be formed into a tape by a lamination method. The Mg in the Fe–Mg alloy diffuses towards the interface during the heat treatment, forming a thin Mg rich layer along the interface. Then, the Mg rich thin layer acts as a source of Mg for MgB_2 formation, which proceeds to the inside of the B layer. A dense structure of MgB_2 with very small amount of MgO impurities can be produced by such formation mechanism, with a J_c value of 3×10^4 A cm^{-2} at 5 K and 7 T.

2.6 Basic Properties of MgB_2

2.6.1 Critical Temperature, T_c

A primary difference between pure MgB_2 and its alloyed forms is that the former is a line compound and, once formed, has the same composition everywhere, whereas the latter is a solid solution and requires diffusion to move alloying elements. Alloying elements might not be distributed homogeneously since defect energies are high, which could have important consequences for the observed superconducting properties.

Unfortunately, there has been no report stating that chemical doping may enhance T_c of MgB_2. One of the difficulties associated with doping of MgB_2 may be the fact that the MgB_2 structure is robust as mixing of the dopant with MgB_2 before or in the process of synthesis is not likely to achieve the substitution. Chemical substitutions change the physical quantities of the system such as carrier density, lattice constants and the crystallinity. The critical temperature of MgB_2 was reported to decrease at various rates for different substitutions.

However, T_c of pure MgB_2 increased from 20 K to 38 K after the processing time increased from 1 h to 24 h, and saturated at 38.7 K for samples sintered longer than 60 h [49]. The improvement of the T_c can be explained by improvements in superconducting transitions with heating time coinciding well with the improvement of crystallinity. As pointed out by Ribeiro et. al, T_c and the residual resistivity ratio (RRR) of MgB_2 bulks are very sensitive to boron purity [101]. The small decrease of T_c is believed to be due to both slightly poor crystallinity and low quality of the starting boron powder containing silicon, iron and carbon as a major impurities.

2.6.2 Critical current, I_c and Flux Pining

Although MgB_2 has a relatively high critical current density, the J_c of pristine MgB_2 drops rapidly with the increasing magnetic field due to its weak vortex pinning strength in magnetic field and low value of H_{c2}. As discussed in the previous section, the critical current density in MgB_2 is influenced by various factors, e.g., the quality and size of the powder particles and the annealing temperature and time. However it is clear that there

are two main obstacles that have to be overcome to enhance the $J_c(H)$: vortex pinning and H_{c2}.

Superconducting properties of MgB_2 wires can be affected not only by a magnetic field, but also by an electric current. In the mixed state of type II superconductors, the field penetrates the superconductor in the form of thin filaments, so called magnetic vortices. Movement of the vortices is associated with a change of magnetic flux in and around the vortices [102]. A current driven by external source will force this vortices to move and this is described on a macroscopic level by a Lorentz Force, F_L, which can be defined as

$$F_L = J \times B \qquad (1)$$

where J and B are spatially averaged transport current density and external magnetic field, respectively.

The moving of the vortices will lead to the dissipative losses in the superconductor and a voltage drop is observed. Pinning centres are defective sites in the superconductor where vortices tend to stick, provided that their size is compatible with the coherence length. They tend to stick there because it requires less energy for the vortices to stay there. When the transport current flows through the superconductor, the vortices will start moving only if the Lorentz force becomes strong enough to overcome pining and tear a vortex away, generating resistance [102]. The current at which the resistance just starts occurring is called the critical current, I_c. Thermal excitations also promote this de-pinning of vortices, resulting in a weaker effective pinning at higher temperatures.

In general, local sharp change in the condensation energy of superconducting carrier is desirable for flux pinning. In other words, transition from superconducting to local weak superconducting or nonsuperconducting regions, such as defects in the crystal lattice, dislocations, twin boundaries, grain boundaries, small precipitates, compositional fluctuations and artificial defects, is sharp and these regions can act as effective pinning sites if their size is comparable to the diameter of the vortices, i.e. ξ. In the case of MgB_2, candidates for effective pinning centres are different form that for high temperature superconductors because of relative long superconducting coherence length and highly isotropic nature of MgB_2.

Attempts to enhance J_c and flux pinning have been made by using several of techniques, including impurity chemical doping, irradiation and thermo-mechanical processing. However, irradiation and thermo-mechanical processing techniques are not suitable for the preparation of MgB_2 wire and tapes because of their complicated nature and the practical difficulty in the use on very large scale. Among these, the doping of chemicals (mostly nano-particle) into MgB_2, which is a low cost fabrication technique to improve the pinning centres, is considered to be the most practical for application. S. Soltanian et al. have shown that grain sizes of the precursor SiC have a strong effect on the critical current density and its field dependence of MgB_2 superconductor. The smaller the SiC grains are, the better is the field performance of J_c and H_{irr} [103]. Nano size pinning has a few main advantages over larger particle dopants. Firstly, a stronger pinning force will be introduced due to their size being comparable to the coherence length (ξ). Secondly, nano size doping would not lower the volume of superconductivity substantially or affect the formation of superconducting phase, but will enable

introduction of large number of pinning centers. In this work, two kinds of nano-particles will be used as the dopants: carbon nanotube, which has nanorod shape with high aspect ratio and nano carbon that is a spherical particle.

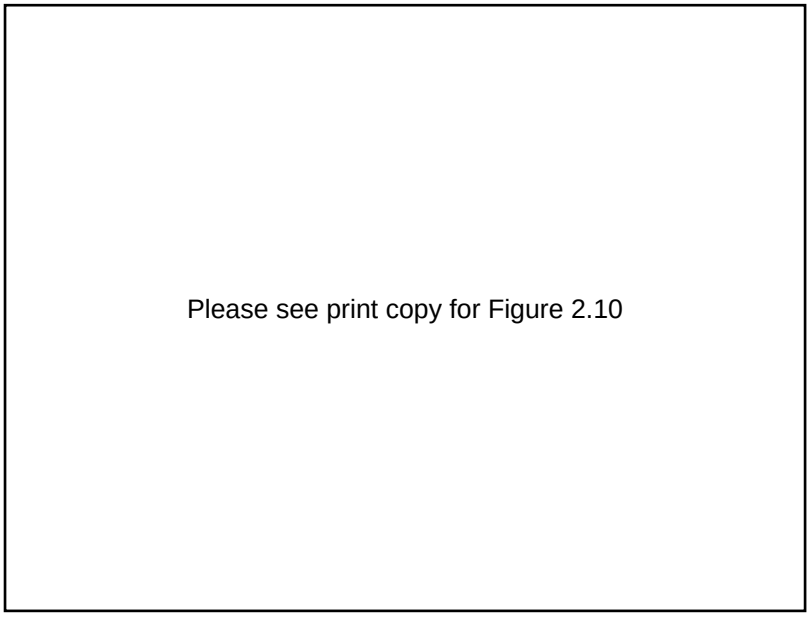

Fig. 2.10 The J_c field dependence of MgB_2 samples doped by 10 wt% of different SiC powders as well as the reference sample at different temperatures of 5, 20 and 30 K [103].

2.6.3 Crystallinity and Grain Size effect on Critical Current Density

It has been reported that grain boundaries are believed to act as pinning centres [104-107]. Yamamoto et al. has systematically studied the crystallinity of MgB_2 by using full width at half maximum (FWHM) value of peaks derived from powder x-ray diffraction (XRD) [108]. FWHM of the [110] peak reflects the in-plane disorder while FWHM of [002] peak reflects the out of plane disorder. The FWHM is apparently larger at low processing temperatures, as compared to the high processing temperatures, suggesting

that poor crystallinity occurred in the low temperature processing reaction. MgB_2 sintered at low temperature was composed of small grains while significant grain growth occurs upon high processing temperature. The degradation of crystallinity originates from disordered crystal lattice caused by various types of lattices defects or intragranular precipitates [109]. These are believed to increase the intraband scattering, shortening the electron mean free path l and ξ according to the equation $1/\xi = 1/l + 1/\xi_0$, where ξ and l are both the coherence length and mean free path, respectively. Since pinning force at grain boundaries, f_{GB}, is proportional to the inverse of grain size and lattice strain, both small crystal size and lattice distortion are considered to enhance the grain boundary pinning [108].

2.6.4 Effect of Mg precursor powder on MgB_2 Superconductivity

It is well known that Mg is highly volatile at high temperatures. Therefore, it is inevitable that Mg is easily lost during the preparing process of the sample. That is to say, the prepared samples usually have Mg deficiency. Nevertheless, Mg, as the other constitutional element, is a very reactive element. Mg powder has a large surface area, and it oxidizes easily during powder production, storage and handling. The effects of MgO on MgB_2 superconducting properties should be studied to facilitate the production of MgB_2 on an industrial scale.

All of the studies on Mg percussor have only focused on the Mg stoichiometry effect while there is no detailed report on effect of purity of Mg on the critical current density and transition temperature [101, 110-113]. However, all the reports on the effect of the

critical temperature so far vary significantly, which is most probably due to different preparing condition and starting precursors. In general, Mg deficiency degrades the critical temperature. According to Lezza et al., inclusion of 5% Mg to MgB_2 powder was found to affect neither J_c nor B_{c2} [114].

Kumakura's group has systematically studied the effect of the Mg on the critical current density. They achieved twice as large J_c by using MgH_2 as Mg source as for samples prepared using the mixture of Mg + B powders [115]. Replacement of commercial Mg powder with nano Mg powder is effective to enhance the reaction between Mg and B and hence improve grain connections. This is because the surface of commercial Mg powder is mostly oxidized, while the nano Mg powder is very active and promotes the reaction between Mg and B.

Yamada et al. has proved that transport J_c values of the non-doped and 10 mol% SiC-doped tapes prepared with nanometer-size Mg powder reached 90 and 250 A/mm^2 at 4.2 K and 10 T, respectively. These values were about five times higher than those of the tapes prepared with commercial Mg powder [51, 116]. The use of ultrafine Mg and B powder mixture prepared by ball milling also effectively improved the grain connections and enhanced the J_c values [64, 117].

2.6.5 Effect of boron precursor powder on Superconductivity

The influence of the nature of the boron precursor on the superconducting properties of polycrystalline MgB_2 was studied, mostly in respect to its effect on critical current

density, resistivity and phase formation [101, 112, 113, 118]. Chen et al. and Zhou et al. showed that samples made from different purity amorphous boron exhibited different J_c, and also that the highest purity boron (99.99%) yielded the highest J_c. In addition, samples made from crystalline boron powders have about an order of magnitude lower J_c compared to those made from amorphous precursors which is due to different reactivity rates and decreases of oxide impurities in the MgB_2. More recently, X. Xu et al. has studied the effect of boron powders on the superconducting properties of MgB_2 [119]. The 92% and 96% purity boron powders produce lower surface reactivity and larger particle size of MgB_2 than the 99% boron powder, indicating that the low purity powders cannot be used to achieve the same superconducting properties as those of samples made from pure 99% boron powder. However, the purity of 92% and 96% boron powders can be improved by using a simple chemical process, leading to enhanced magnetic critical current densities J_c.

2.6.6 Porosity and Density Effect

On the other hand, MgB_2 bulks synthesized from the powder mixture of magnesium (1.74 g/cm^3) and boron (2.2 g/cm^3) have porous microstructure, having low bulk density, approximately 50% of the theoretical density (2.62 g/cm^3). With larger particle size of Mg, large voids will be formed in MgB_2 matrix when Mg diffuses into B to form MgB_2 as shown in the figure. This leads to the artifact of the sample size-dependent critical current density J_c and irreversibility field obtained from magnetic measurements, due to the different length scales of superconducting screening in the magnetic measurement [120]. Besides that, grain size of MgB_2 is much dependent on

the B powder and smaller grain size is preferable for enhanced J_c where grain boundary is believed to contribute to the flux pinning. If the highly dense MgB_2 bulks or tapes are easily obtained, higher J_c will be expected because of an increase of effective cross-section area for superconducting current.

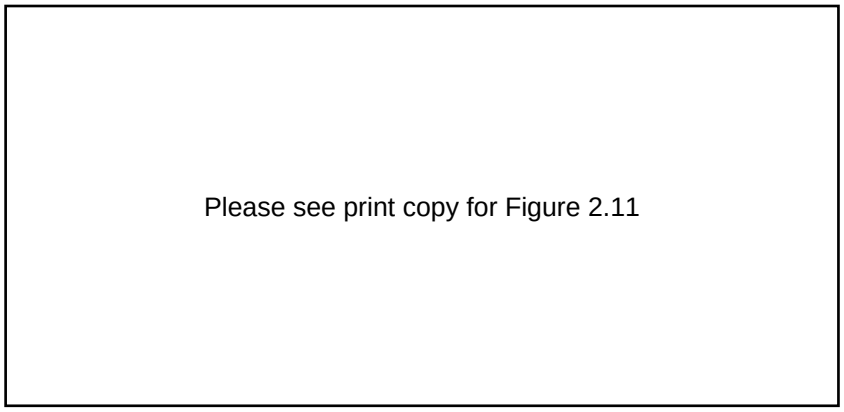

Figure 2.11 Theoretical concept of "in-situ" reaction of Mg and B [1].

2.7 Effect on Chemical Doping on MgB_2 Superconductivity

2.7.1 Carbon doping

Aimed at substitution of boron in MgB_2, various carbon sources, like SiC, TiC, B_4C, C, Na_2CO_3, diamond, graphite, carbon nanohorn and CNT, have been studied aggressively by several groups as shown in the table 2.2. However, among all the reports on C doping, most of the studies only focused on the effect on superconductivity, particularly on the two-band superconductivity and the solubility of C in MgB_2 [101, 121-153]. In

this section, the topic of C solubility and the flux pinning of most of the carbon doped MgB_2 will be reviewed.

Due to the difference between the nominal and actual C substitution level, the correlation between the C substitution and superconducting properties of MgB_2 is obscured. The inconsistencies originate from the precursor materials, fabrication techniques and processing conditions used. Early study on the carbon solubility ranging from 1.25% to 30% was reported when elemental magnesium, boron, and carbon were used as starting materials [122, 128]. Recent studies seem to agree that C can be introduced substitutionally to Boron sites by up to 10% when B_4C was used as a carbon source [134]. However, another study shows that a higher substitution of boron for carbon can be obtained, as revealed by the magnitude of the measured decrease of T_c and the change of a-lattice parameter for C doped MgB_2 samples [143]. By using the neutron diffraction study to estimate C concentration, Avdeev et al. found a linear relation between the unit cell parameter-*a* and the C concentration. The authors also showed that earlier reports overestimated the carbon content in MgB_2 because polycrystalline-carbon-substituted samples may contain significant amounts of impurity phases and the nominal content was assumed most often to be equal to the actual one [134]. S. Jemima et al have evaluated the actual C fraction substituted into the polycrystalline MgB_2 matrix by conventional solid–vapour reaction route and discovered that the actual composition is in disagreement with the nominal composition as plotted in the figure 2.12 [143].

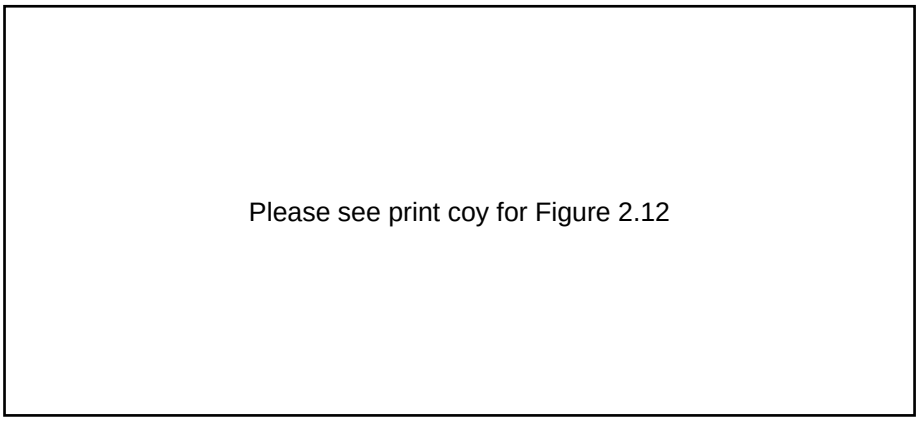

Figure 2.12 Variation of the actual carbon plotted against the nominal carbon in the $MgB_{2-x}C_x$ [143].

Another approach for carbon substitution of MgB_2 was suggested by Mickelson *et al.* to overcome the diffusion problem by using C as starting material [125]. Using boron carbide B_4C as a source of carbon they achieved better mixing of B and C atoms. The samples had an estimated composition $Mg(B_{0.9}C_{0.1})_2$, and T_c was decreased by 7 K. However, the synthesis using B_4C yields multiphase samples containing another borocarbide MgB_2C_2. Ribeiro *et al.* followed this approach and reported the optimization of synthetic conditions of carbon doped samples leading to nearly single-phase $Mg(B_{1-x}C_x)_2$ with T_c=22 K [130].

Ueda et al. and Yamamoto et al. showed that C could substitute at the B site with synthesis temperature of 850^{o}C using B_4C as starting materials [154-156]. Substantially enhanced J_c properties under high magnetic fields were observed in the B_4C doped samples due to low temperature heating and carbon substitution effects. On the other hand, the values of the Full Width Half-Maximum (FWHM) of the MgB_2 (110) peak for

the B_4C doped samples increased with increase of its doping levels, suggesting the introduction of lattice defects and/or decrease of the crystal size of MgB_2 occurring upon B_4C doping. Furthermore, the reactivity of B_4C with magnesium and boron was found to be much higher than that of graphite.

Wilke et al. used chemical vapour deposition, CVD, method to co-deposit B together with a doping element to form long lengths of carbon doped boron fibre [140]. More recently, Senkovicz et al. bulk samples of milled carbon and MgB_2 with hot isostatic pressing and Mg vapour annealing have achieved upper critical fields in excess of 32 T and critical current density approaching 10^6 A/cm^2 which was due to lattice disorder introduced in the milling process and high normal state resistivity shown by the samples [67].

The effect of C doping on the flux pinning and critical current density in MgB_2 using amorphous carbon, diamond, Na_2CO_3, carbon nanohorn and graphite have been studied, all showing improvement of J_c at elevated field. The effective pinning improvement of all the samples are mainly attributed to partial C substitution despite finely dispersed small particles like MgO and MgB_2C_2 in MgB_2 the matrix. All kinds of carbon sources with the magnetic field and transport $J_c(H)$ at 5K and 20K are shown in the table 1.

The improvement of critical current of MgB_2 has been confirmed to be the most effective by doping with SiC fine powder. Although their density was only half of the theoretical density, a 10wt% SiC-doped MgB_2 bulk samples showed H_{irr}~8T and J_c~10^5 Acm^{-2} under 3T at 20K. In fact, the SiC-doped MgB_2 achieved the highest J_c in fields at

20K ever reported for MgB_2 wires and bulks [78, 157]. At 20 K and 2 T, the J_c for the doped sample was $2.4x10^5$ A/cm^2, which is comparable to J_c values for the best Ag/Bi-2223 tapes [78]. At 20 K and 4 T, J_c was twice as high as for the best MgB_2 thin films and an order of magnitude higher than for the best pure MgB_2/Fe tapes, as shown in Figure 2.13.

There are a few reasons nano-SiC can be considered as a good substitution in the MgB_2:

1) Carbon is the only element confirmed to be able to partially substitute at the B site and enhance the $J_c(H)$ in all forms and sources.
2) SiC was found to provide moderate amounts of carbon substitution, largely independent of heating temperature
3) The enhancement of $J_c(H)$ extends to all temperatures, even at the temperatures close to T_c, unlike certain doping elements that show effective pinning only at low temperature.
4) Besides the partial substitution effect, highly dispersed fine particles (< 10nm) like $MgSi_2$, BC, BO_x and $SiBO_x$ match the coherence length of MgB_2, making them good pinning centers.
5) T_c reduction is not pronounced even in the heavy SiC doped sample
6) Partial C substitution in the B causes disorder on the B sites which results in the impurity scattering and contributes to the enhancement of H_{c2}.
7) SiC can provide suitable amount of carbon into MgB_2 even through the reaction below the melting point of magnesium. This advantageous point is desirable for low temperature synthesis of MgB_2, which shows high critical current performance due to smaller grains of MgB_2 with poor crystallinity.

Several leading groups all around the world like NISM and Hyper Tech Research Centers have confirmed the significant enhancement of J_c and H_{c2} for SiC doped MgB_2. Nowadays, most of the commercial MgB_2 wires are prepared with the nano SiC doping. Serquis et al. demonstrated that the high critical current of SiC doped MgB_2 can be retained in longer wire lengths. They made a 6 layers coil using 25 meters of wire [158]. All of these results demonstrated that the enhancement effect on the $J_c(H)$ performance from SiC doping is highly reproducible.

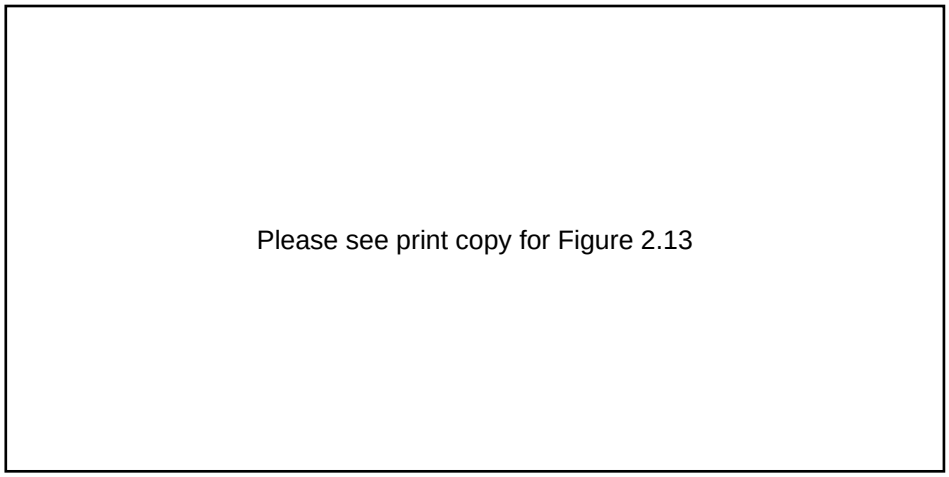

Figure 2.13 Significant enhancement of transport $J_c(H)$ by SiC doping [77].

2.7.2 Carbon Nanotube (CNT) doping

Among various carbon precursors, CNT [159] may have the potential to improve the mechanical and thermal properties of MgB2 wires since CNT's have been used as

component for a number of composites to improve their mechanical properties [160, 161]. This is in addition to improving the superconducting properties of MgB_2. It has been demonstrated that carbon nanotubes can be embedded in Bi-2212, thus offering a promising method for introduction of extended defects in superconductor [162]. The magneto-optical image investigations have revealed that CNT's are functioning like columnar defects, enhancing J_c in the Bi-based superconductor [163]. However, the flux-pinning properties were improved only at low temperatures, below 52 K. Similar method has been reported by Yang et al for a significant enhancement in $J_c(H)$ for high temperature superconductors by introducing nanorods as columnar pinning centers into the composites [164-166]. Recently, Wei et al. have studied the superconductivity of MgB_2-carbon nanotube composites [167]. However, the effect of carbon nanotube doping on critical current density and flux pinning has not been reported.

The advantages of CNT doping over other additives can be described as follows.

(1) Multiwalled CNT's can carry current densities up to 10^9 – 10^{10} A/cm^2 and remain stable for extended period of time [168]. The CNT doping can improve the current path and connectivity between grains in MgB_2.

(2) The thermal conductivity for isolated multiwall CNT's is estimated to be over 3000 W/mK at room temperature, which is higher than that of graphite [169] and hence could benefit the heat dissipation and thermal stability of the MgB_2 wires.

(3) Bundled CNT's have very high axial strength and stiffness, approaching that for ideal carbon fibres [170]. CNT is typically one-dimensional with high aspect ratio of several orders of magnitude and can act as good pinning centres.

Table 2.2 Comparison of magnetic and transport $J_c(H)$ at 4 and 20K for different carbon doping sources. All the $J_c(H)$ were determined by the magnetization unless stated.

Carbon source	Type	J_c at 8T (A/cm^2)	J_c at 6T (A/cm^2)	J_c at 2T (A/cm2)	Reference
4.2/5K					
Graphite	Wire/SS	Transport $2x10^4$	$8x10^3$		[171]
Carbon nanohorn	Wire (suspension spinning method)	Transport $4x10^3$	$4x10^3$	$4x10^3$	[172]
Carbon	Tape/Fe	Transport $4.4x10^4$			[173]
	Bulk 4x3x0.5 mm^3	$3x10^3$	$2x10^4$		[174]
	Bulk 2.87x2.70x3.12 mm^3			$3x10^5$	[175]
	Bulk	$7x10^4$	10^5		[67]
	CVD with Mg vapor			$2x10^3$	[151]
	Transport thin film	$6x10^4$	$2x10^5$	10^6	[176]
B_4C	Bulk			$>8x10^5$	[154]
	Bulk			$2x10^4$	[155, 156]
0.5%Ti+1.1%C	Bulk			$2x10^5$	[147]
SiC	Bulk			$>8x10^5$	[156]
	Bulk 4x2.8x0.7 mm^3			$2.4x10^4$	[157]
	Bulk 0.56x2.17x3.73 mm^3	$2.5x10^4$	$9x10^4$		[78]
	Wire	Transport $4.1x10^4$	$8.4x10^4$		[78]
	Tape/Fe	Transport $3x10^4$			[85]
	Tape/Fe	$2x10^4$			[177]
	Tape/Fe	Transport $3x10^4$			[50]
	Tape/Fe	Transport $6x10^4$			[51]
	Strand(1m)	Transport $2x10^5$	$3x10^5$	$4x10^5$	[98]
		J_c at 4T (A/cm^2)	J_c at 2T (A/cm^2)	J_c at 0T (A/cm^2)	
20K					
Graphite	Wire(SS)	Transport 10^3	$8x10^3$	$>10^4$	[171]
Diamond	Bulk 0.7x2.1x2.7 mm^3	$8x10^3$	$7x10^4$	$5x10^5$	[178]
Carbon	Bulk 4x3x0.5 mm^3	$5x10^3$	10^5	$3x10^5$	[174]
	Bulk 2.87x2.70x3.12 mm^3		$2x10^4$	$3x10^5$	[175]
	Bulk	10^4	$7x10^4$		[67]
	CVD with Mg vapor		$5x10^2$	$>10^5$	[151]
	Thin film	$7x10^4$	$2x10^5$	$4x10^6$	[176]
B_4C	Bulk	10^4	10^5	$7x10^5$	[154]
	Bulk	10^4	$8x10^4$	$4x10^4$	[155, 156]

Na2CO3	Bulk	$8x10^3$	$9x10^4$	$5x10^5$	[179]
SiC	Bulk	$6x10^3$	$2x10^5$	$7x10^5$	[154]
	Bulk 0.56x2.17x3.73 mm^3	$5x10^4$	$2x10^5$	$7x10^5$	[78]
	Wire/Fe	Transport $3.2 x10^4$	$>10^5$		[78]

2.7.3 Metal doping

The effects of metals doping in MgB_2 have been reported due to that many metals can form metal borides, having AlB_2 structure. Some metals were found to be partially substituted in the Mg site while some do not substitute into MgB_2 phase and form other impurities with B.

2.7.3.1 Al doping

Although most of the reports on the Al substitution at the Mg site reveal dramatic decrease of J_c [180-182] due to change of carrier density and density of states at the Fermi surface, Berenov et al. have successfully improved the J_c, particularly at lower fields at 20 K, for example at 5 T J_c was enhanced by a factor of 20 for a doping level of 1 at.% Al. The critical temperature (T_c) remained largely unchanged, which may be the effect of low doping levels of Al on the crystal structure and superconducting properties of MgB_2 [183]. On the other hand double doping with Al and Zn or Li show improvement of the J_c compared to the single Al doping but the value is still well below the pure MgB_2 [184].

2.7.3.2 Zn doping

However, measurements by Martínez et al. demonstrated that single Zn doping does not improve, nor deteriorate the field dependence of the superconducting wires and powders [185]. The results indicate that the solubility limit of Zn in the MgB_2 structure is very small and a very small amount of Zn enters the Mg site thus, it does not alter significantly the superconducting properties.

2.7.3.3 Au coating

The effect of a gold coating on MgB_2 thin film has been studied by Choi et al. where they believe that the good thermal conduction of the gold film helps the thermal stability of the MgB_2 thin film [186]. When the thickness of the thin gold film was increased, the suppression of the J_c due to flux jump was drastically reduced and J_c is fully recovered.

2.7.3.4 Cd doping

Similar with the Zn doping, Cd does not occupy the atomic Mg sites in the MgB_2 crystal structure, but merely reacts with Mg and forms $MgCd_3$ phase. It is striking to note that although the nonsuperconducting phase $MgCd_3$ is as high as about 67 vol.% in $Mg_{0.5}Cd_{0.5}B_2$ (nominal composition), the J_c of 5.0 × 105 A/cm^2 (5 K, 0 T) has been achieved. It is suggested that the improvement in J_c in $Mg_{0.5}Cd_{0.5}B_2$ is primarily due to pinning effects induced by $MgCd_3$ and better grain linkage provided by the $MgCd_3$ [187].

2.7.3.5 Ti doping

Several groups have studied the effect of Ti doped into MgB_2 in the form of bulk, wire and tape and all the reports showed positive results [188-198]. Zhao *et al* have observed a 1 nm TiB_2 layer at grain boundaries in *in situ* synthesized MgB_2 bulk material with titanium inclusions [198]. This, they argue, contributes significantly to flux pinning and also prevents coarsening of the MgB_2, producing a grain size of just 20 nm. Similar substantial increases in performance have been reported for Ti inclusions to *in situ* high pressure synthesized MgB_2 bulk material [196]. In the magnetic fields up to 2 T, high-pressure synthesized MgB_2 (with 10% of Ti) at 20 K has a critical current density comparable to that of Nb_3Sn at 4.2 K. Finnemore et al. and Anderson et al. have introduced a new processing method for the doping of magnesium diboride wire by using the chemical vapour deposition (CVD) to produce long lengths of suitably doped starting boron fibre [194, 195]. It was found CVD methods are an effective way to distribute the Ti impurities and can be used to produce conductors with J_c values in the range of 10,000 A/cm^2 at 25 K and 1.3 T. The samples show a fine dispersion of Ti through out the grains and no conspicuous precipitation of TiB_2 on the MgB_2 grain boundaries. This is to be contrasted with the precipitation of TiB_2 on MgB_2 grain boundaries observed for samples prepared by solid state reaction of Ti, Mg, and B powders.

2.7.3.6 Fe doping

Jin et al. have studied the effect of Fe inclusion on T_c and the J_c–H characteristics of MgB_2 [72]. They found that 5 wt% Fe inclusions had no effect on T_c and a negative effect on J_c. However, it had the least negative effect on the J_c–H behaviour of all the

elements that they studied, including Cu, Ag, Y, Ti and Mo. Dou et al. discovered that the $J_c(H)$ performance was severely depressed at above 2% doping level of Fe in the MgB_2 sample [199]. The detrimental effect of nanoscale Fe doping on $J_c(H)$ is attributable to both the Fe substitution for B in the lattice structure and the inclusions of Fe and FeB which act as weak links at grain boundaries.

2.7.3.7 La doping

High density of LaB_6 nanoparticle inclusions were found in MgB_2 grains in the La doping MgB_2 sample as major impurity [200, 201]. In fact, the production of nano-particles LaB_6 impurity phase within the bulk MgB_2 is believed to be responsible for the enhancement of J_c. The optimum result on J_c is obtained for $Mg_{0.97}La_{0.03}B_2$ at 5 K; J_c reaches ~1.4×10^7 A cm^{-2} in self-field, ~2.1×10^6 A cm^{-2} at 1 T, ~2.5×10^5 A cm^{-2} at 2.5 T and ~1.8×10^4 A cm^{-2} at 4.5 T.

2.7.3.8 Zr doping

Similar to Ti doping, the majority of Zr atoms form ZrB_2 phase while a small amount of Zr atoms may be introduced into the lattice of MgB_2 [189, 202-204]. The combination of good grain connection, the reduction of grain size and small ZrB_2 particles in the sample may be responsible for the significant enhancement of J_c in Zr-doped samples

2.7.3.9 Ta doping

Prikhna et al. have observed the positive influence of Ta during high pressure (HP) synthesis of MgB_2 on the critical current density in the fields up to 3 T and irreversible fields of the material [205]. At 20 K HP-synthesized MgB_2 has critical current density

of 68 kA/cm^2 in the 1 T field and of 160 kA/cm^2 in the zero field, its field of irreversibility at 20 K being 5.7.

2.7.3.10 Other metal doping

Tachikawa *et al* explored doping *ex situ* wire in nickel sheaths by different kinds of metal powder like Ag, Cu and Ni and also low melting point metal powders of Sn and In [206, 207]. They have shown that 10 wt% indium inclusion increased J_c values by a factor of 6–7, which was attributed to the improvement of weak inter-grain links that would consist mostly of unsintered MgB_2 powder particles. But this J_c increase is still one order of magnitude lower than that achieved by high temperature annealing which causes the whole MgB_2 core to recrystallize.

Cimberle et al. attempt to introduce defects in the MgB_2 structure by different chemical treatments like substitution of lithium on the magnesium site and doping of the precursor boron powders with Si [181]. J_c always increased in doped or substituted samples (up to a factor 3) and this fact is meaningful, in particular in the light of the small level of substitution. The best result in terms of J_c is achieved by Si doping that, moreover, does not significantly decrease the transition temperature. However, neutron diffraction and Rietveld analysis showed no evidence of Si doping into the lattice in the Si doped MgB_2 samples [208]. Nano-particle inclusions, such as Mg_2Si, precipitates of MgO, unreacted nano particles observed using TEM are proposed to be responsible for the enhancement of flux pinning in high fields.

A wide variety of metal powders, including Nb, Hf and W have all been used at the 10 wt% in the *ex situ* wires by Kovac's et al. [202]. Transport current measurements have shown that metal particle inclusion leads to an especially significant improvement in current carrying capacity. The presence of normal particles influences both the resistivity and also the thermal conductivity of the MgB_2 core, and the improved internal stability may be responsible for the increased critical current values. Goto et al. have proved that J_c values were also improved to $4.8x10^5$ A/cm^2 with 1% Hf doping [188]. On the other hand, the value of MgB_2 tapes was increased from 1500 A/cm^2 to 4500 A/cm^2 at 4.2 K and 5 T with Cu inclusion [209].

2.7.4 Oxide and other compound Doping

2.7.4.1 Al_2O_3 doping

Delfany et al. have reported that J_c values decrease by more than one order of magnitude in the AlO_2 doped MgB_2 whereby the amount of MgO was found to increase with increasing Al_2O_3 level [210]. However, smaller decrease of J_c is observed by Rui's group when they used a nano alumina dopant [211]. It is believed that the nanocomposite superconductor consists of MgB_2 grains with nano-alumina (10–50 nm) inside the grains and at grain boundaries could be strong pinning centers, unlike in the case of doping with the coarse alumina.

2.7.4.2 Bi-2212 doping

Shen et al. [212] found that J_c of bulk polycrystalline MgB_2 is significantly enhanced by the Bi-2212 inclusion. Microstructural analysis indicates that a small amount of Bi-2212

is decomposed into Cu_2O and other impurity phases while a significant amount of not decomposed Bi-2212 particles remains in MgB_2 matrix, and these act as effective pinning centres for vortices. The enhanced pinning force is mainly attributable to these highly dispersed inclusions inserted in the MgB_2 grains.

2.7.4.3 Fe_2O_3 doping

Prozorov et al. have performed a study on magnesium diboride slurries with magnetic Fe_2O_3 nanoparticles. By using ultrasonic method, considerable enhancement of magnetic hysteresis of such MgB_2 was observed, which implies an increase of vortex pinning strength due to embedded magnetic nanoparticles [213].

2.7.4.4 MgO doping

Besides the main phase of MgB_2, MgO is always present as the major impurity phase in MgB_2 superconductor. It was shown that an MgO layer on the surface of MgB_2 grains would cause a strong depression of I_c [73]. However, Kovac et al. have concluded that by controlling the amount of MgO, pinning in *ex situ* MgB_2 wires can be increased. The level of MgO should be optimized as a compromise between inter-grain connectivity and introducing pinning centres in ex-situ MgB_2 wire [214]. It was found that light doping of nano-MgO (62.5 wt.%) could increase the J_c property of MgB_2 tapes through enhancing the grain connectivity and core density. A 50% enhancement in J_c (10 T, 4.2 K) was obtained when adding 1.25 wt % of nano-MgO into MgB_2 [215]. In the mean time, Perner et al. discovered that doping with MgO improves J_c (i.e. 1.6 $x10^6$ A cm^{-2} at 7.5 K in self field), which is more effective than doping with SiO_2 [65, 216].

2.7.4.5 Silicides doping

Both Ma et al. and Matsumoto et al. obtained J_c enhancement for silicide impurities like WSi_2, $ZrSi_2$, Mg_2Si, and SiC, except for SiO_2 [217-219]. Among these additives, the best result in terms of J_c was achieved for $ZrSi_2$ doping, by up to a factor of 3.4 at 4.2 K in magnetic fields up to 12 T. Scanning electron microscopy investigation revealed that the WSi_2 and $ZrSi_2$, doping enhanced intergranular connectivity, thus the critical temperature for the doped tapes decreased slightly less than 0.7 K. Under the EDX, small precipitates and homogenous segregation of each elements were observed in the SiC doped MgB_2 which explained why SiC doped MgB_2 is much better than other silicides impurities [218].

2.7.4.6 SiO_2 doping

Microstructural analysis reveals that a high density of $MgSi_2$ nanoparticles (10–50 nm) exists inside the SiO_2 nanoparticles added MgB_2 grains, leading to the formation of a nanocomposite superconductor [220]. The lattice constant in the *c* direction increases with additive content due to a small amount of Si being doped into the lattice of the MgB_2. The inclusion of SiO_2 nanoparticles also improves the J_c–H and H_{irr}–T characteristics of MgB_2 when the additive content is lower than 7%. However, the degradation of J_c values was obtained by using MgH_2 as a precursor instead of Mg in SiO_2 doping [85]. It was speculated that the H_2 released from the decomposition of MgH_2 deoxidizes SiO_2 to form H_2O and this H_2O degrades the MgB_2 core.

2.7.4.7 Nb_xB_2 doping

The crystal structure of Nb_xB_2 is similar as MgB_2 in both AlB_2-type structure and in values of the lattice parameters [221]. So, utilizing Nb_xB_2 as the additive for strong

pinning centre for theMgB_2 tape is expected to have some advantages with respect to matching the MgB_2 grains, densification of the tape core and alignment of the grains. The best $J_c(H)$ value was more than 1000 A/cm^2 for 5 mol % of Nb_xB_2 at 4.2 K and 12T.

2.7.4.8 Mg_2Cu doping

Kikuchi's group have studied the Mg_2Cu (568^{o}C) doping that has a lower melting point than a pure MgB_2 (600^{o}C), thus promoting a diffusion reaction for synthesizing MgB_2 through their liquid states [223]. Both J_c and H_{irr} at 4.2 K improve with decreasing the size of Mg_2Cu powders as a starting material. 10^4 Acm $^{-2}$ was obtained at 4.2 K and 4 T for the Fe-sheathed MgB_2 wire made by using Mg_2Cu powder with a diameter of a few microns. These improvements may be due to the enhancement of homogeneity of the powder mixture with small $MgCu_2$ particles with a size of about 10 nm, which were dispersed in the MgB_2 matrix.

2.7.4.9 O_2 doping

Haruta et al. has showed that effective pinning centres can be introduced by the deposition of the MgB_2 thin film in an O_2 atmosphere [224]. The values of J_c of the O_2-doped film have exceeded those of the non-doped film in magnetic fields applied perpendicular and also parallel to the *c*-axis. The peak of J_c caused by the *c*-axis correlated pinning centres has been observed in the angular dependence of J_c. It is found that B_{c2} increased by the introduction of O_2 in both the directions of the applied field. For example at 15T, both B_{c2}, (B$\perp$c) and (B//c), of O_2-doepd film were enhanced by a factor of 1.1 compared to the pure MgB_2 thin film at 15.5 K and 13 K respectively.

2.7.4.10 TiO_2 doping

Xu et al. have achieved an increase of H_{irr} and J_c performance of TiO_2 doping [225]. The H_{irr} at 20 K increases from 4.3 to 4.9 T as the TiO_2 content increases from 0 to 10 wt%, and the J_c increases from 450 to 4250 A/cm^2 at 4.2 T. Besides TiO_2, the Mg-deficiency and existence of MgO are suggested to be an important factor in increasing the H_{irr} and J_c.

2.7.4.11 ZrB_2 doping

According to Bhatia et al. an increase in H_{c2} from 20.5 T to 28.6 T and enhancement of H_{irr} from 16 T to 24 T were observed in the ZrB_2 doped sample as compared to the pure MgB_2 sample at 4.2 K [226]. In addition, the critical field increases similarly as for SiC doped MgB_2 at 4.2 K.

2.7.4.12 ZrO_2 doping

The *in situ* and *ex situ* ZrO_2 doped MgB_2 was studied by Chen et al. in order to understand the contamination effect by mechanical alloying [227]. Short milling ZrO_2 and MgB_2 powders (> 4 hours) results in no new phases, while 400 h milled powder was partially amorphized and showed the formation of a minority ZrB_2 phase. The results of the magnetic measurement shows that J_{c} of MgB_2 is deteriorated by *in situ* ZrO_2 inclusion while *ex situ* ZrO_2 inclusion with annealing did not degrade the T_{c} of MgB_2. However, there is no report on the J_c of the *ex situ* ZrO_2 inclusions doped MgB_2.

2.7.4.13 ZrH_2 doping

Xu et al. used ZrH_2 as another form of Zr for doping effect in the MgB_2 as ZrH_2 decomposes to Zr and H_2 at high temperature [228]. Some J_c values of the undoped wires are higher than those of the doped samples, due to the microstructure caused by the ZrH_2 doping and the processing temperature. J_c values of all the doped MgB_2 wires decrease with the increase of processing temperature, but the optimum doping ratio goes up correspondingly.

2.7.4.14 WB doping

The effect of WB inclusion on the microstructure and superconducting properties of MgB_2 tapes has been investigated by Fuji et al. [229]. The microstructure was not influenced appreciably by the inclusion, whereas the superconducting properties changed. However, the transport critical current density at 4.2 K increased about twice by the 5 mol% inclusion and reached 15 and 5 kA cm^{-2} at 8 and 10 T, respectively, suggesting that pinning centres effective in a high-field region were introduced.

2.7.4.15 Y_2O_3 doping

Wang et al. doped MgB_2 with 5, 10, and 15 wt% Y_2O_3 nanoparticles, using a simple solid-state reaction route [79]. Transmission electron microscopy showed a fine nanostructure consisting of 3–5 nm YB_4 nanoparticles embedded within MgB_2 grains of 400 nm size. Compared to an undoped control sample, an improvement in the in-field critical current density J_c was observed in the 10% doping sample with a value of 2 x 10^5 Acm^{-2} at 4.2 K and 2T

2.7.4.16 Dy_2O_3 doping

Recently, Chen et al. studied the rare earth oxide, Dy_2O_3 nano particles by in-situ method [230]. They found that the T_c remained largely unchanged, as J_c was enhanced by a factor of 4, as compared to the pure sample at 20K and 1T.

Table 2.3 Comparison of magnetic and transport $J_c(H)$ at 4.2/5K and 20K for other sources of inclusion doping . All the $J_c(H)$ were determined by the magnetization unless stated.

Dopant	Type	J_c at 8T (A/cm^2)	J_c at 6T (A/cm^2)	J_c at 2T (A/cm2)	Reference
4.2/5K					
Al	Bulk		$2x10^3$	$2x10^4$	[180]
	Bulk 2x2x3 mm^3			$1x10^4$	[181]
	Bulk	$7x10^2$	$1.5x10^5$		[182]
Al_2O_3	Bulk 0.5×1.7×2.9mm^3			$4x10^3$	[210]
Au	Thin film			$4x10^5$	[186]
BN	Wire(ex-situ)	transport	$5x10^2$		[202]
Cd	Bulk			$2x10^5$	[187]
Cu	Tape(insitu) magnetic	$5x10^2$	$5x10^3$		[209]
Dy_2O_3	Bulk			$2.9\ x10^5$	[230]
Fe	Bulk			$2x10^5$	[199]
Hf	Wire(ex-situ)	Transport 10^3	$8x10^3$		[202]
In	Wire(ex-situ)	transport		$2x10^4$	[206,207]
La	bulk			$2x10^5$	[200]
Li	Bulk 2x2x3 mm^3			$7x10^3$	[181]
MgO	Wire(insitu-Fe sheath)	transport		$3x10^5$	[215]
MgSi	Insitu Tape	transport $0.5x10^4$	$4x10^4$		[217]
Na	Bulk	$7x10^3$	$2x10^5$		[182]
Nb	Wire(ex-situ)	transport $8x10^2$	$6x10^3$		[202]
N_xB_2	In-situ Tape	transport $1.5x10^4$	$5x10^4$		[222]
Nb_2O_5	Wire(ex-situ)	transport $6x10^2$	$5x10^3$		[202]
Si	Bulk 2x2x3 mm^3			$1.5x10^4$	[181]
SiO	Insitu Tape	transport $4x10^3$	10^4		[218, 85]
Sn	Wire(ex-situ)	transport		$1x10^4$	[206, 207]
Ti	Bulk		$2x10^4$	$6x10^5$	[189, 191]
	Bulk		$4x10^3$		[193]
	Chemical Vapor			$2x10^6$	[194, 195]

	Deposition(CVD) conductor				
TiO_2	Wire(ex-situ)	transport 6x10	$6x10^2$		[202]
	Bulk 1.35x2.83x 4.45 mm^3			$8x10^5$	[225]
W	Wire(ex-situ)	transport 10^3	$6x10^3$		[202]
WB	Wire(insitu)	transport $2x10^4$	$7x10^4$	$7x10^5$	[229]
WSi_2	In-situ Tape	transport $8x10^3$	$2x10^4$		[217-219]
Y_2O_3	Bulk	$2x10^3$	10^4	$2x10^5$	[79]
Zn	Bulk	$2x10^4$	$2.5x10^5$		[182]
Zn	Wire magnetic			10^4	[185]
Zr	Bulk		$2x10^3$	$2x10^5$	[189]
	Bulk 0.7x0.9x1.4 mm^3		10^4	$8x10^5$	[203]
	Wire(ex-situ)	$6x10^2$	$5x10^3$		[202]
ZrB_2	In-situ Tape	transport $8x10^3$	$2x10^4$		[217]
$ZrSi_2$	In-situ Tape	transport $8x10^3$	$2x10^4$		[217-219]
		J_c at 4T (A/cm^2)	J_c at 2T (A/cm^2)	J_c at 0T (A/cm^2)	
20K					
Al	Bulk	8x10	$7x10^3$	$7x10^4$	[180]
			$2x10^5$	$4x10^5$	[183]
Li and Al	Bulk		$7.8x10^4$	10^6	[184]
Zn and Al	Bulk		$7x10^5$	$2x10^6$	[184]
Al_2O_3	Bulk 20x10x2mm^3		$2x10^2$	10^5	[211]
	Bulk 0.5×1.7×2.9mm^3		$2x10^2$	$4x10^4$	[210]
Bi-2212	Bulk 1.4 × 1.5 ×3.0 mm^3		$5x10^4$	10^6	[212]
Cd	Bulk	10^2	10^4	$2x10^5$	[187]
Dy_2O_3					[230]
Fe	bulk		$4x10^4$	$4x10^5$	[199]
Hf	bulk	$7x10^2$	$3x10^4$	$3x10^5$	[188]
La	bulk		$2x10^3$	10^5	[200]
MgO	Wire(in situ-Fe sheath)	transport $4x10^3$	$8x10^4$	$3x10^5$	[215]
O	Thin film (B⊥c)	$5x10^4$	10^5		[224]
Si	Bulk 0.56x2.7 x 3.73 mm^3	$2x10^4$	$2x10^5$	$9x10^5$	[208]
SiO	Bulk (0.21x0.21x 0.21 mm^3)	$2x10^3$	10^5	$7x10^5$	[220]
Ta	bulk	10^3	$4x10^4$	$1.5x10^5$	[209]
Ti	bulk	10	10^5	10^6	[189, 191]

	In-situ Ta/Cu tape magnetic			$9x10^5$	[190, 192]
	Bulk	$6x10^2$	$3x10^4$	$3x10^5$	[188]
	Bulk	10^4	$2x10^5$	$5x10^5$	[193]
	Bulk	$3x10^4$	$2x10^5$	$5x10^5$	[196]
	Bulk	$4x10^4$	$2x10^5$	$4x10^5$	[197]
TiO	Bulk 1.35x2.83x 4.45 mm^3	$6x10^3$	$2x10^5$		[224]
Y_2O_3	Bulk	10^4	10^5	$3.5x10^5$	[79]
Zr	Bulk	10	$5x10^4$	$8x10^5$	[189]
	Bulk 0.7x0.9x1.4 mm^3	$2x10^2$	10^5	$7x10^6$	[203, 204]
	Bulk	$2x10^3$	$3x10^4$	$3x10^5$	[188]
ZrB_2	Bulk			$3x10^5$	[226]

2.8 Practical Applications and challenges of MgB_2

In the past three years, rapid R&D progress of MgB_2 towards its development as a technical conductor has reached remarkable milestones. With the knowledge of the basic properties of the MgB_2 like the H_{c2}, H_{irr}, two-gap superconductivity, flux-pinning mechanism and weak link free grain, the problems of fabricating MgB_2 conductors commercially are being addressed by Hyper Tech Research in Columbus, Ohio [231-233], Columbus Superconductors based in Genova, Italy [234], Japan based Hitachi which has collaborated with National Institute of Material Science (NIMS), Japan [218], Diboride Conductors in Cambridge and many other laboratories worldwide. All these groups have emerged to exploit MgB_2 in applications ranging from fault current limiters for electrical power transmission systems to low field magnetic resonance imaging (MRI). Besides that, it is believed that MgB_2 will eventually find its way into generators and motors in ships and marine systems, as such superconducting components would be smaller and lighter than conventional conductor version. Because the promised HTS superconductors such as, $YBa_2Cu_3O_7$ coated conductor are still in a very infant stage of scaling up and also suffer from low engineering critical

current density, J_{ceng}, this opens up a possibility of MgB_2 to compete with the well established Nb-based low temperature superconductors, LTS, such as NbTi and Nb_3Sn that represent 99.99% of world production of superconducting materials. The prospects for an operation of MgB_2 around 20-25K and fields up to 5T in the cryocooler cooled magnet (~20K) (MRI with field 2-5T), high field magnet (~4.2K), liquid hydrogen cooled electrical transmission system and superconducting magnetic-energy storage, SMES, will give a very competitive challenge to the LTS. The demonstration of coils with magnetic field exceeding 1 T at 25K under self-field and 4K under 1.25 T has demonstrated the advanced MgB_2 competitiveness with LTS for superconducting transformer and low field MRI [235, 236]. Figure 2.14 shows the critical current density of MgB_2 in comparison to other commercial superconductor materials. One can note that the value of J_c for the SiC doped MgB_2 stands very strongly at 20K and low fields and it is comparable to the value of J_c for Nb-Ti at 4.2K, which is very useful for application of MRI.

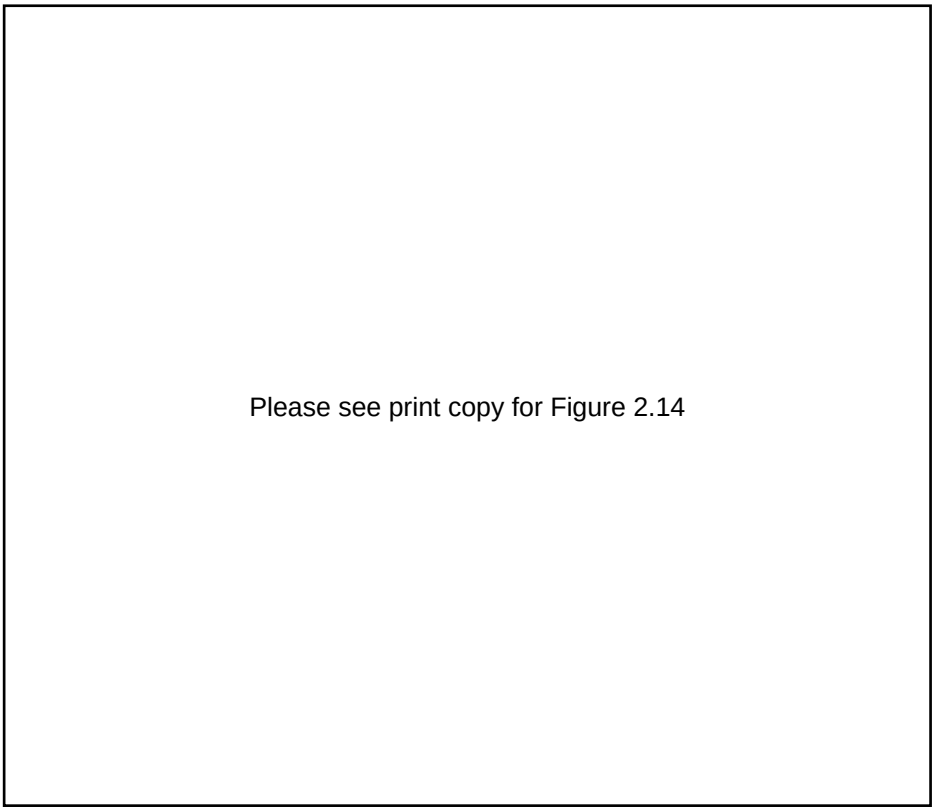

Figure 2.14 Comparison of J_c of MgB_2 with other commercial superconducting wire [237]. All results were measured at 4.2 K unless labelled otherwise.

On the economic side, dramatic savings could be achieved if the superconductors can be put to practical use. Advantage of MgB_2 is that the raw material costs of both B and Mg are low; reasonable estimates suggest that even for appropriately purified material, they will be several times less than those of Nb-based superconductors. And instead of requiring a silver cladding, like Bi2223/Ag, MgB_2 works just fine with a sheath of cheap metal, such as iron. Even though low-temperature superconductors, such as niobium-titanium (NbTi), cost only $1 kA/m to produce, they must be cooled to 4 K with expensive liquid helium. Operating at 77 K, HTS wire allows the use of cheap liquid nitrogen to cool the material to its operating temperature. However, the first generation of HTS wires cost around US$200 per kA/m although large-scale

manufacturing might drive the cost down to US$50 per kA/m. MgB_2 becomes superconducting below 39 K and it will operate at temperatures between 20 and 30 K. In fact, 20 K is good news for many applications, because it allows the use of inexpensive cryocoolers, a type of hassle free refrigerators that can be plugged into the wall power socket. After factoring in all the costs for wire, the cooling equipment and electrical losses MgB_2 wire will eventually be better than HTS and standard copper wire as in figure 2.15 [238]. Predictions that the annual market for HTS-based wire and machinery will approach $2 billion by 2025 suggest that there's plenty of room for sales of MgB_2. According to Hyper Tech Research, they will drive down the prices to around US$ 5 to 7/kA/m at 20K in a 2T field, with a 200A of current by 2009. If successful, this price will match the US$ 13/kAm price tag on the copper wire used in electric motors.

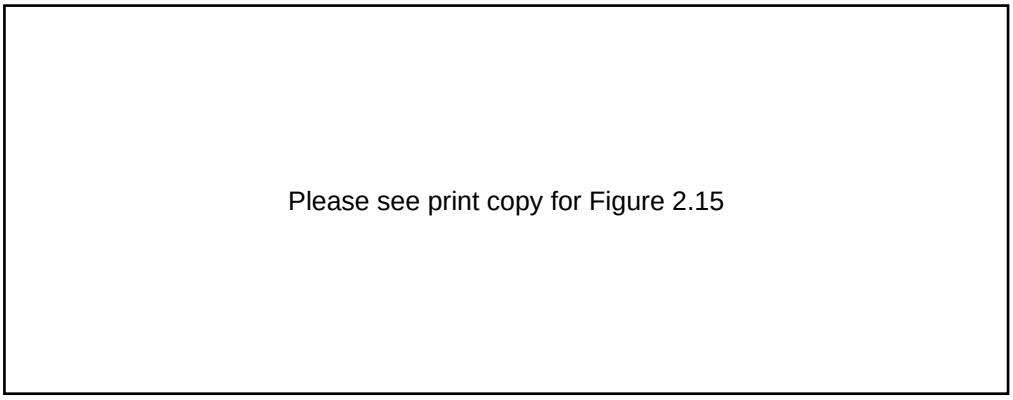

Figure 2.15 MgB_2 wire cost less than those based on copper or high-temperature superconductors [238].

Despite all the optimistic prospects, many problems have yet to be tackled in the development of MgB_2 conductors. Iron can be used as a protective layer between MgB_2 and a stabilizing outer copper layer while providing the magnetic shield of the filaments

as well. However, Fe barrier provides a poor thermal stability to MgB_2 due to the electrical resistivity, and does not have the same flow stress as the high-purity Cu or Ag needed for electrical stabilization. This leads to drawing instabilities, and wire failure. The mechanical reinforcement of conductor is important to withstand handling during coil winding, thermal stress and Lorentz forces in magnetic field. Study on E(I) transition are commonly described by means of a power law equation, $V=I^n$ which defines a characteristic exponent, the so called n-value. In fact, n-value of a superconducting wire or tape has to exceed the value of 30 to be used for magnets in persistent mode [237, 240].

Although high n values above 100 were observed for MgB_2 conductors at low fields [114, 241-245], variety of fundamentals properties that influenced the n values like sheath materials, filament size and geometry still need to be addressed. Poor thermal stabilization of high current-carrying MgB_2 wires and tapes leads to burn-out even for currents below the true I_c. In AC-applications, superconductor exhibits AC-losses, which should be minimized since they translate into cooling costs during normal operation. Besides that, the design of the conductor composites and the choice of sheath materials have to meet several important technical conductor specifications which cannot be fulfilled in the single sheath core material. As a result, development of high quality multi filament wire geometries is now becoming important for reasons of strain tolerance, flux jump stability, transport current stability and AC loss reduction.

2.9 References

[1] T. Muranaka, Y. Zenitani, J. Shimoyama and J. Akimitsu, Superconductivity in MgB_2 Frontier in Superconducting Materials, 2005 Springer-Verlag Berlin Heidelberg.

[2] C. Buzea and T. Yamashita, *Supercond. Sci. Technol*. **14**, R115 (2001).

[3] M. I. Eremets, V.V. Struzhkin, H. K. Mao and R. J. Hemley, *Science* **293**, 272 (2001).

[4] L. Leyarovska and E. Leyarovski, *J. Less Common Met*. **67,** 249 (1979).

[5] A. S. Copper, E. Corenzwit, L. D. Longinotti, B. T. Matthias and W. H. Zachariasen, *Proc. Natl. Acad. Sci.* U.S.A. **67**, 313 (1970).

[6] K A. Yamamoto, C. Takao, T. Masui, M. Izumi and S. Tajima, *Physica C* **383**, 197 (2002).

[7] D. P. Young, R. G. Goodrich, P. W. Adams, Julia Y. Chan, Frank R. Fronczek, F. Drymiotis, L. L. Henry, *Phys. Rev*. B **65**, 180518(R) (2002).

[8] V. A. Gasparov, N. S. Sidorov, I. I. Zver'kova, and M. P. Kulakov, *JETP Letters* **73**, 532-535 (2001).

[9] D. Kaczorowski, A. J. Zaleski, O. J. Zogal, J. Klamut, *Preprint cond-mat/0103571* (2001).

[10] L. H. He, L, G. Q. Hu, P. L. Zhang, Q. W. Yan, *Chin. Phys*. **10**, 343 (2001).

[11] G. Y. Sung, S. H. Kim, J. H. Kim, D. C. Yoo, J. W. Lee, J. Y. Lee, C. U. Jung, M. S. Park, W. N. Kang, Z. L. Du and S. I. Lee, *Supercond. Sci. Tech.* **14**, 880 (2001).

[12] S. Margadonna, T. Muranaka, K. Prassides, I. Maurin, K. Brigatti, R. M. Ibberson, M. Arai, M. Takata, J. Akimitsu, *J. Phys-:Condens. Matter*. **13** L795-L802 (2001).

[13] R. C. Yu, S. C. Li, Y. Q. Wang, X. Kong, J. L. Zhu, F. Y. Li, Z. X. Liu, X. F. Duan, Z. Zhang and C. Q. Jin, *Physica C* **363**, 184 (2001).

[14] D. Larbalestier, A. Gurevich, D. Matthew Feldmann and A. Polyanskii, *Nature* **414**, 368 (2001).

[15] I. I. Tupitsyn *Sov. Phys. Solid State* **18** 1688 (1976).

[16] D. R. Armstrong and P. G. Perkins, *J. of the Chem. Soc., Faraday Transactions 2* **75**, 12 (1979).

[17] N. I. Medvedeva, A. L. Ivanovskii, J. E. Medvedeva and A. J. Freeman, *Phys. Rev. B* **64**, 020502 (2001).

[18] A. I. Ivanovskii and N. I. Medvedeva, *Russ. J. Inorg. Chem*. **45** 1234 (2000)

[19] J. Kortus, I. I. Mazin, K. D. Belashchenko, V. P. Antropov, and L. L. Boyer, *Phys. Rev. Lett*. **86**, 4656–4659 (2001).

[20] J. M. An and W. E. Pickett, *Phys. Rev. Lett*. **86**, 4366-4369 (2001).

[21] G. Satta, G. Profeta, F. Bernardini, A. Continenza, and S. Massidda, *Phys. Rev. B* **64**, 104507 (2001).

[22] K. D. Belashchenko, M. V. Schilfgaarde, and V. P. Antropov, *Phys. Rev. B* **64**, 092503 (2001).

[23] P. C. Canfield and G. W. Grabtree, *Physics Today* **56**, 34 (2003).

[24] H. Suhl, B. T. Matthias, and L. R. Walker, *Phys. Rev. Lett*. **3**, 552 (1959).

[25] L. Y. L. Shen, N. M. Senozan, and N. E. Phillips, *Phys. Rev. Lett*. **14**, 1025 (1965).

[26] R. Radebaugh and P. H. Keesom, *Phys. Rev*., **149**, 209 (1996).

[27] G. Binnig, A. Baratoff, H. E. Hoenig, and J. G. Bednorz, *Phys. Rev. Lett*. **45**, 1352 (1980).

[28] S. V. Shulga, S. L. Drechsler, G. Fuchs, K. H. Müller, K. Winzer, M. Heinecke, and K. Krug, *Phys. Rev. Lett*. **80**, 1730 (1998).

[29] A. Gurevich, *Phys. Rev. B* **67**, 184515 (2003).

[30] V. Braccini, A. Gurevich, J. E. Giencke, M. C. Jewell, C. B. Eom, D. C. Larbalestier, A. Pogrebnyakov, Y. Cui, B. T. Liu, Y. F. Hu, J. M. Redwing, Q. Li, X. X. Xi, R. K. Singh, R. Gandikota, J. Kim, B. Wilkens, N. Newman, J. Rowell, B. Moeckly, V. Ferrando, C. Tarantini, D. Marré, M. Putti, C. Ferdeghini, R. Vaglio, E. Haanappel, *Phys. Rev.B* **71**, 012504-1 (2005).

[31] R. S. Gonnelli, D. Daghero, A. Calzolari, G. A. Ummarino, V. Dellarocca, V. A. Stepanov, S. M. Kazakov, N. Zhigadlo, J. Karpinski, *Phys. Rev.B* **71**, 060503-1 (2004).

[32] R. S. Gonnelli, D. Daghero, G.A. Ummarino, A. Calzolari, V. Dellarocca, V. A. Stepanov, S.M. Kazakov, J. Jun, J. Karpinski, Prepint Cond-matt 0407267

[33] E. Ohmichi, T. Masui, S. Lee, S. Tajima and T. Osada, *J. Phys. Soc. of Jap*. **73**, 2065 (2004).

[34] A. Y. Liu, I. I. Mazin, and J. Kortus, *Phys. Rev. Lett*. **87**, 087005 (2001).

[35] D. G. Hinks, H. Claus and J. D. Jorgensen, *Nature* **411**, 457(2001).

[36] S. L. Bud'ko, G. Lapertot, C. Petrovic, C. E. Cunningham, N. Anderson and P. C. Canfield, *Phys. Rev. Lett.* **86** 1877 (2001).

[37] P. C. Canfield, S. L. Bud'ko, D. K. Finnemore, *Physica C* **385** 1 (2003)

[38] S. L. Bud'ko, V. G. Kogan and P. C. Canfield, *Preprint* cond-mat/0106577(2001)

[39] S. Lee, H. Mori, T. Masui, Y. Eltsev , A. Yamamoto and S. Tajima, *J. Phys. Soc. Jpn*. **70**, 2255 (2001).

[40] M. Xu, H. Kitazawa, Y. Takano, J. Ye, K. Nishida, H. Abe, A. Matsushita and G. Kido, *Appl. Phys. Lett.* **79**, 2779 (2001).

[41] C. Panagopoulos, B. D. Rainford, T. Xiang, C. A. Scott, M. Kambara and I. H. Inoue, *Phys. Rev.* B **64**, 094514 (2001).

[42] A. V. Pronin, A. Pimenov, A. Loidl and S. I. Krasnosvobodtsev, *Phys. Rev. Lett*. **87**, 097003 (2001)

[43] N. Klein, B. B. Jin, J. Schubert, M. Schuster, H. R. Yi, A. Pimenov, A. Loidl and S. I. Krasnosvobodtsev, *Preprint* cond-mat/0107259 (2001)

[44] R. Jin, M. Paranthaman, H. Y. Zhai, H. M. Christen, D. K. Christen and D. Mandrus, *Phys. Rev. B* **64**, 220506 (2001).

[45] F. Marsiglio, *Phys. Rev. Lett*. **87**, 247001 (2001).

[46] J. E. Hirsch, *Phys. Lett. A* **282**, 392 (2001).

[47] J. E. Hirsch and F. Marsiglio, *Phys. Rev. B* **64**, 144523 (2001).

[48] T. B. Massalski 1990 Binary Alloy Phase Diagrams. 2nd ed (Materials Park, OH: ASM International).

[49] A. Yamamoto, J. I. Shimoyama, S. Ueda, Y. Katsura, S. Horii, K. Kishio, *Supercond. Sci. Tech*. **18**, 116 (2005).

[50] H. Kumakura, H. Kitaguchi, A. Matsumoto, H. Hatakeyama, *Appl. Phys. Lett*. **84**, 3669 (2004).

[51] H. Yamada, M. Hirakawa, H. Kumakura, A. Matsumoto, H. Kitaguchi, *Appl. Phys. Lett*. **84**, 1728 (2004).

[52] S. K. Chen, Z. Lockman, M. Wei, B. A. Glowacki, and J. L. MacManus-Driscolla, *Appl. Phys. Lett*. **86**, 242501 (2005).

[53] N. A. Frederick, S. Li, M. B. Maple, V. F. Nesterenko, and S. S. Indrakanti, *Physica C* **363**, 1, (2001).

[54] S. S. Indrakanti, V. F. Nesterenko, M. B. Maple, N. A. Frederick, W. M. Yuhasz, and S. Li, *Philos. Mag. Lett*. **81**, 849-857 (2001).

[55] A. Serquis, X. Z. Liao, Y. T. Zhu, J. Y. Coulter, J. Y. Huang, J. O. Willis, D. E. Peterson, F. M. Mueller, N. O. Moreno, J. D. Thompson, V. F. Nesterenko and S. S. Indrakanti, *J. Appl. Phys*. **92**, 351 (2002).

[56] A. Serquis, L. Civale, D. L. Hammon, X. Z. Liao, J. Y. Coulter, Y. T. Zhu, M. Jaime, D. E. Peterson, F. M. Mueller, V. F. Nesterenko and Y. Gu, *Appl. Phys. Lett*. **82**, 2847 (2003).

[57] L. Schultz and J. Eckert, in *Glassy Metals III, Topics in Applied Physics*, edited by H. Beck and H. J. Günterodt (Springer, Berlin 1994), Vol. **72**, p. 69.

[58] A. Gűmbel, J. Eckert, G. Fuchs, K. Nenkov, K. H. Műller and L. Schultz, *Appl. Phys. Lett*. **80**, 2725 (2002).

[59] A. Gűmbel, O. Perner, J. Eckert, G. Fuchs, K. Nenkov, K. H. Műller and L. Schultz, *IEEE Trans. Appl. Supercond*. **13**, 3064 (2003).

[60] J. Eckert, O. Perner, G. Fuchs, K. Nenkov, K. H. Műller, W. Häßler, C. Fischer, B. Holzapfel and L. Schultz, *Advances in Solid State Physics*, ed. by B Kramer (Berlin: Springer 2003) Vol. 43 p. 703.

[61] H. Abe, M. Naito, K. Nogi, M. Matsuda, M. Miyake, S. Ohara, A. Kondo and T. Fukui, *Physica C* **391**, 211 (2003).

[62] S. K. Chen, B. A. Glowacki, J. L. MacManus-Driscoll, M. Majoros, M. Vickers and S. H. Pawar EUCAS 2003 (Poster presentation) (2003).

[63] W. Hassler, C. Rodig, C. Fischer, B. Holzapfel, O. Perner, J. Eckert, K. Nenkov and G. Fuchs, *Supercond. Sci. Technol*. **16**, 281 (2003).

[64] C. Fischer, C. Rodig, W. Hassler, O. Perner, J. Eckert, K. Nenkov, G. Fuchs, H. Wendrock, B. Holzapfel and L. Schultz, *Appl. Phys. Lett*. **83**, 1803 (2003).

[65] O. Perner, W. Hassler, C. Fischer, G. Fuchs, B. Holzapfel, L. Schultz, and J. Eckert, *IEEE Trans. Appl. Supercond* **15**, 3192 (2005).

[66] Y. D. Gao, J. Ding, G. V. S. Rao, B. V. R. Chowdari, W. X. Sun and Z. X. Shen, *Phys. Status Solid A* **191**, 548(2002).

[67] B. J. Senkowicz, J. E. Giencke, S. Patnaik, C. B. Eom, E. E. Hellstrom, and D. C. Larbalestier, *Appl. Phys. Lett*. **86**, 202502 (2005).

[68] M. Kambara, N. H. Babu, E. S. Sadki, J. R. Cooper, H. Minami, D. A. Cardwell, A. M. Campbell, I. H. Inoue, *Supercond. Sci. Technol*. **14**, L5 (2001).

[69] Y. Takano, H. Takeya, H. Fujii, H. Kumakura, T. Hatano, K. Togano, *Appl. Phys. Lett*. **78**, 2914 (2001).

[70] M. Dhalle, P. Toulemonde, C. Beneduce, N. Musolino, M. Decroux, R. Flukiger, *Physica C* **363**, 155 (2001).

[71] B. A. Glowacki, M. Majoros, M. Vikers, J. E. Evetts, Y. Shi and I. Mcdougall, *Supercond. Sci. Technol.* **14**, 193 (2001).

[72] S. Jin, H. Mavoori, C. Bower and R. B. van Dover *Nature* **411**, 563, (2001).

[73] S. Soltanian, X. L. Wang, I. Kusevic, E. Babic, A. H. Li, H. K. Liu, E.W. Collings, and S. X. Dou, *Physica C* **361**, 84, (2001).

[74] G. Grasso, A. Malagoni, C. Ferdeghini, S. Roncallo, V. Braccini, M. R. Cimberle, and A. S. Siri, *Appl. Phys. Lett.* **79**, 230 (2001).

[75] H. Kumakura, A. Matsumoto, H. Fujii, and K. Togano, *Appl. Phys. Lett.*, **79**, 2435 (2001).

[76] A. Matsumoto, H. Hatakeyama, H. Kitaguchi, H. Fujii, K. Togano, and K. Kumakura, *Physica C*, **382**, 207 (2002).

[77] H. L. Suo, C. Beneduce, M. Dhalle, N. Musolino, J. Y. Genoud, and R. Flukiger, *Appl. Phys. Lett*. **79**, 3116 (2001).

[78] S. X. Dou, S. Soltanian, J. Horvat, X. L. Wang, S. H. Zhou, M. Ionescu, H. K. Liu, P. Munroe, M. Tomsic, *Appl. Phys. Lett*. **81**, 3419 (2002).

[79] J. Wang, Y. Bugoslavsky, A. Berenov, L. Cowey, A.D. Caplin, L.F. Cohen, J.L. MacManus-Driscoll, L.D. Cooley, X. Song and D.C. Larbalestier, *Appl. Phys. Lett*. **81**, 2026 (2002).

[80] S. X. Dou, A.V. Pan, S. Zhou, M. Ionescu, H.K. Liu, P.R. Munroe, *Supercond. Sci. Technol*. **15**, 1587 (2002).

[81] K. Tanaka, H. Kitaguchi, H. Kumakura, M. Hirakawa, H. Yamada and M. Okada, *IEEE Trans. Appl. Supercond.* **15**, 3180 (2005)

[82] G. Grasso *et al. 17th Int. Symp. on Superconductivity (Niigata, 2004)*

[83] A. Serquis, L. Civale, D. L. Hammon, J. Y. Coulter, X. Z. Liao, Y. T. Zhu, D. E. Peterson and F. M. Mueller, *Appl. Phys. Lett*. **82**, 1754-1756 (2003)

[84] K. J. Song, N. J. Lee, H. M. Jang, H. S. Ha, D. W. Ha, S. S. Oh, M. H. Sohn, Y. K. Kwon and K. S. Ryu, *Physica C* **370**, 21 (2002).

[85] A. Matsumoto H. Kumakura, H. Kitaguchi, H. Hatakeyama, *Supercond. Sci. Technol.* **16**, 926 (2003).

[86] H. Kumakura, A. Matsumoto, Kitaguchi H and H. Hatakeyama, *Physica C* **182**, 93 (2002).

[87] A. K. Pradhan, Y. Feng, Y. Zhao, N. Koshizuka, L. Zhou, P. X. Zhang, X. H. Liu, P. Ji, S. J. Du and C. F. Liu, *Appl. Phys. Lett*. **79**, 1649 (2001).

[88] W. Goldacker, S. I. Schlachter, B .Obst, B. Liu, J. Reiner, S. Zimmer, *Supercond. Sci. Technol.* **17**, 363 (2004).

[89] S. X. Dou, J. Horvat, S. Soltanian, X. L. Wang, M. J. Qin, S. H. Zhou, H. K. Liu, P. G. Munroe, *IEEE Trans. Appl. Supercond.* **13**, 3199 (2003).

[90] P. Kovac, I. Husek, W. Pachla, T. Melisek, R. Diduszko, K. Frohlich, A. Morawski, A. Presz and D. Machajdik, *Supercond. Sci. Technol.* **15**, 1127 (2002).

[91] T. B. Masalski, (ed.) Binary Alloy Phase Diagrams. Vol. 46, 1,434 2nd edition Materials Park, Ohio : ASM International, 1990

[92] H. Fujii, H. Kumakura and K. Togano, *J. Mater. Res*. **17**, 2339 (2002).

[93] J. Horvat, X. L. Wang, S. Soltanian, S. X. Dou, *Appl. Phys. Lett*. **80**, 829 (2002).

[94] J. Horvat, S. Soltanian, X. L. Wang, S. X. Dou, *IEEE Trans. Appl. Supercond* **13**, 3324 (2003).

[95] M. Majoros, B. A. Glowacki, and A. M. Campbell, *Physica C*. **334**, 129 (2001).

[96] R. Flukiger , H. L. Suo, N. Musolino, C. Beneduce, P. Toulemonde, P. Lezza, *Physica C* **385**, 286 (2003).

[97] P. C. Canfield, D. K. Finnemore, S. L. Budko, J. E. Ostenson, G. Lapertot, C. E. Cunningham, C. Petrovic, *Phys. Rev. Lett*. **86**, 2423 (2001).

[98] M. D. Sumption, M. Bhatia, S. X. Dou, M. Rindfliesch, M. Tomsic, L. Arda, M. Ozdemir, Y. Hascicek and E.W. Collings, *Supercond. Sci. Technol.* **17**, 1180 (2004).

[99] G. Giunchi, S. Ceresara, G. Ripamonti, A. Di Zenobio, S. Rossi, S. Chiarelli, M. Spadoni, R. Wesche and P. L. Bruzzone, *Supercond. Sci. Technol*. **16**, 285 (2003).

[100] K. Togano, T. Nakane, H. Fujii, H. Takeya and H. Kumakura, *Supercond. Sci. Technol*. **19**, L17 (2006).

[101] R. A. Ribeiro, S. L. Bud'ko, C Petrovic and P. C. Canfield, *Physica C* **385**, 16 (2003).

[102] J. Bardeen, L. N. Copper and J. R. Schriefffer, *Phys. Rev*. **108**, 1175 (1957).

[103] S. Soltanian, X. L. Wang, J. Horvat, M. J. Qin, H. K. Liu, P. R. Munroe, and S. X. Dou, *IEEE Trans. Appl. Supercond*. **13**, 3273 (2003).

[104] D. C. Larbalestier, L. D. Cooley, M. O. Rikel, A. A. Polyanskii, J. Jiang, S. Patnaik, X. Y. Cai, D. M. Feldmann, A. Gurevich, A. A. Squitieri, M. T. Naus, C. B. Eom, E. E. Hellstrom, R. J. Cava, K. A. Regan, N. Rogado, M. A. Hayward, T. He, J. S. Slusky, P. Khalifah, K. Inumaru, and M. Haas, *Nature* **410**, 186 (2001).

[105] H. Kitaguchi, A. Matsumoto, H. Kumakura, T. Doi, H. Yamamoto, K. Saitoh, H. Sosiati, and S. Hata, *Appl. Phys. Lett*. **85**, 2842 (2004).

[106] X. Y. Song, S. E. Babcock, C. B. Eom, D. C. Larbalestier, K. A. Regan, R. J. Cava, S. L. Bud'Ko, P. C. Canfield, and D. K. Finnemore, *Supercond. Sci. Technol.* **15**, 511 (2002).

[107] L. Cooley, X. Y. Song, and D. Larbalestier, *IEEE Trans. Appl. Supercond*. **13**, 3280 (2003).

[108] A. Yamamoto, J. Shimoyama, S. Ueda, Y. Katsura, I. Iwayama, S. Horii, K. Kishio, *Appl. Phys. Lett*. **86**, 212502 (2005).

[109] A. Serquis, Y. T. Zhu, E. J. Peterson, J. Y. Coulter, D. E. Peterson, and F. M. Mueller, *Appl. Phys. Lett*. **79**, 4399 (2001).

[110] H. Xiao, W. Peng, W.H. Song , R.C. Ma , L. Zhang , J.J. Du , Y.P. Sun, *Physica C* **386**, 648 (2003).

[111] C. M. Franco , B. Ferreira , C. A. M. dos Santos , L. Ghivelder , H. J. I. Filho , A. J. S. Machado, *Physica C* **408–410**, 130 (2004).

[112] R. Ribeiro , S.L. Bud'ko, C. Petrovic, P.C. Canfield, *Physica C* 382 194 (2002).

[113] S. H. Zhou, A. V. Pan, J. Horvat, M. J. Qin and H. K. Liu, *Supercond. Sci. Technol*. **17**, S528 (2004).

[114] P. Lezza, V. Abacherli, N. Clayton, C. Senatore, D. Uglietti, H. L. Suo, R. Flukiger, *Physica C* **401**, 305 (2004).

[115] H. Fujii, K. Togano and H. Kumakura, *Supercond. Sci. Technol*. **15**, 1571 (2002).

[116] H. Yamada, M. Hirakawa, H. Kumakura, A. Matsumoto, and H. Kitaguchi, *IEEE Trans. Appl. Supercond.* **15**, 3337, (2005).

[117] H. Fang, S. Padmanabhan, Y. X. Zhou, and K. Salama, *Appl. Phys. Lett.* **82**, 4113 (2003).

[118] S. K. Chen, K. A. Yates, M. G. Blamire and J. L. MacManus-Driscoll, *Supercond. Sci. Technol*. **18**, 1473 (2005).

[119] X. Xu, M. J. Qin, K. Konstantinov, Dayse I dos Santos, W. K. Yeoh, J. H. Kim and S. X. Dou, *Supercond. Sci. Technol*. **19** 466 (2006).

[120] J. Horvat, S. Soltanian, A. V. Pan, and X. L. Wang, *J. of Appl. Phys*. **96**, 4342 (2004).

[121] T. Takenobu , T. Ito , D. H. Chi, K. Prassides and Y. Iwasa, *Phys. Rev.* B **64**, 134513 (2001).

[122] M. Paranthaman, J. F. Thompson and D. K. Christen, *Physica* C **355**, 1 (2001)

[123] J. S. Ahn and E. J. Choi *Preprint* cond-mat/0103169 (2001)

[124] M. J. Mehl, D. A. Papaconstantopoulos, and D. J. Singh, *Phys. Rev. B* **64**, 140509(R) (2001).

[125] W. Mickelson, J. Cumings, W. Q. Han and A. Zettl, *Phys. Rev.* B **65**, 052505 (2002).

[126] I. Maurin, S. Margadonna, K. Prassides, T. Takenobu, Y. Iwasa and A. N. Fitch *Chem. Mater.* **14** 3894 (2002).

[127] I. Maurin, S. Margadonna, K. Prassides, T. Takenobu, T. Ito, D. H. Chi, Y. Iwasa and A. Fitch, *Physica* B **318**, 392 (2002).

[128] A. Bharathi, S. J. Balaselvi, S. Kalavathi, G. L. N. Reddy, V. S. Sastry, Y. Haritharan and T. S. Radhakrishnan, *Physica* C **370**, 211 (2002)

[129] Y. Yan and M. M. Al-Jassim, *J. of Appl. Phys*. **92**, 7687 (2002).

[130] R. A. Ribeiro, S. L. Budko, C. Petrovic and P. C. Canfield, *Physica* C **384**, 227 (2003).

[131] S. Lee, T. Masui, A. Yamamoto, H. Uchiyama and S. Takama, *Physica* C **397**, 7 (2003).

[132] P. Samuely, Z. HoIanova, P. Szabo, J. Kacmarcık, R. A. Ribeiro, S. L. Budko and P. C. Canfield, *Phys. Rev.* B **68**, 020505(R) (2003).

[133] H. Schmidt, K. E. Gray, D. G. Hinks, J. F. Zasadzinski, M. Avdeev, J. D. Jorgensen and J. C. Burley *Phys. Rev.* B **68**, 060508(R) (2003).

[134] M. Avdeev , J. D. Jorgensen, R. A. Ribeiro, S. L. Bud'ko and P. C. Canfield, *Physica* C **387**, 301 (2003).

[135] P. P. Singh, *Solid State Comm.* **127**, 271 (2003).

[136] K. Papagelis, J. Arvanitidis, I. Margiolaki, K. Brigatti, K. Prassides, A. Schenck, A. Lappas, A. Amato, Y. Iwasa, T. Takenobu, *Physica B* **326**, 346 (2003).

[137] M. Pissas, D. Stamnopoulos, S. Lee and S. Tajima *Phys. Rev. B* **70**, 134503 (2004).

[138] T. Masui, S. Lee and S. Tajima, *Phys. Rev. B* **70**, 024504 (2004)

[139] E. Ohmichi, T. Masui, S. Lee, S. Tajima and T. Osada, *Phys. Rev. B* **70**, 174513 (2004)

[140] R. H. T. Wilke, S. L. Bud'ko, P. C. Canfield, D. K. Finnemore, R. J, Suplinskas and S. T. Hannahs *Phys. Rev. Lett.* **92**, 217003 (2004)

[141] S. Lee, T. Masui, A. Yamamoto, H. Uchiyama, S. Tajima, *Physica C* **412–414**, 31 (2004).

[142] E. Ohimichi, T. Masui, S. Lee, S. Tajima and T. Osada, *J. of the Phys. Soc. of Jap*. **73**, 2065 (2004).

[143] S. Jemima Balaselvi, N. Gayathri, A. Bharathi, V. S. Sastry, Y. Hariharan, *Physica C* **407**, 31 (2004).

[144] Z. Holanova, J. Kacmarcık, P. Szabo, P. Samuely, I. Sheikin, R. A. Ribeiro, S. L. Bud'ko, P.C. Canfield, *Physica C* **404**, 195 (2004).

[145] T. Masui, S. Lee, A. Yamamoto, H. Uchiyama and S. Tajima, *Physica C* **412–414**, 303 (2004).

[146] G. A. Ummarino, D. Daghero, R. S. Gonnelli and A. H. Moudden, *Phys. Rev. B* **71**, 134511 (2005).

[147] R. H. T. Wilke, S. L. Budko, P. C. Canfield, M. J. Kramer, Y. Q. Wu, D. K. Finnemore, R. J. Suplinskas, J. V. Marzik, S. T. Hannahs, *Physica C* **418**, 160 (2005).

[148] S. M. Kazakov, R. Puzniak, K. Rogacki, A. V. Mironov, N. D. Zhigadlo, J. Jun, Ch. Soltmann, B. Batlogg, and J. Karpinski, *Phys. Rev. B* **71**, 024533 (2005).

[149] D. Kasinathan, K. W. Lee, W. E. Pickett, *Physica C* **424**, 116 (2005).

[150] J. Kortus, O. V. Dolgov, R. K. Kremer and A. A. Golubov, *Phys. Rev. Lett.* **94**, 027002 (2005).

[151] R. H. T. Wilke, S. L. Budko, P. C. Canfield, D. K. Finnemore, Raymond J. Suplinskas and S. T. Hannahs, *Physica C* **424**, 1 (2005).

[152] R. S. Gonnelli, D. Daghero, A. Calzolari, G. A. Ummarino, Valeria Dellarocca, V. A. Stepanov, S. M. Kazakov, N. Zhigadlo, and J. Karpinski, *Phys. Rev. B* **71**, 060503(R) (2005).

[153] D. A. Tenne, X. X. Xi, A. V. Pogrebnyakov, and J. M. Redwing, *Phys. Rev. B* **71**, 132512 (2005).

[154] S. Ueda, J. I. Shimoyama, A. Yamamoto, Y. Katsura, I. Iwayama, S. Horii, K. Kishio, *Physica C* **426-431**, 1225 (2005).

[155] A. Yamamoto, J. I. Shimoyama, S. Ueda, Y. Katsura, S. Horii, K. *IEEE Trans. Appl. Supercond.* **15**, 3292 (2005).

[156] A. Yamamoto, J. I. Shimoyama, S. Ueda, I. Iwayama, S. Horii, K. Kishio, *Supercond. Sci. Technol*. **18**, 1323 (2005).

[157] S. Soltanian, X. L. Wang, J. Horvat, S. X. Dou, M. D. Sumption, M. Bhatia, E. W. Collings, P. Munroe and M. Tomsic, *Supercond. Sci. Technol*. **18**, 658 (2005).

[158] A. Serquis, L. Civale, D. L. Hammon, G. Serrano, V. F. Nesterenko, *IEEE Trans. Appl. Supercond*. **15**, 3188 (2005).

[159] S. Iijima, *Nature* **354**, 56 (1991).

[160] Y. Li, I. A. Kinloch, and A. H. Windle, *Science*, **304**, 276 (2004).

[161] E. S. Choi, J. S. Brooks, D. L. Eaton, M. S. Al-Haik, M. Y. Hussaini, H. Garmestani, D. Li and K. Dahmen, *J. of Appl. Phys.*, **94**, 6034 (2003)

[162] K. Fossheim, E. D. Tuset, T. W. Ebbesen, M. M. J. Treacy and J. Schwartz, *Physica C* **248**, 195 (1995).

[163] S. Huang, M. R. Koblischka, K. Fossheim, T. W. Ebbesen and T. H. Johansen, *Physica C* **311**, 172 (1999).

[164] P. Yang and C.M. Lieber, *Science* **273**, 1836 (1996).

[165] P. Yang and C.M. Lieber, *Appl. Phy. Lett.* **70**, 3158 (1997).

[166] P. Yang and C.M. Lieber, *J. of Mat. Res.* **12**, 2981 (1997).

[167] J. Wei, Y. Li, C. Xu, B. Wei and D. Wu, *Materials Chemistry and Physics* **78**, 785 (2003).

[168] B. Q. Wei, R. Vajtai, and P. M. Ajayan, *Appl. Phys. Lett.*, **79**, 1172 (2001).

[169] P. Kim, L. Shi, A. Majumdar, and P. L. McEuen, *Phys. Rev. Lett*. **87**, 215502. (2001).

[170] M. M. J. Treacy, T. W. Ebbesen and J. M. Gibson, *Nature* **381**, 678 (1996).

[171] H. L. Xu, Y. Feng, Z. Xu, G. Yan, L.Z. Cao and X.G. Li Xiao, *Chin. Phys. Lett*. **21**, 2511 (2004).

[172] E. Ban, R. Sakaguchi, Y. Matsuoka, T. Goto, K. Watanabe, G. Nishijima *Physica C* **426–431**, 1249 (2005).

[173] Y. Ma, X. Zhang, G. Nishijima, K. Watanabe,S. Awaji and X. Bai, *Appl. Phys. Lett* **88**, 072502 (2006).

[174] S. Soltanian, J. Horvat, X. L. Wang, P. Munroe, S. X. Dou, *Physica C* **390**, 185 (2003).

[175] Z. H. Cheng, B. G. Shen, J. Zhang, S. Y. Zhang, T. Y. Zhao and H. W. Zhao, *J. Appl. Phys.* **91**, 7125 (2002).

[176] A. V. Pogrebnyakov, X. X. Xi, J. M. Redwing, V. Vaithyanathan, D. G. Schlom, A. Soukiassian, S. B. Mi, C. L. Jia, J. E. Giencke, C. B. Eom, J. Chen, Y. F. Hu, Y. Cui, and Qi Li, *Appl. Phys. Lett*. **85**, 2017 (2004).

[177] H. Kumakura, H. Kitaguchi, A. Matsumoto, and H. Hatakeyama, *IEEE Trans. Appl. Supercond.***15**, 3184 (2005).

[178] Y. Zhao, C. H. Cheng X. F. Rui, H. Zhang P. Munroe H. M. Zeng N. Koshizuka and M. Murakami, *Appl. Phys. Lett*. **83**, 2916 (2003).

[179] S. Ueda, J. Shimoyama, A.Yamamoto, S. Horii and K. Kishio, *Supercond. Sci. Technol*. **17**, 926 (2004).

[180] J. Y. Xiang, D. N. Zheng , J. Q. Li, S. L. Li, H. H. Wen, Z. X. Zhao, *Physica C* **386**, 611 (2003).

[181] M. R. Cimberle, M. Novak, P. Manfrinetti and A. Palenzona, *Supercond. Sci. Technol*. **15**, 43 (2002).

[182] P. Toulemonde, N. Musolino and R. Flukiger, *Supercond. Sci. Technol*. **16**, 231 (2003).

[183] A. Berenov, A. Serquis, X. Z. Liao, Y. T. Zhu, D. E. Peterson, Y. Bugoslavsky, K. A. Yates, M. G. Blamire, L. F. Cohen and J. L. MacManus-Driscoll, *Supercond. Sci. Technol*. **17**, 1093 (2004).

[184] G. J. Xu , J. C. Grivel , A. B. Abrahamsen, X. P. Chen, N. H. Andersen, *Physica C* **403**, 113 (2004).

[185] E. Martínez, L. A. Angurel, R. Navarro, A. Millán, C. Rillo, and M. Artigas, *IEEE Trans. Appl. Supercond.* **13**, 3210 (2003).

[186] E. M. Choi, H. S. Lee, H. J. Kim, S. I. Lee, H. J. Kim and W. N. Kang *Appl. Phys. Lett*. **84**, 82 (2004).

[187] S. F. Wang, S. Y. Dai, Y. L. Zhou, Y. B. Zhu, Z. H. Chen, H. B. Lu and G. Z. Yang, *J. Supercond.,* **17**, 397 (2004).

[188] D. Goto, T. Machi , Y. Zhao, N. Koshizuka, M. Murakami, S. Arai *Physica C* **392–396**, 272 (2003).

[189] Y. Zhao, Y. Feng, D. X. Huang, T. Machi, C. H. Cheng, K. Nakao, N. Chikumoto, Y. Fudamoto, N. Koshizuka, M. Murakami, *Physica C* **378**, 122 (2002).

[190] B. Q. Fu, Y. Feng, G. Yan, Y. Zhao, A. K. Pradhan, C. H. Cheng, P. Ji, X. H. Liu, C. F. Liu, L. Zhou, K. F. Yau, *J. Appl Phys*. **92**, 7341 (2002).

[191] Y. Zhao, Y. Feng, T. Machi, C. H. Cheng, D. X. Huang, Y. Fudamoto, N. Koshizuka and M. Murakami, *Europhys. Lett.*, **57**, 437 (2002).

[192] B. Q. Fu , Y. Feng, Y. Zhao, A. K. Pradhan, C. H. Cheng, P . Ji, X. H. Liu, C. F. Liu, G. Yan and L. Zhou, *Physica C* **386**, 659 (2003).

[193] S. H. Zhou, H. K. Liu, J. Horvat and S. X. Dou *J. Low Temp. Phys*. **131**, 687 (2003).

[194] N. E. Anderson Jr., W. E. Straszheim, S. L. Budko, P. C. Canfield, D. K. Finnemore and R. J. Suplinskas, *Physica C* **390**, 11(2003).

[195] D. K. Finnemore, W. E. Straszheim, S. L. Budko, P. C. Canfield, N. E. Anderson Jr. and R. J. Suplinskas, *Physica C* **385**, 278 (2003).

[196] T. A. Prikhna, W. Gawalek, Y. M. Savchuk, V. E. Moshchil, N. V. Sergienko, T. Habisreuther, M. Wendt, R. Hergt, Ch. Schmidt, J. Dellith, V. S. Melnikov, A. Assmann, D. Litzkendorf and P. A. Nagorny, *Physica* C **402**, 223 (2004).

[197] S. Haigh, P. Kovac, T. A. Prikhna, Y. M. Savchuk, M. R. Kilburn, C. Salter, J. Hutchison and C. Grovenor, *Supercond. Sci. Technol*. **18**, 1190 (2005).

[198] Y. Zhao, D. X. Huang, Y. Feng, C. H. Cheng, T. Machi, N. Koshizuka and M. Murakami *Appl. Phys. Lett.* **80**, 1640 (2002).

[199] S. X. Dou, S. Soltanian, Y. Zhao, E. Getin, Z. Chen, O. Shcherbakova and J. Horvat, *Supercond. Sci. Technol*. **18**, 710 (2005).

[200] C. Shekhar, R. Giri, R. S. Tiwari, D. S. Rana, S. K. Malik and O. N. Srivastava, *Supercond. Sci. Technol*. **18**, 1210 (2005).

[201] Y. Kimishima , M. Uehara, T. Kuramoto, S. Takano, S. Takami, *Physica C* **412–414**, 402 (2004).

[202] P. Kovac, I. Husek, T. Melisek, C. R. M. Grovenor, S. Haigh and H. Jones *Supercond. Sci. Technol*. **17**, 1225 (2004).

[203] Y. Feng, Y. Zhao, Y. P. Sun, F. C. Liu, B. Q. Fu, L. Zhou, C. H. Cheng, N. Koshizuka, M. Murakami, *Appl. Phys. Lett*. **79**, 3983 (2001).

[204] Y. Feng, Y. Zhao, A. K. Pradhan, C. H. Cheng, J. K. F. Yau, L. Zhou, N. Koshizuka and M. Murakami, *J. Appl. Phys.* **92**, 2614 (2002).

[205] T. A. Prikhna, W. Gawalek, A. B. Surzhenko, V. E. Moshchil, N. V. Sergienko, Y. M. Savchuk, V. S. Melnikov, P. A. Nagorny, T. Habisreuther, S. N. Dub, M. Wendt, D. Litzkendorf, J. Dellith, C. Schmidt, G. Krabbes, A. V. Vlasenko, *Physica* C **372**, 1543 (2002)

[206] K. Tachikawa, Y. Yamada, M. Enomoto, M. Aodai, and H. Kumakura, *IEEE Trans. Appl. Supercond.*, **13**, 3269 (2003).

[207] K. Tachikawa, Y. Yamada, M. Enomoto, M. Aodai, H. Kumakura, *Physica C* **392–396**, 1030 (2003).

[208] X. L. Wang, S. Soltanian, M. James, M. J. Qin, J. Horvat, Q. W. Yao, H. K. Liu, S. X. Dou, *Physica C* **408–410**, 63 (2004).

[209] J. W. Ko, J. Yoo, Y. K. Kim, H. D. Kim, K. H. Oh, S. J. Choe, H. Chung, S. J. Chung, H. Kumakura, A. Matsumoto, and K. Togano, *IEEE Trans. Appl. Supercond.* **13**, 3214 (2003).

[210] M. Delfany, X. L. Wang, S. Soltanian, J. Horvat, H. K. Liu, S. X. Dou, *Ceramics International* **30**, 1581 (2004).

[211] X. F. Rui, J. Chen, X. Chen, W. Guo, H. Zhang, *Physica C* **412**, 312 (2004).

[212] T. M. Shen, G. Li, X. T. Zhu, C. H. Cheng and Y. Zhao, *Supercond. Sci. Technol*. **18**, L49 (2005).

[213] T. Prozorov, R. Prozorov, A. Snezhko and K S. Suslick, *Appl. Phys. Lett*. **83**, 2019 (2003).

[214] P. Kovac, I. Husek, T. Melisek, J. C. Grivel, W. Pachla, V. Strbık1, R. Diduszko, J. Homeyer and N. H. Andersen, *Supercond. Sci. Technol*. **17**, L41 (2004).

[215] C. H. Jiang, H. Hatakeyama and H. Kumakura, *Physica C* **423**, 45 (2005)

[216] O. Perner , W. Hassler, J. Eckert , C. Fischer , C. Mickel, G. Fuchs, B. Holzapfel , L. Schultz, *Physica C* **432**, 15 (2005).

[217] Y. Ma, H. Kumakura, A. Matsumoto, H. Hatakeyama and K. Togano, *Supercond. Sci. Technol*. **16**, 852 (2003).

[218] A. Matsumoto, H. Kumakura, H. Kitaguchi and H. Hatakeyama, *Supercond. Sci. Technol*. **17**, S319 (2004).

[219] Y. Ma, H. Kumakura, A. Matsumoto, and K. Togano, *Appl. Phys. Lett.* **83**, 1181 (2003).

[220] X. F. Rui, Y. Zhao, Y. Y. Xu, L. Zhang, X. F. Sun, Y. Z. Wang and H. Zhang, *Supercond. Sci. Technol*. **17**, 689 (2004).

[221] A. Yamamoto, C. Takao, T. Masui, M. Izumi and S. Tajima, *Physica* C **383**, 197 (2002).

[222] T. Nakane, H. Takeya, H. Fujii and H. Kumakura, *Supercond. Sci. Technol*. **18**, 521 (2005).

[223] A. Kikuchi, Y. Iijima, N. Banno, T. Takeuchi, and K. Inoue, *IEEE Trans. Appl. Supercond.* **15**, 3207 (2005).

[224] M. Haruta, T. Fujiyoshi, T. Sueyoshi, K. Miyahara, T. Doi, H. Kitaguchi, S. Awaji and K. Watanabe, *Supercond. Sci. Technol*. **18**, 1460 (2005).

[225] G. J. Xu, J. C. Grivel, A. B. Abrahamsen, N. H. Andersen *Physica C* **406**, 95 (2004).

[226] M. Bhatia, M. D. Sumption, E. W. Collings, and S. Dregia, *Appl. Phys. Lett.* **87**, 042505 (2005).

[227] S. K. Chen, B. A. Glowacki, J. L. MacManus-Driscoll, M. E. Vickers and M. Majoros, *Supercond. Sci. Technol*. **17**, 243 (2004).

[228] H. L. Xu, Y. Feng, Z. Xu, C. S. Li, G. Yan, Y. F. Wu, Z. L. Chen, E. Mossang, A. Sulpice, *Physica C* **426–431**, 1244 (2005).

[229] H. Fujii, K. Togano and H. Kumakura, *Supercond. Sci. Technol*. **16**, 432 (2003)

[230] S. K. Chen, M. Wei and J. L. MacManus-Driscoll, *Appl. Phys. Lett*. **88**, 192512 (2006).

[231] M. D. Sumption, M. Bhatia, F. Buta, S. Bohnenstiehl, M. Tomsic, M. Rindfleisch, J. Yue, J. Phillips, S. Kawabata, E. W. Collings, *Supercond. Sci. Technol.* **18**, 961 (2005).

[232] M. D. Sumption, M. Bhatia, M. Rindfleisch, M. Tomsic, E. W. Collings, *Appl. Phys. Lett.* **86**, 102501 (2005).

[233] E. W. Collings, E. Lee, M. D. Sumption, M. Tomsic, X. L. Wang, S. Soltanian, S. X. Dou, *Physica C* **386**, 555 (2003).

[234] G. Grasso , A. Malagoli, M. Modica, A. Tumino, C. Ferdeghini, A. S. Siri, C. Vignola, L. Martini, V. Previtali, G. Volpini, *Supercond. Sci.* Technol. **16**, 271 (2003)

[235] M. D. Sumption, M. Tomsic, M. Bhatia, Y. Hascieck, S. X. Dou, E. W. Collings, Presented at the ICMC Topical Conferences Feb 10-13 2004, Wollongong, Australia.

[236] A. Serquis, L. Civale, J. Y. Coulter, D. L. Hammon, X. Z. Liao, Y. T. Zhu, D. E. Peterson, F. M. Mueller, V. F. Nesterenko, S. S. Indrakanti, *Supercond. Sci. Technol*. **17**, L35 (2004).

[237] H. Kumakura, Short Course presentation in the Applied Superconductivity Conference 2004 Jacksonville, Florida, USA.

[238] MgB_2 Trades Performance for A Shot at the Real World, *Science* **295**, 786 (2002).

[239] B. Seeber, in: B. Seeber (Ed.), Handbook of Applied Superconductivity, Institute of Physics Publishing, Bristol, 1998, p. 307.

[240] W. H. Tschopp, D. D. Laukien, in: B. Seeber (Ed.), Handbook of Applied Superconductivity, Institute of Physics Publishing, Bristol, 1998, p. 1191

[241] H. L. Suo, P. Lezza, D. Uglietti, C. Beneduce, V. Abächerli, and R. Flükiger, *IEEE Trans. Appl. Supercond*, **13**, 3265 (2003)

[242] R Flükiger, P Lezza, C Beneduce, N Musolino and H L Suo, *Supercond. Sci. Technol*. **16**, 264 (2003).

[243] H. Kitaguchi, A. Matsumoto, H. Hatakeyama, H. Kumakura, *Physica C* **401**, 246 (2004).

[244] P. Kováč, I. Hušek, T. Melišek, *Physica C* **401**, (2004) 282.

[245] W. Goldacker, S. I. Schlachter, B. Liu, B. Obst, E. Klimenko, *Physica C* **401**, 80 (2004).

Chapter 3: Experimental

3.1 Bulk sample preparation

Polycrystalline samples of MgB_2 were prepared through solid state reaction in-situ process, as described in the previous chapter. The starting powders were magnesium, amorphous boron, multi-walled carbon nanotubes (MWCNT), C nano-particle and SiC nano-particle powder. The details of the powders used were listed in the table 1. The aim of this work is to systematically study the effect of the carbon substitution effect in the MgB_2. As a result, two main series-MWCNT and nano C doped MgB_2 have been prepared with nominal atomic ratio of $MgB_{2-x}Z_x$ as x = 0, 0.05, 0.1, 0.2, 0.3,(Z = dopants). Besides that, the 5% wt SiC doped samples were synthesized for reference and comparison. All the elements were weighed out according to the stociometry and well-mixed through grinding. The powders were pressed into pellets of 13 mm in diameter and 1 mm in thickness using a hydraulic press. The pellets were sealed in Fe tubes, then heat treated at 650^{o}C to 1000^{o}C for 10 to 120 min in flowing high purity Ar followed by a furnace cooling to room temperature. We stress that the values for x are the nominal values throughout the paper, and actual substitution of B for C will be shown to be less than these values.

Table 3.1 Details of various percursors materials used in this work

Element	Purity	Outside Diameter (nm)	Inside Diameter (nm)	Length (μm)	Particle size (nm)
Magnesium	99%	n/a	n/a	n/a	$44x10^6$
Boron	99%	n/a	n/a	n/a	$1\text{-}2\ x10^6$
MWCNT	>95%	8-15	3-5	0.5	n/a
	>95%	20-30	5-10	0.5	n/a
	>95%	30-50	5-15	0.5	n/a
	>95%	<8	2-5	0.5-200	n/a
	>95%	8-15	3-5	0.5-200	n/a
	>94%	20-30	16-28	0.5-2	n/a
	>95%	60-100	5-10	5-15	n/a
Nano Carbon	99%	n/a	n/a	n/a	<20
Nano-SiC	99 %	n/a	n/a	n/a	<20

3.2 Fabrication of MgB_2 Wires and Tapes

MgB_2/Fe monofilament wires were prepared by an in-situ reaction process, using the powder-in-tube method (PIT). The well-mixed powders were packed into Fe tubes with a length of 140 mm, an outer diameter (O.D) of 10 mm, and an inner diameter (I.D) of 8 mm and both ends of the tube were sealed by pieces of aluminium foil. Each tube was subsequently drawn to wire 1.4 mm in diameter. Drawing process was carried out by passing the tube through the conical hole of successive round dies at a speed of a few cm/s. A deformation rate of no more than 15% per pass was used in the whole mechanical deformation procedure. For tape making, short wire samples (4 cm each), were cold rolled to the flat tape with a thickness of 500 μm and 3 mm width. All the samples were sealed in Fe tubes or Zr foil, then heat treated with a heating rate of 5^oC/min in flowing high purity Ar at 700-1000 ^oC for 30 minutes, followed by a furnace cooling to room temperature.

3.3 Samples Characterizations

3.3.1 X-ray Diffraction (XRD)

X-ray diffraction (XRD) was used to examine the microstructure, phase formation, and study of the texture, as well as calculation of the lattice parameters. In this work two XRD instruments were used for microstructure characterization: Philips PW1730 and MAC MO3XHF. In both diffractometers, CuK_α radiation with wavelength of 1.5405 Å was used to index the peak by the Bragg's law from 20-70^0 (2 theta). The average grain size can be quantitatively estimated, as the average crystallite is inverse proportional to the width of a reflection peak at half maximum intensity (FWHM). The lattice parameters and unit cell volumes were estimated from the (002) and the (100) peaks. Si powder was used as an internal standard to calculate the lattice parameters.

3.3.2 Scanning electron microscopy (SEM) and Energy dispersive X-ray spectrometry (EDS)

A direct observation of microstructure as well as the investigation of morphology can be made using the SEM. Although the resolution of the SEM is not high enough to image down to the atomic scale, SEM is a non-destructive characterization method to image a comparatively large area of the specimen for measuring the nature of the specimen. Depending on the instrument, the resolution can fall somewhere between less than 1 nm and 20 nm.

Energy dispersive X-ray spectroscopy (EDX or EDS) is a method used to determine the energy spectrum of X-ray radiation to characterize the elemental composition of the samples area as small as a few cubic micrometers. Nevertheless, EDS cannot detect light elements, like B. A thin layer of gold was deposited on the specimens to increase the electric conductivity.

3.3.3 Transmission Electron Microscopy (TEM)

The TEM allows not only structural information to be obtained, but also crystallographic studies of materials are routinely possible. Transmission Electron Microscopy permits a direct observation and characterization of atomic resolution imaging, unlike the SEM. In this work, three kinds of TEM facilities were used: JEOL 3000F High Resolution Transmission Electron Microscope (HRTEM) at University of Sydney, Australia, Phillips CM 200 Field Emission Gun Transmission Electron Microscope at University of New South Wales, Australia and JOEL 2011 analytical electron microscope with JOEL EDS system at University of Wollongong, Australia

The microscopes are also equipped with energy dispersive X-ray spectroscopy system (EDAX) and Electron Energy Loss Spectroscopy (EELS), which can provide information on elemental concentrations and distributions from regions as small as 10 nm in diameter. Specimens were prepared by pulverizing the powder with mortar and pestle, then dispersing it in ethanol by using sonication. The suspension was then pipetted on to holey-carbon coated copper grids.

3.3.4 Critical Current Density, T_c, Measurements

T_c of the superconducting materials can be determined by using the resistance or the magnetic ac susceptibility measurement. Both of the measurements were performed with a Quantum Design Physical Property Measurement Systems (PPMS). The resistance measurement requires the sample to be contacted with four leads. The two outer leads are for current and the two inner leads are for voltage. Besides that, we can determine the resistivity of MgB_2 samples from room temperature to superconducting temperature by using this method with sensitivity up to 1 μΩ.

In the ac susceptibility measurement, the sample will be located in a system consisting of a primary and secondary coils. The primary coils produce an excitation field set to an amplitude of 0.1 Oe and frequency of 117Hz. The sample was placed in the secondary pick-up coils, where the change of the induction voltage across the coils due to the superconducting shielding current can be detected by the Lock-In Amplifier. In that case, T_c was defined as the onset of the diamagnetism by measuring the real part of the ac susceptibility with a sensitivity of up to 10^{-8} emu.

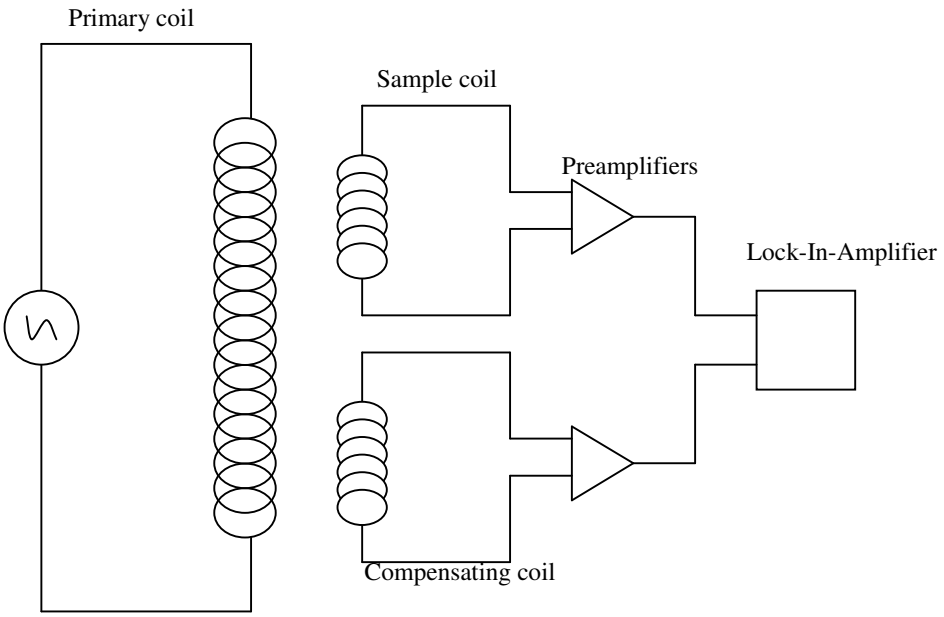

Figure 3.1 Schematic diagram of mutual inductance technique for measuring the critical temperature.

3.3.5 Critical Current Density, J_c, Measurements

Similar to the critical temperature, critical current density can be determined by the transport method or the DC magnetization measurement.

The critical current, I_c, was measured by a conventional four point-probe resistive method at 4.2 K in magnetic field below 12 T. Current leads and voltage taps were directly soldered to the sheath materials of the wire/tape. The maximum current of power supply was 1000 A and a nanovoltmeter was used to detect the signal of sample. A magnetic field was applied parallel to the tapes/wires. The criterion of I_c definition was 1 μV/cm. Critical current density, J_c, was obtained by dividing I_c by the cross-sectional area of the MgB_2 core.

DC magnetization measurements were carried out on MgB_2 samples using the Quantum Design Physical Property Measurement System (PPMS). The sample moves in a constant magnetic field and the waveform signal from the sample is picked up by detection coil. The signal is then fitted with the known calibration waveform, where the magnetic moment of the sample is a fitting parameter. The magnetic hysteresis loop was measured over a temperature range of 5 to 30 K in a time-varying magnetic field with sweep rate 50 Oe/s and amplitude 8.5T. J_c can be calculated from the measured magnetic hysteresis loop based on the Critical State Model [1], as shown below.

For bar shape (b >a)

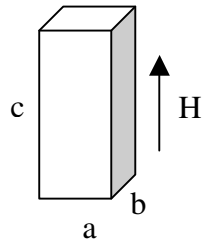

J_c=20 ΔM/[a(1-a/3b)]

For cylinder shape (diameter 2a)

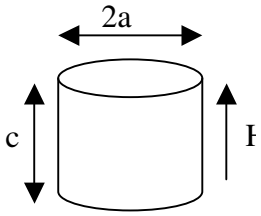

B // axis
J_c=15 ΔM/[$a^3c\pi$]

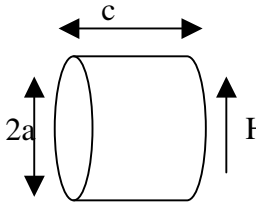

B ⊥ axis
J_c=15 ΔM/[$4a^3c$]

In this relation, a, b and c are the dimensions of sample in cm. J_c and ΔM are in A/cm^2 and in emu/cm^3, respectively. Bar shaped samples (3 x 1.5 x 1 mm^3) and wire shaped samples (c=140 mm, a=1.0-0.7mm) were cut from each pellet and extracted out from the wire for magnetic measurements. The low field J_c below 10 K could not be measured due to flux jumping.

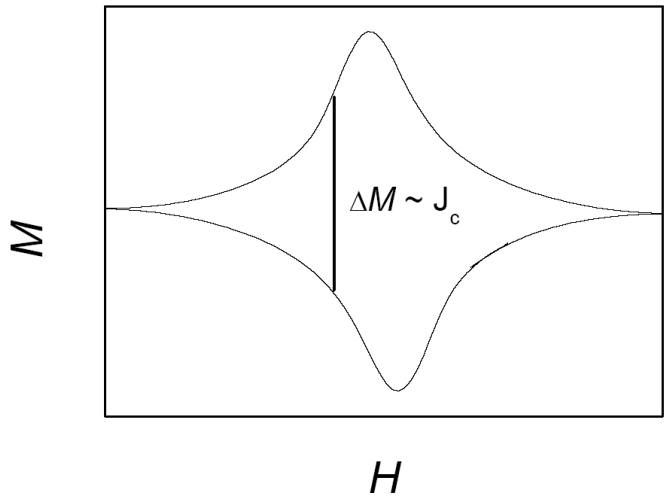

Figure 3.2: Schematic diagram of magnetic hysteresis loop of a superconductor showing the width of the magnetic hysteresis loop ΔM

3.3.6 Upper Critical field, H_{c2} and Irreversibility Field, H_{irr}

H_{c2} value was determined by using two methods: the resistivity versus temperature and the ac susceptibility versus temperature measurements. Both measurements were taken using Quantum Design PPMS system, with fields up to 8.7 T. For the resistivity method, $H_{c2}(T)$ and $H_{irr}(T)$ were obtained by measuring the temperature at which the normal-state resistivity of the sample drops by 10% and 90% of its normal state value, respectively, for a particular field (figure 3.3a). For the magnetization measurements, the $H_{c2}(T)$ was estimated by the onset of diamagnetic

screening for a particular field. In general, a criterion of J_c = 100 A cm^{-2} is used to define $H_{irr}(T)$ at particular measuring temperature (Fig.3.3.b).

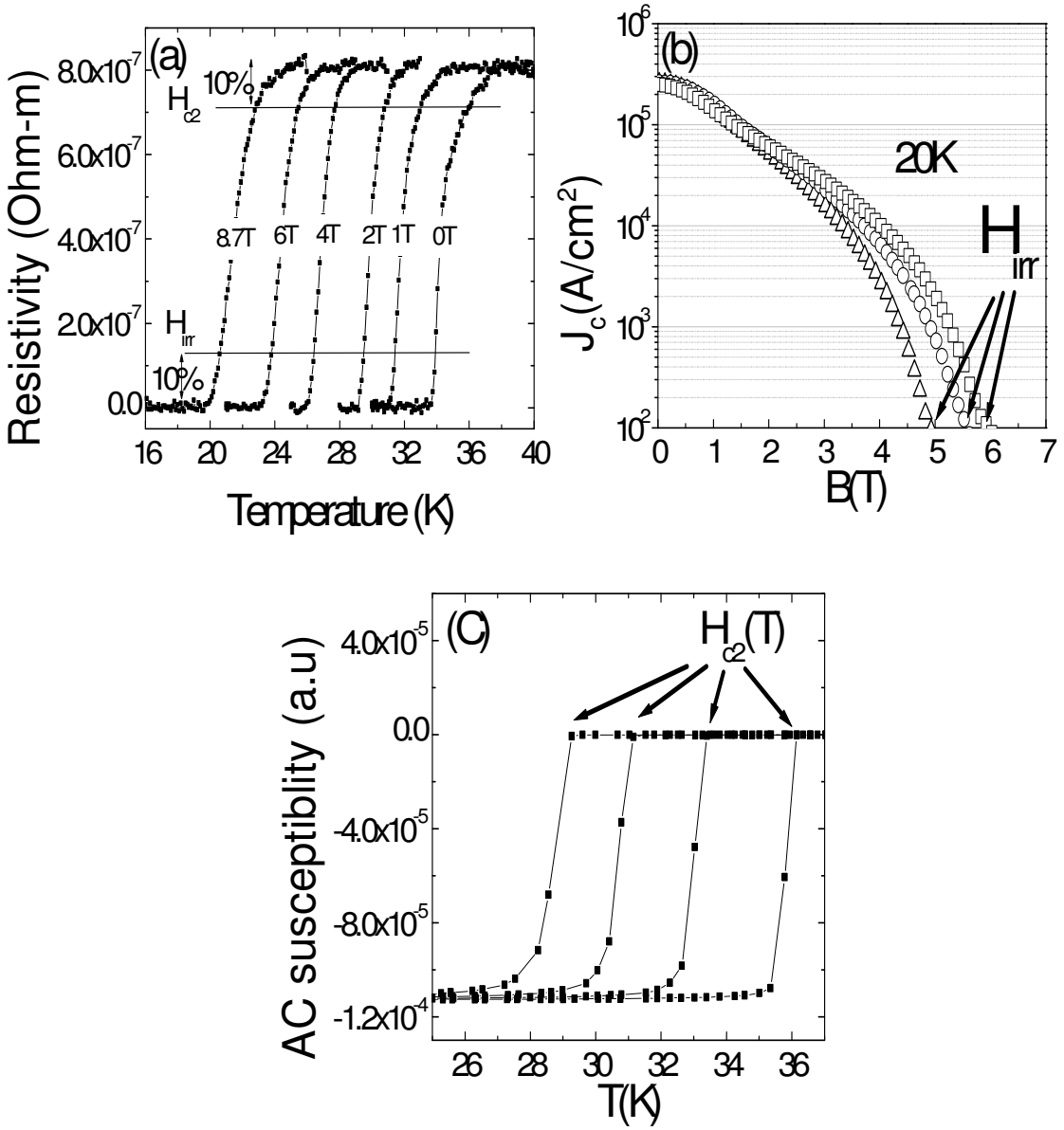

Figure 3.3 (a) resistivity method to measure the H_{c2} and H_{irr} (b) H_{irr} determined by using the criteria of J_c =100A/cm^2 (c) Magnetization method to determine the H_{c2}.

3.3.7 Reference

[1] C. P. Bean, *Rev.Mod.Phys*. **36**, 31-36 (1964).

Chapter 4: Strong pinning and high critical current density in carbon nanotube doped MgB_2

4.1 Introduction

MgB_2 has been proven to have good grain connectivity, large coherence lengths and low anisotropy, which all makes it a potential material for practical cable applications. However, there are two disadvantages of MgB_2 compared to the classical superconductors: low upper critical field H_{c2} and relatively rapid decrease of J_c with magnetic field. The key to high magnetic field application is to improve the pinning centres through chemical doping, which is a low cost fabrication technique. The doping can also increase H_{c2} through impurity scattering of charge carriers, which was used quite efectivelly for MgB_2 [1]. Nano defects will be the best pinning centres since MgB_2 has a coherent length of ~10 nm. The results of the nanoparticle doping are best seen by the significant improvement in $J_c(H)$ and irreversibility field, H_{irr} , through the nano-SiC doping [2]. However, inducing the defects in the MgB_2 matrix is also counterproductive, leading to a decrease of critical temperature T_c.

The substitution of boron for carbon has a great impact on the carrier density and impurity scattering, because MgB_2 is a two-gap superconductor. It is expected that the carbon, which has one more electron than boron, will donate electrons to the σ band [3-5]. This would suggest that the superconductivity in MgB_2 is substantially modified by carbon doping. As a result, this opens up the possibility for an optimised simultaneous

enhancement of the upper critical field, the irreversibility field, and the critical current by a controlled carbon doping.

The effect of C doping on superconductivity in MgB_2 compound has been widely studied by several groups [6–24]. Past studies have shown that carbon does substitute into the boron site, causing a decrease in the T_c and in the *a*-lattice parameter, but not the *c*-lattice parameter. The results on C solubility and the effect of C-doping on T_c reported so far vary significantly due to the precursor materials, fabrication techniques and processing conditions used. It appears that lower sintering temperatures and short sintering times result in an incomplete reaction and hence lower C solubility in MgB_2. Ribeiro et al. used Mg and B_4C as precursors to synthesize C doped MgB_2 by heat processing at 1200^oC for 24 hours [25]. A neutron diffraction study confirmed that the most likely solubility of C in MgB_2 is up to around 10% of C in the boron sites, resulting in a large drop of both T_c and the *a*-axis lattice parameter [20]. Lee et al. synthesized C-doped single crystalline MgB_2 at high pressure (5GPa) and high temperature (1600^0C), obtaining the C solubility of 15% at the boron sites and T_c depression to below 3K [16]. From the applications point of view, the effect of C doping on the flux pinning properties is crucially important.

The effects of C doping on the flux pinning and critical current density in MgB_2 has been studied using amorphous carbon [26] and diamond [27], both showing improvement of J_c at elevated magnetic fields. Wei et al. have studied the superconductivity of MgB_2-carbon nanotube composites [28]. However, the effect of carbon nanotube doping on critical current density and flux pinning has not been

reported. Among various carbon precursors, carbon nanotubes are particularly interesting as their special geometry (high aspect ratio and nanometer diameter) may induce more effective pinning centres compared to other carbon-containing precursors. In this chapter we report the results on control of the extent of carbon nanotube substitution and inclusion to achieve an enhancement of critical current density and flux pinning by two orders of magnitude in magnetic fields. Besides that, we show that CNT doping improves both H_{irr} and H_{c2}. The improvement of H_{c2} was predicted by the theory of two-band scattering, where homogeneously distributed impurities in the crystal lattice are expected to increase H_{c2}. We show that some of the carbon from the CNT's substitutes boron in the MgB_2 crystalline lattice (depending on the sintering temperature), improving the H_{c2} and probably also the vortex pinning. On the other hand, some of CNT's do not decompose, but become a part of the crystal matrix as a whole, where they are effective pining centres, resulting in improved irreversibility field and field dependence of J_c.

4.2 Experimental

Polycrystalline samples of $MgB_{2-x}C_x$ were prepared through in-situ solid state reaction process. High purity powders of magnesium (99%), amorphous boron (99%) and multi-walled carbon nanotubes of 20-30nm diameter were weighed out according to the nominal atomic ratio of $MgB_{2-x}C_x$ with x = 0, 0.05, 0.1, 0.2, 0.3, and well-mixed through grinding. The powders were pressed into pellets of 10 mm in diameter and 1 mm in thickness and then sealed in Fe tubes before heat treated at 700 to 1000^{o}C for 10 to 120min in flowing high purity Ar. The phase and crystal structure of all the samples

was obtained from X-ray diffraction (XRD) patterns with Si powder used as an internal standard. The grain morphology and microstructure were also examined by scanning electron microscope (SEM) and transmission electron microscope (TEM).

The magnetization was measured over a temperature range of 5 to 30 K using a Physical Property Measurement System (PPMS, Quantum Design) using a time-varying magnetic field with sweep rate 50 Oe/s and amplitude 8.5T. Bar shaped samples with a size of 3 x 1.5 x 1 mm^3 were cut from each pellet for magnetic measurements. The magnetic measurements were performed by applying the magnetic field parallel to the longest sample axis. The magnetic J_c was calculated from the height of the magnetization loop ΔM using the critical state model: J_c=20 ΔM/[a(1-a/3b)], with a and b as the dimensions of the sample perpendicular to the direction of applied magnetic field and $a < b$. J_c versus magnetic field has been measured up to 8.5 T. The low field J_c below 10 K could not be measured due to flux jumping. T_c was obtained from the measurements of AC susceptibility at a frequency of 117 Hz and an external magnetic field of 0.1 Oe. The H_{c2} values have been determined from resistivity versus temperature data up to 8.7 T taken on Quantum Design, PPMS. $H_{c2}(T)$ was obtained by measuring the temperature at which the normal-state resistivity of the sample drops by 10% of its value at 43 K for a particular field. This field is then H_{c2} for the thus obtained temperature.

4.3 Results and Discussions:

Figure 4.1 shows the XRD pattern for the series of $MgB_{2-x}CNT_x$ with x= 0, 0.05, 0.1, 0.2 and 0.3 sintered at 800^{o}C for 30 min. All the peaks can be indexed, where the majority phase corresponds to the MgB_2, hexagonal, P6/mmm structure up to x = 0.3 The XRD patterns reveal that the (100) peak shifts substantially to higher angle for nominal doping level up to x = 0.3 while the (002) peak remains unchanged with increasing carbon content as shown in the figure 4.2. This is in agreement with most of the reports that carbon substitution leads to the decrease of lattice parameter a and no effect on the lattice parameter c. The lattice contraction is probably due to the average atomic radius for C (0.91 Å) being smaller than for B (1.17 Å). Therefore, the lattice reduction shows some level of substitution of C in the B site. Impurities like MgO can be detected in all samples including the pure MgB_2 and again there is no strong change of intensity of MgO peaks with the carbon content. However, there is no evidence that B_4C, unreacted C and Mg, MgB_4 or MgB_2C_2 are present, except for sample with x = 0.3 that shows the presence of uncreated C.

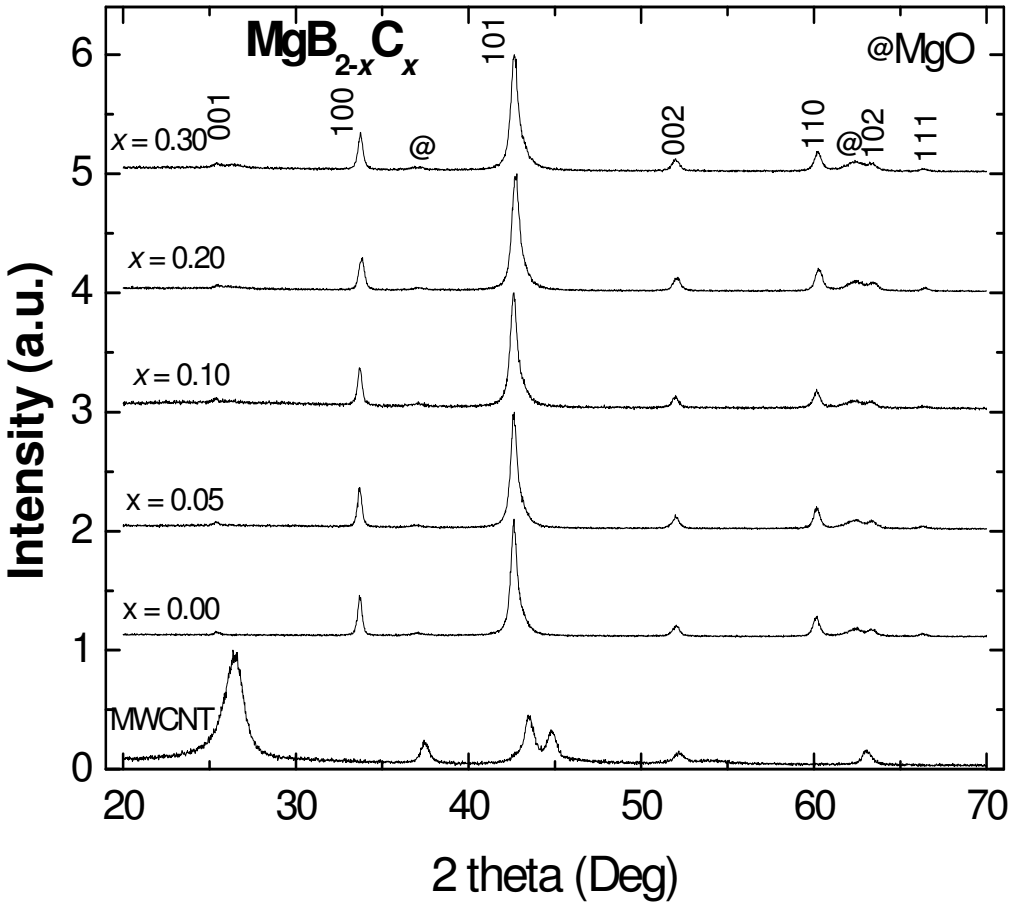

Figure 4.1 XRD pattern for carbon nanotube doped $MgB_{2-x}C_x$ with x = 0, 0.05, 0.1, 0.2 and 0.3, sintered at temperatures at 800°C for 30 min.

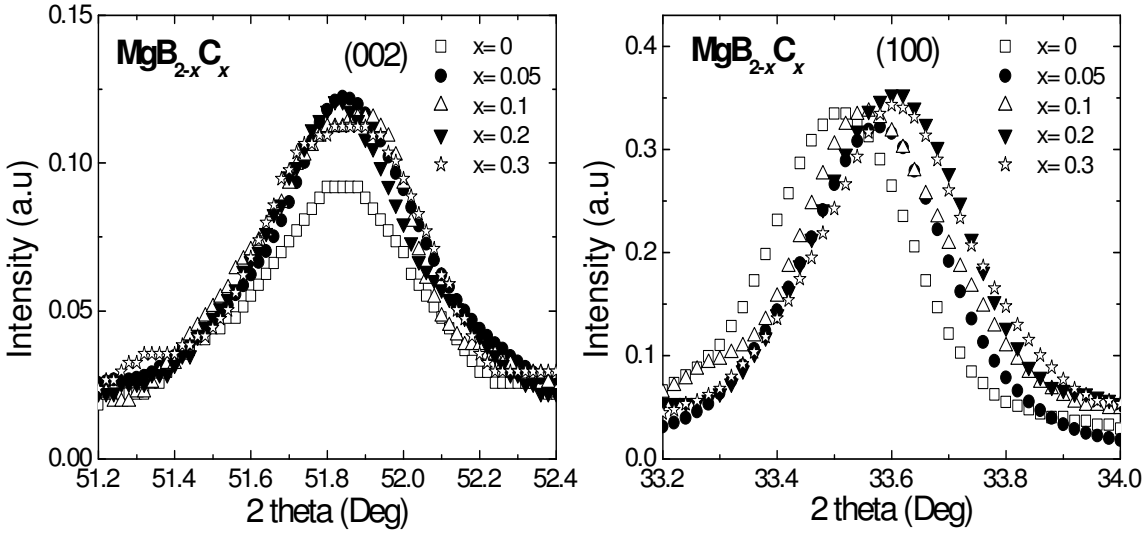

Figure 4.2: XRD pattern of (002) and (100) peak for carbon nanotube doped $MgB_{2-x}C_x$ with x = 0, 0.05, 0.1, 0.2 and 0.3.

Fig. 4.3 shows lattice parameter *a,* and unit cell volume vs. sintering temperature for samples doped at $x = 0.2$. The lattice parameter *a* decreases monotonically with increasing sintering temperature. The lattice parameter *c* varies very little with the sintering temperature and consequently the volume changes in a similar manner as *a*. As the decrease of lattice parameter *a* is an indication of the boron substitution for carbon and the decrease of lattice parameter *a* is more pronounced at temperatures above 900^{o}C, enhanced carbon substitution occurs at these high temperatures, which is consistent with several recent papers [16, 19]. However, the substitution reaction in the present work is far from its maximum achievable level even at sintering temperature of 1000^{o}C, in comparison with those treated at a higher temperature (1600^{o}C) and high pressure [16]. Thus, we achieved a condition of partial substitution of B for C. The majority of the carbon from the added CNT's stays within CNT's and small proportion of it is substituted for boron in MgB_2. Small amounts of carbon from CNT can also react with B to form BC, as detected using EELS [29]. Inset to Fig.4.3 shows the XRD data for carbon nanotube doped samples, sintered at three different temperatures. The sample was a well developed MgB_2 phase, with only a small amount of MgO present. No other impurities phase was detected by XRD even at high sintering temperature of 1000^{o}C.

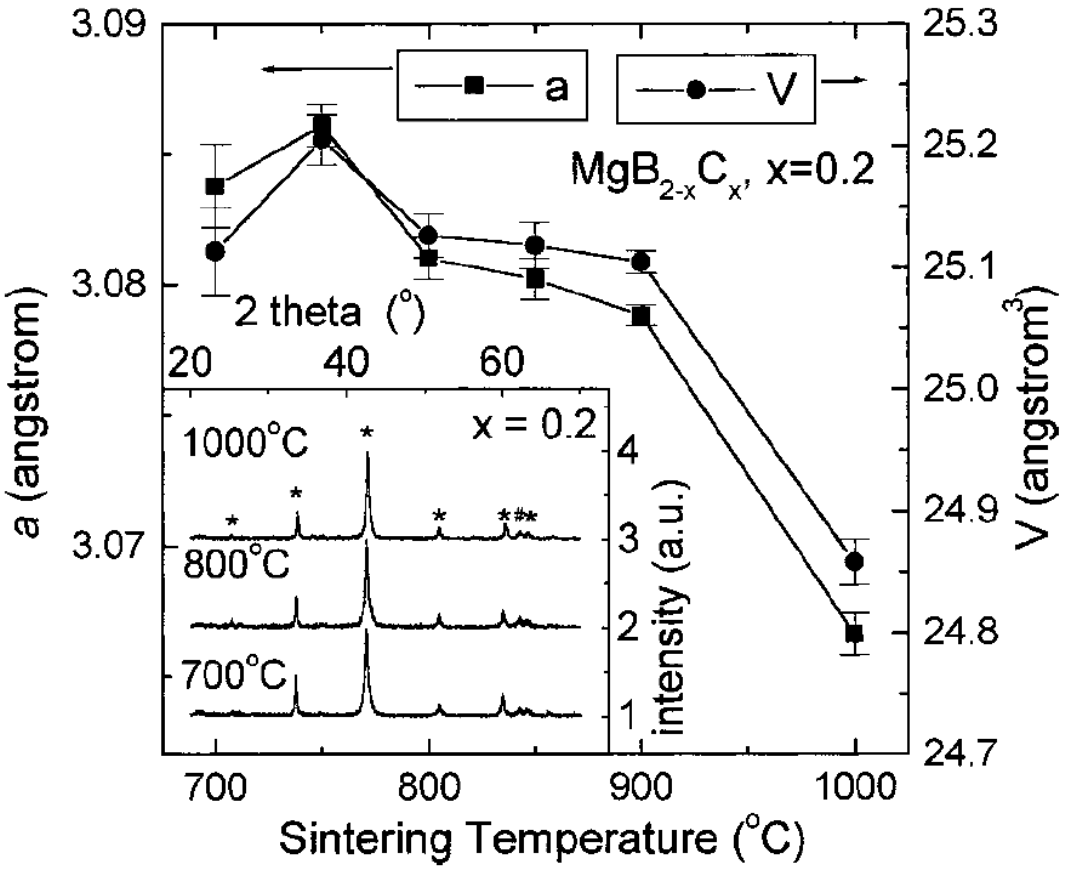

Figure 4.3: Variation of lattice parameter a and unit cell volume of $MgB_{2-x}C_x$, with nominal $x = 0.2$, with sintering temperature. The carbon was in the form of multi-walled carbon nanotubes. Inset: XRD pattern for carbon nanotube doped MgB_2, sintered at temperatures as indicated in the Figure. Symbols * and # indicate the XRD peaks for MgB_2 and MgO, respectively.

Figure 4.4 shows the shift in lattice parameter a as a function of the transition temperature, T_c for doped and undoped samples. The T_c obtained for the undoped sample is 37.5 K. For the doped samples, the T_c decreases with increasing carbon doping, which is consistent with recent reports [7,13,14,16,19,23,24,28,30]. The total T_c drop is only 2K with the nominal CNT doping level up to $x = 0.3$. The change of the lattice parameter a was rather small even up to 15% of nominal carbon content in the MgB_2 which is consistent with the small decrease of T_c. A similar decrease has also observed in the CNT samples prepared by Wei et. al [28]. The moderate shift of the

lattice parameter *a* may indicate the small fraction of carbon substitution in the boron site, which is due to the low sintering temperature (800^{o}C) and the short sintering time (30 min) where substantial carbon substitution is unlikely to happen. It should be noted that the values of *x* are the nominal values and actual substitution of C into B is expected to be less than these values.

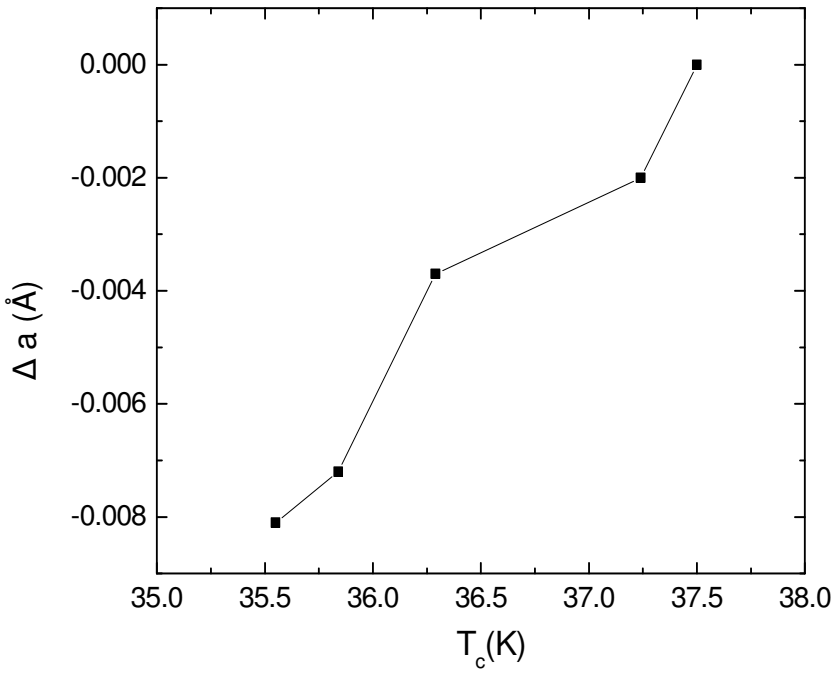

Figure 4.4. Difference in lattice parameter *a* as a function of transition temperature for CNT doped MgB_2 samples.

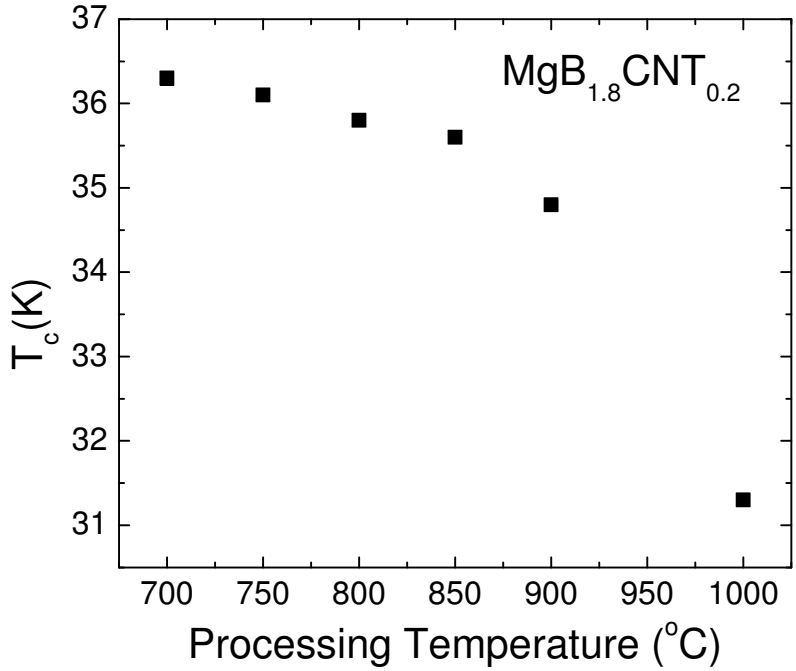

Figure 4.5 T_c determined by magnetic AC as a function of processing temperature for $MgB_{2-x}C_x$ with 30 minutes as the period of sintering.

Fig. 4.5 shows the transition temperature (T_c) for the sample doped at x=0.2 (10% of B) and sintered for a fixed period of 30min under different sintering temperatures. The T_c decreases with increasing sintering temperature, with a sharp drop to 31 K for the sintering temperature of 1000°C. This indicates that the extent of C substitution reaction increases with increasing sintering temperature, resulting in T_c depression, which is consistent with the lattice parameter a change in figure 4.4. These results confirm that only a small amount of C nanotube powder was substituted in the B position in the samples sintered at low temperature and a short period, consistent with small crystal lattice contraction. In order to improve the J_c at higher temperature, such as 20K, it is essential to maintain high T_c. The results indicate that by manipulating the processing parameters we could control the T_c while achieving a high level of C inclusion into MgB_2 sample, up to 10% of B. Because such C inclusion has little effect on T_c, the

partial substitution of boron for carbon and partial inclusion of nanocarbon particles into MgB_2 matrix may enhance flux pinning within a wide range of temperatures.

Therefore, we use two different types of incorporation of carbon into MgB_2: substitution and inclusion to improve the field dependence of J_c. The substitution effect is achieved when the C of CNT replaces the B site in the MgB_2, while the inclusion effect is due to the existing high aspect ratio of CNT embedded in the MgB_2 matrix.

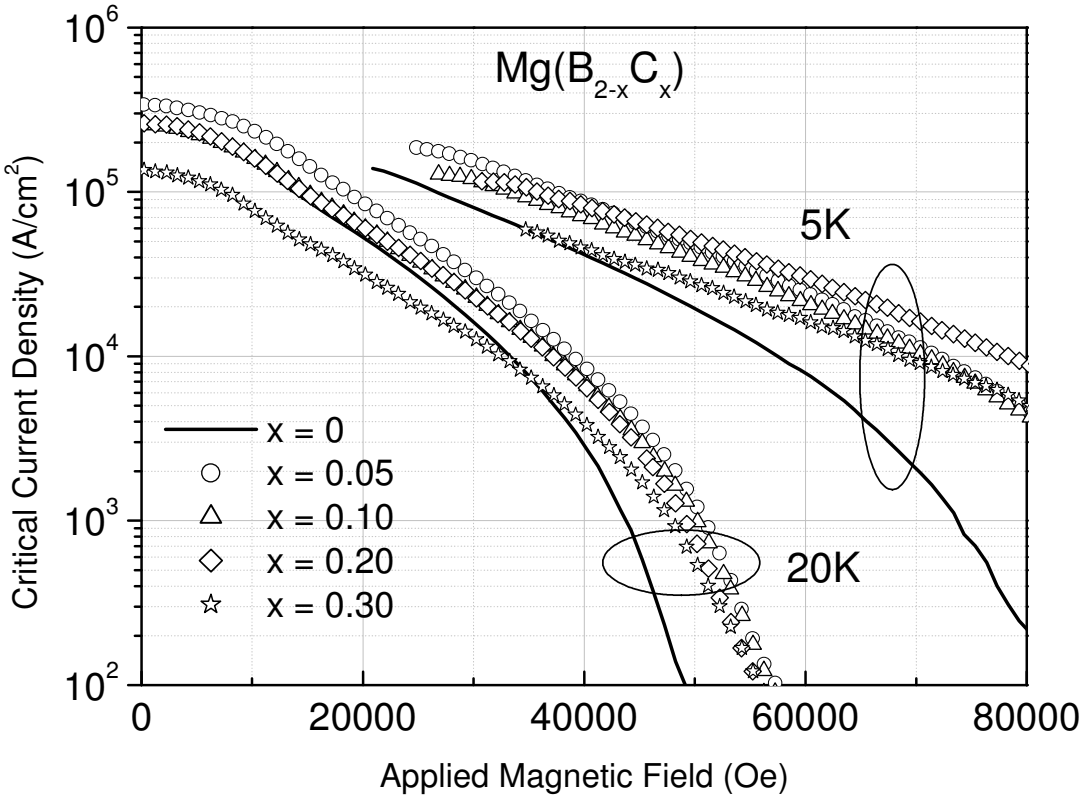

Figure 4.6. Critical current density as a function of magnetic field at 5K and 20K for different doping level of multi-walled carbon nanotubes.

Fig. 4.6 shows the $J_c(H)$ curves at 5K and 20K for the samples of $MgB_{2-x}C_x$, where x = 0, 0.05, 0.1, 0.2 and 0.3 are the nominal values for C content, with all the samples sintered at 800°C for 30min. All the $J_c(H)$ curves for doped samples have a higher J_c

than the undoped samples at high fields. The sample doped with 10% of carbon nanotubes (x = 0.2) gives the best J_c at high fields: J_c increases by a factor of 45 at 5K for the field of 8T, and at 20K for the field of 5T, as compared to the undoped sample. At higher doping level (x = 0.3), although the J_c in low field regime was depressed, the rate of J_c drop with H is much slower than for all other samples, clearly indicating strong flux pinning induced by the C nanotube doping.

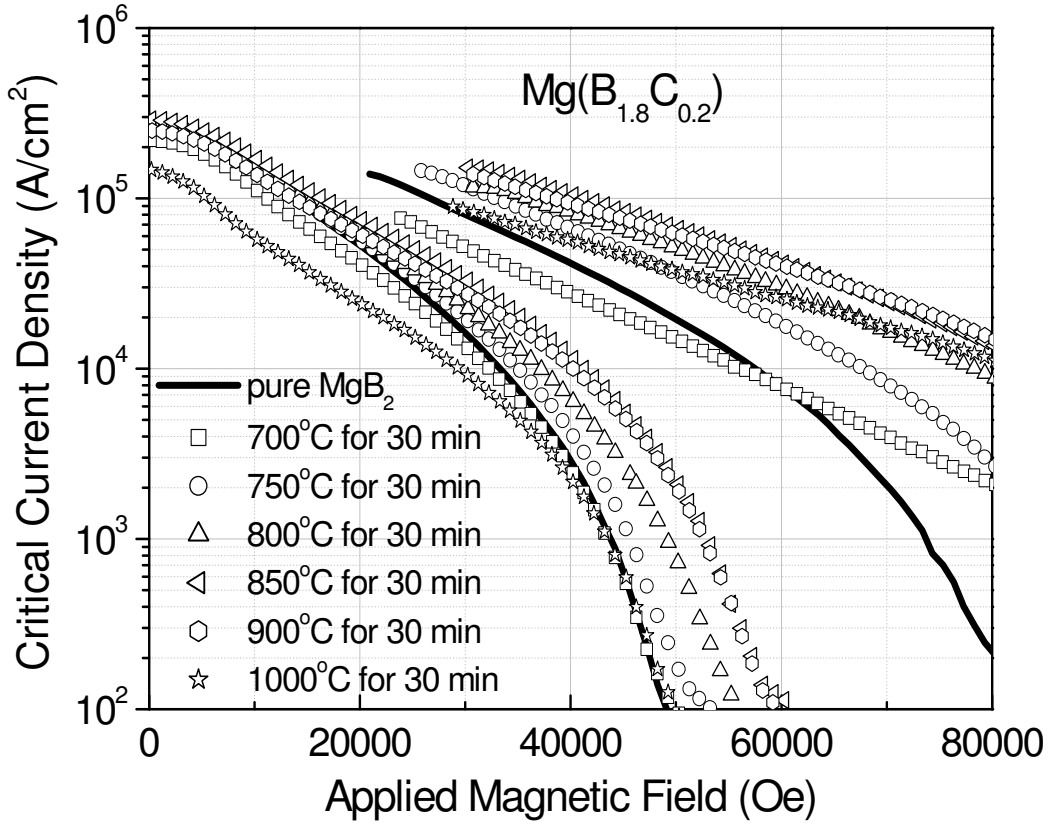

Figure 4.7. Critical current density as a function of magnetic field at 5K and 20K for $MgB_{1.8}C_{0.2}$, sintered at different temperatures for 30 minutes. The carbon was in the form of multi-walled carbon nanotubes.

Fig. 4.7 shows the $J_c(H)$ curves at 5 K and 20K for $MgB_{1.8}C_{0.2}$ sample sintered at temperatures from 700-1000°C for 30min. For comparison, the $J_c(H)$ curve for the undoped sample, MgB_2 sintered at 800°C is included. It is noted that the sintering temperature has a significant effect on the J_c performance in the field. A general trend is

such that the $J_c(H)$ characteristic is improved with increasing sintering temperature. Although the sample sintered at 1000°C has lower J_c values in low field regime, its $J_c(H)$ curve crosses over the $J_c(H)$ for the other samples in higher fields. As higher sintering temperature promotes the C substitution reaction for B, the improved field dependence of J_c measured at lower temperatures is clearly attributable to the C substitution. However, because C substitution depresses T_c, the $J_c(H)$ behaviour for samples processed at high temperatures deteriorates above 20K. Thus, it is important to control the extent of C nanotube substitution and inclusion to achieve the best combination of the substitution induced flux pinning and C nanotube additive pinning.

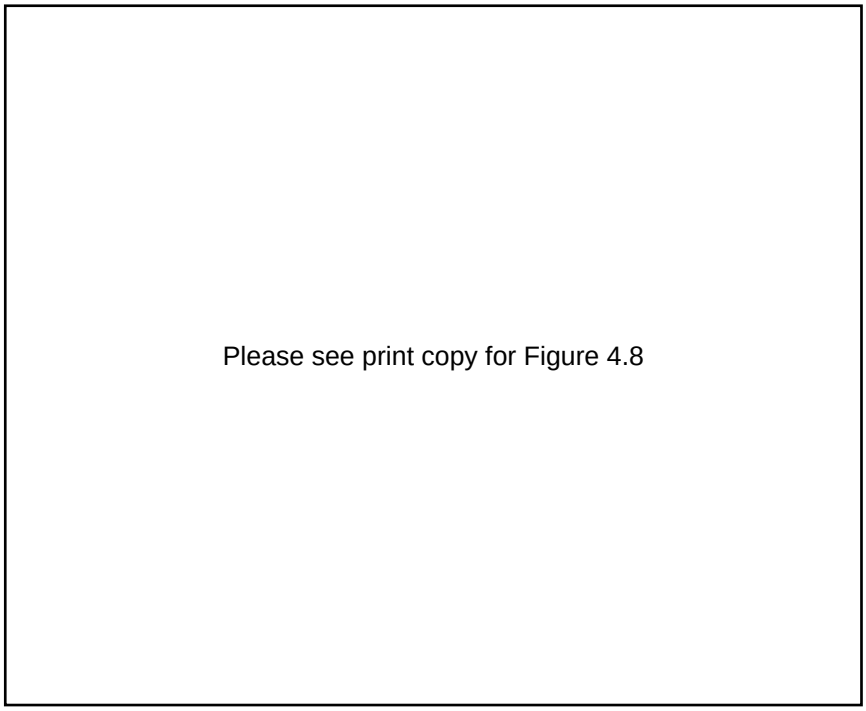

Figure 4.8. Irreversibility field for H_{irr} as a function of sintering time for $MgB_{1.8}C_{0.2}$ sintered at 900 and 1000 °C. H_{irr} obtained from $\Delta M(H)/V = 0.1\Delta M(0)/V$ is shown by triangles. H_{irr} obtained from $\Delta M(H)/V = 0.1\Delta M(0)/V$, but only for the screening around the whole of the sample, is shown by squares. The inset shows H_{irr} taken with the commonly used criterion of $J_c = 100$ A cm^{-2}. For more detail please refer to [31].

Figure 4.8 shows the irreversibility field H_{irr} as a function of the sintering time at 900 and 1000 °C and $T = 0.8\ T_c$. H_{irr} was defined in three different ways. The inset to figure 7 shows the results for the commonly defined H_{irr} as the field at which $J_c = 100$ A cm^{-2}. However, because superconducting screening in the bulk MgB_2 occurs at three different length scales [31], there is a pronounced step in $J_c(H)$, corresponding to superconducting screening on the length scale smaller than 1 μm. H_{irr} defined by $J_c =$ 100 A cm^{-2} is at this step [31] which may lead to wrong conclusions due to the observed difference of the microstructure of the measured samples. To avoid this, we also study the irreversibility field defined by $J_c/J_{c0} = 0.1$, above the large step in $J_c(H)$. Further, there is a smaller step in $J_c(H)$ at about 2 T, arising from another tier of superconducting screening on the length scale of 10 μm, as described in [31]. To avoid the artifacts that may arise from this superconducting screening, H_{irr} was also defined by $J_c/J_{c0} = 0.1$, but for J_c pertinent to the superconducting screening around the whole of the sample only. This J_c was obtained following the procedure described in [31]. Apparently, the results for all three H_{irr} show the same trend, ruling out the effects of the microstructure on the qualitative behaviour of H_{irr} with CNT doping and sintering at different temperatures. H_{irr} is the largest for 1000 °C sintering temperature, for all measured sintering times. The dependence of the lattice parameter a on the temperature of sintering shows that carbon substitution increases with the sintering temperature, especially above 900 °C. This would indicate that the carbon substitution introduces pinning centres and increases H_{irr}, in addition to increasing H_{c2}.

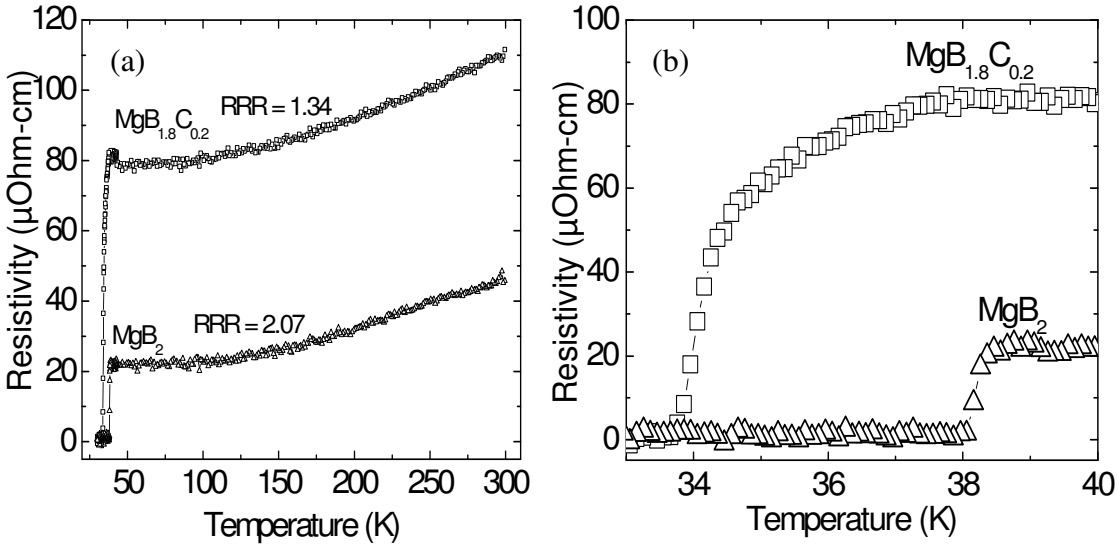

Figure 4.9. (a) Resistivity vs temperature for undoped and doped sample from 300K to 30K. (b) shows the transition near T_c.

Figure 4.9 displays resistivity of doped and undoped sample. Both samples show the metallic behaviour in the normal state resistivity. The resistivity of pure MgB_2 at 300K, ρ(300K), and 40K, ρ(40K), has the value of 46 μΩ-cm and 21 μΩ-cm respectively, described as the intermediate resistivity by Rowell [32]. The doped sample shows a higher value in both resistivities , 110 μΩcm and 81 μΩcm, respectively. Residual resistivity ratio, RRR, for doped and undoped sample is 1.34 and 2.07, respectively. Figure 4.9(b) is the close look to the temperature near T_c for two samples. The zero-field T_c for the undoped and doped sample is in agreement with AC susceptibility measurement. The undoped sample shows a sharp transition at T_c as compared to the doped sample. The $T_{c\text{-}onset}$ and the $T_{c\text{-}zero}$ of the undoped sample are higher than the doped samples by 0.7 K and 4.5 K, respectively. The increase of resistivity in the doped sample is due to the impurities between the superconducting grains (i.e. CNT's).

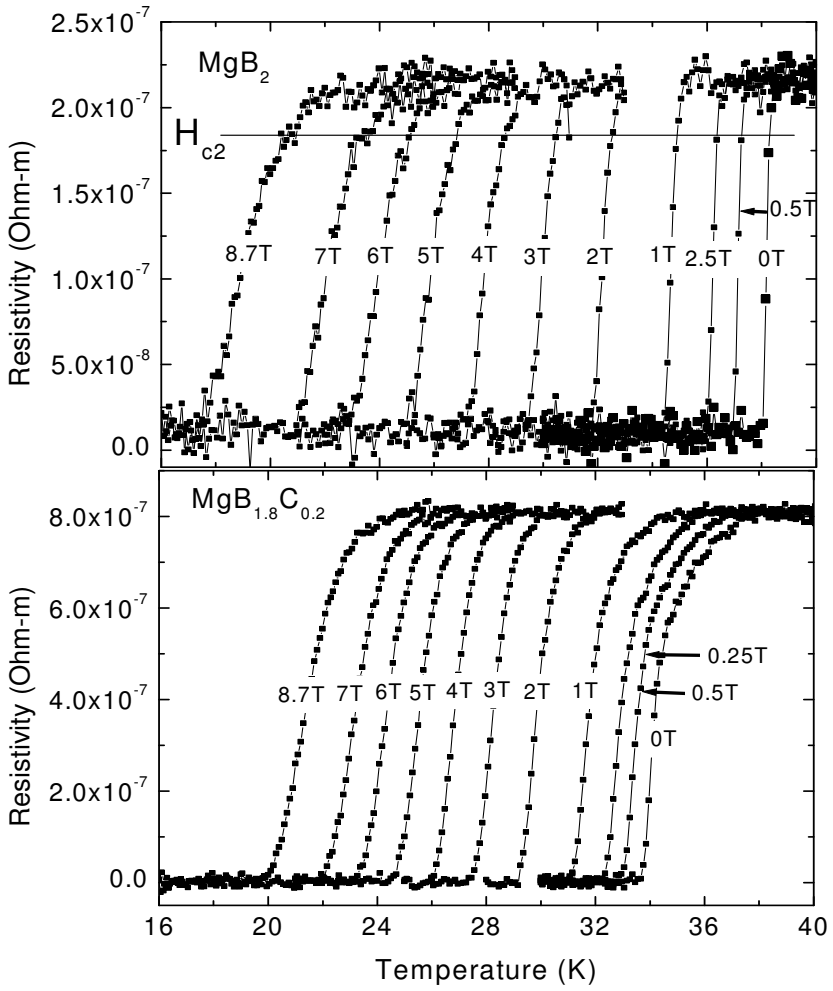

Figure 4.10. Temperature variation of electrical resistivity for magnetic filed H = 0,0.25, 0.5, 1, 2, 3, 4, 5, 6, 7 and 8.7 T for pure MgB_2 and $MgB_{1.8}C_{0.2}$.

Figure 4.10 shows the resistivity transitions in fields H ≤ 8.7T for undoped and doped samples. Although the T_c at H=0 decreases by C-substitution, the reduction of T_c by magnetic field becomes much smaller for the C-substituted sample than for the undoped one. This reflects an improvement of H_{c2} by carbon substitution through CNT doping .

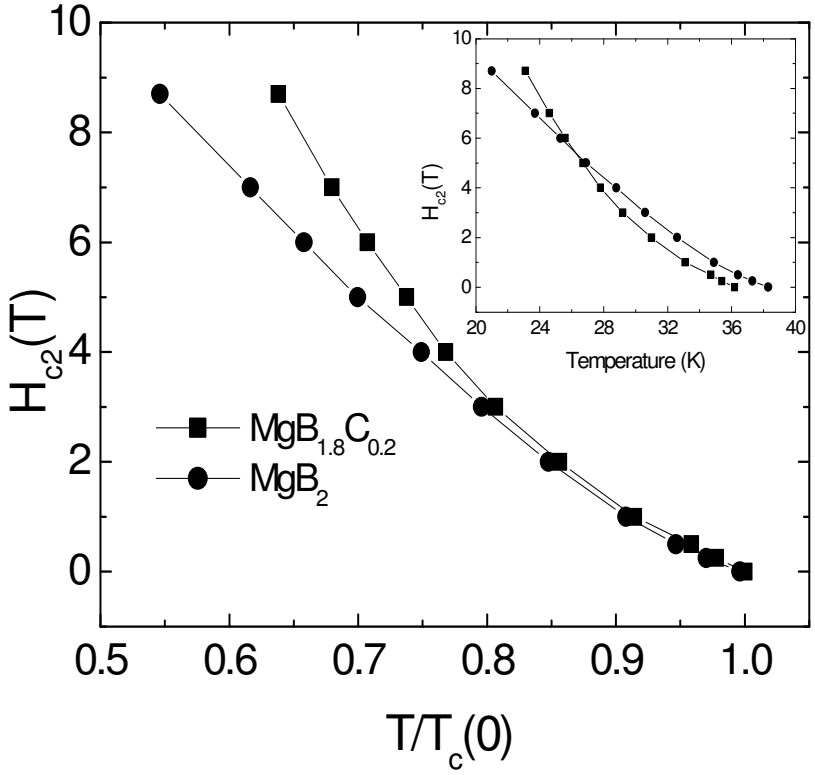

Figure 4.11. Normalized temperature *(T/T_c(0))* dependence of the upper critical field, H_{c2}, for pure MgB_2 and $MgB_{1.8}C_{0.2}$ with both samples processed at 900 °C. Inset: the same dependence, but versus the temperature.

Figure 4.11 compares the upper critical fields $H_{c2}(T)$ defined at 10% of normal state resistivity in the temperature dependence of resistivity curve. The values of H_{c2} are higher for CNT doped samples than for the pure MgB_2 at the same value of T/T_c. The inset to figure 4.11 shows H_{c2} as a function of temperature. Even though the value of T_c decreased with CNT doping, H_{c2} for the doped samples is still higher than for the pure MgB_2 for T < 26 K. The increase of H_{c2} indicates the increase of impurity scattering. Namely, $H_{c2}=\Phi_0/(\pi\xi_{ab})$ and coherence length ξ_{ab} decreases with the decrease of mean free path of charge carriers, l, due to impurity scattering, as expected from the relation $\xi_{ab}^{-1} \approx \xi_{0ab}^{-1} + l_{ab}^{-1}$. Here, ξ_{0ab} is in plane coherence length in clean limit [1]. The decrease of ξ_{ab} is due to the change from clean superconductor to a dirty superconductor

with CNT content, which has been seen as an increase of residual resistivity ratio in the doped samples.

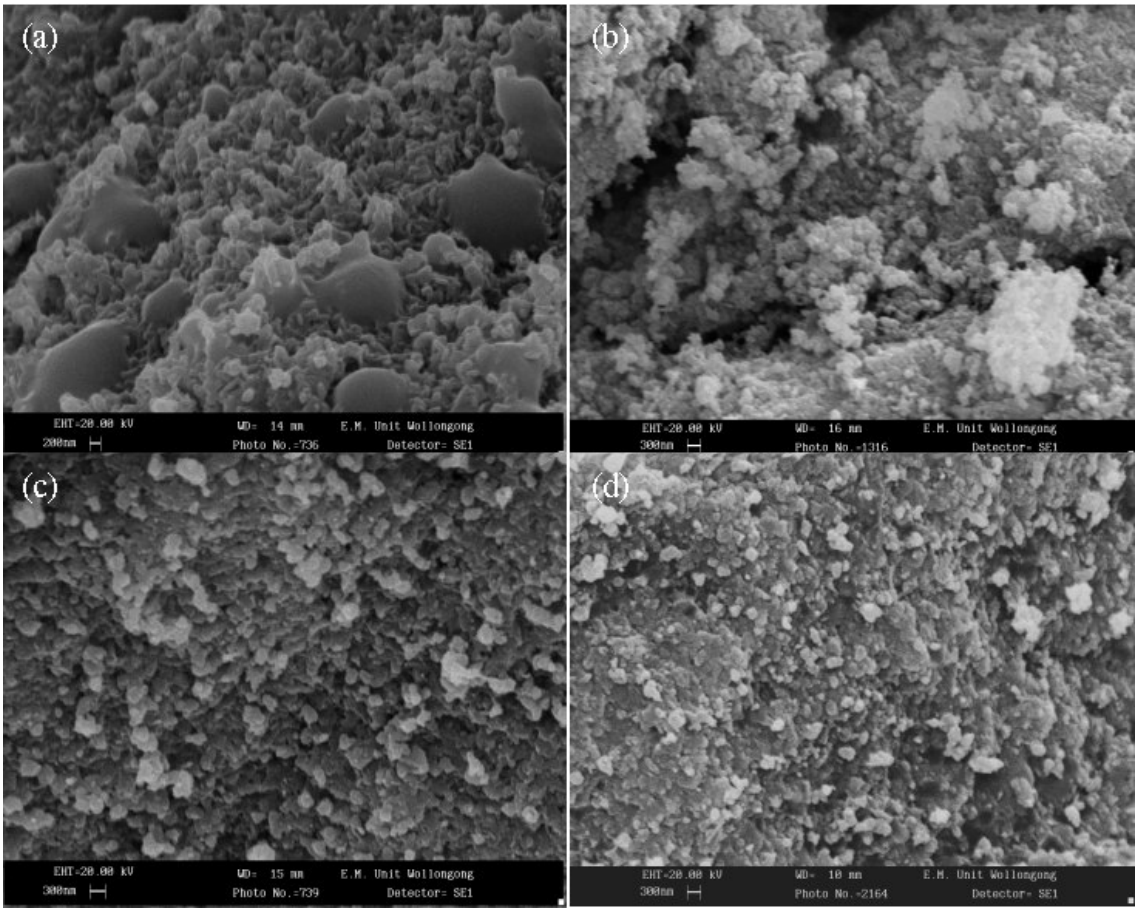

Figure 4.12. SEM images of (a) pure MgB_2 (b) $MgB_{1.8}C_{0.2}$ processed at 750^{o}C/30min (c) $MgB_{1.8}C_{0.2}$ processed at 900^{o}C/30min (d) $MgB_{1.8}C_{0.2}$ processed at 1000^{o}C/30min

SEM images of samples processed at different reaction temperatures, with 30 min of sintering time, are shown in figure 4.12, including the pure MgB_2. The images show a surface transition from 750 ˚C low reaction temperature to 900 and 1000 ˚C. Pure MgB_2 shows rough surfaces with a number of flakes observed within the grains. We believe that the poorer performance in $J_c(H)$ of pure MgB_2 is a consequence of the flakes which are the main obstacle for current flowing in MgB_2. This suggests that the CNT is playing an important role as a centre of formation of MgB_2. The samples synthesised at

1000 and 900 °C have a smaller grain size and better connectivity between the grains as compared to the other two samples.

Small particles of different size are found between the MgB_2 grains in the CNT doped samples, and the number of particles increases with the increase of reaction temperature. However, sample (c) shows a better performance in $J_c(H)$ (~11 times at high field and low temperature) than sample (d) although they share similar microstructure. This has excluded the possibility that improvement in $J_c(H)$ is due entirely to the finer microstructure, implying that defects like carbon substitution act as pinning centres in theMgB_2 grains that enhance the $J_c(H)$.

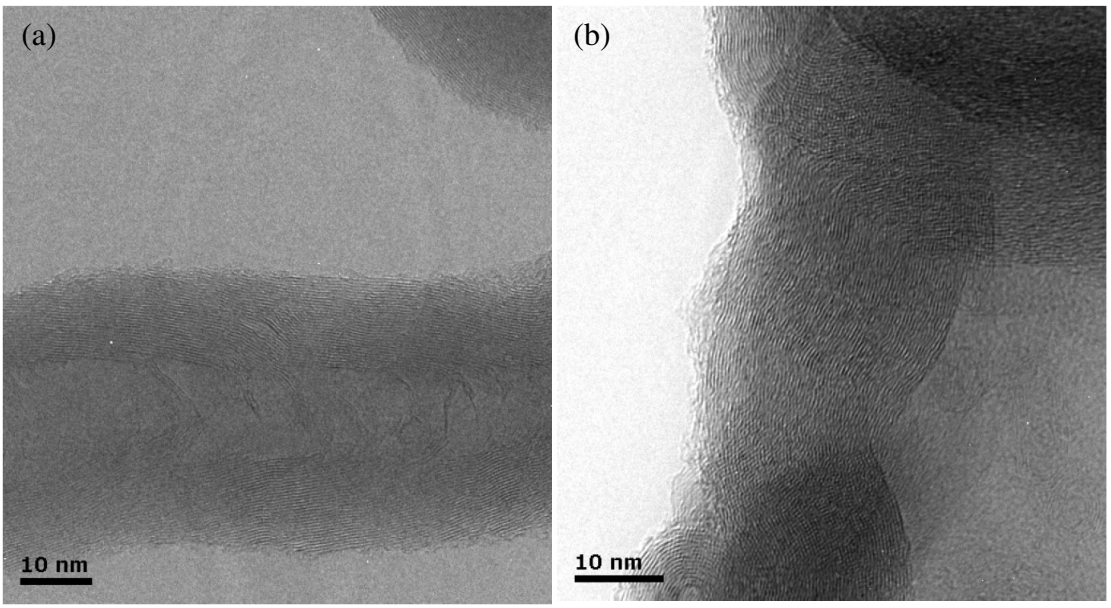

Figure 4.13. TEM images of enlarge CNT that was doped in the samples processed at 750 °C (a) and 900 °C (b) for $MgB_{1.8}C_{0.2}$.

Figure 4.13 shows the enlarged image of CNT in the samples processed at 750°C and 900°C. For the synthesis temperature of 750 °C, the undistorted CNT's can be clearly observed (see figure 4.13 (a)). For the synthesis temperature of 900 °C, CNT's are still

present; however, they are distorted. This distortion indicates that some of the carbon from the nanotubes was substituted into the MgB_2 crystals for high sintering temperatures, which is in agreement with the faster decrease of the lattice parameter *a* for synthesis temperatures higher than 900 °C. This again implies that the high synthesis temperatures induce distortion and carbon substitution in the MgB_2 thus, enhancing the vortex pinning.

4.4 Conclusion

In summary, the effect of C nanotube doping on lattice parameters *a* and *c*, critical transition temperature (T_c) , critical current density (J_c) and flux pinning in MgB_2 was investigated under a wide range of processing conditions. It was found that substitution of B for C from CNT enhances the flux pinning but depresses T_c slightly. By controlling the processing parameters, an optimized $J_c(H)$ performance is achieved under a partial C substitution and CNT inclusion. Under these conditions, J_c was enhanced by two orders of magnitude at 8 T and 5 K, and at 7T and 10 K. The J_c was more than 10,000A/cm^2 at 20 K in field of 4 T and at 5 K in field of 8.5 T, respectively. Carbon nanotube inclusions and B substitution for C are proposed to be responsible for the enhancement of flux pinning in high fields.

Nevertheless, enhancement of H_{c2} and H_{irr} shown by CNT doped samples show that the effect of CNT doping is two-fold. Incorporation of whole CNT's into the crystal matrix, obtained with synthesis at temperatures below 900 °C, increases the vortex pinning. This is because the size of the nanotubes is of the same order as the coherence length of MgB_2. Synthesis at higher temperatures results in partial decomposition of the

nanotubes and substitution of boron in MgB_2 crystals for carbon released from the CNT's. This results in an increase of H_{c2}, as predicted by the theory of two-band scattering [1], and in further improvement of vortex pinning.

4.5 References

[1] A. Gurevich, *Phys. Rev. B* **67**, 184515 (2003).

[2] S. X. Dou, S. Soltanian, J. Horvat, X. L. Wang, P. Munroe, S. H. Zhou, M. Ionescu, H. K. Liu and M. Tomsic, *Appl. Phys. Lett.* **81**, 3419 (2002).

[3] J. Kortus, I. I. Mazin, K. D. Belashchenko, V. P. Antropov, and L. L. Boyer, *Phys. Rev. Lett*. **86**, 4656 (2001).

[4] J. M. An and W. E. Pickett, *Phys. Rev. Lett*. **86**, 4366 (2001).

[5] I. I. Mazin and V. P. Antropov, *Physica C* **385**, 49 (2003).

[6] T. Takenobu, T. Ito, D. H. Chi, K. Prassides and Y. Iwasa, *Phys. Rev.* B **64**, 134513 (2001)

[7] M. Paranthaman, J. F. Thompson and D. K. Christen, *Physica* C **355** 1 (2001)

[8] J. S. Ahn and E. J. Choi *Preprint* cond-mat/0103169 (2001)

[9] W. Mickelson, J. Cumings, W. Q. Han and A. Zettl, *Phys.Rev.* B **65**, 052505 (2002)

[10] Z. H. Cheng, B. G. Shen, J. Zhang, S. Y. Zhang , T. Y. Zhao and H. W. Zhao H-W *J. Appl. Phys.* **91**, 7125 (2002)

[11] I. Maurin, S. Margadonna, K. Prassides, T. Takenobu, Y. Iwasa and A. N. Fitch, *Chem. Mater.* **14**, 3894 (2002)

[12] I. Maurin, S. Margadonna, K. Prassides, T. Takenobu, T. Ito, D. H. Chi, Y. Iwasa and A. Fitch, *Physica* B **318**, 392 (2002)

[13] A. Bharathi, S. Jemina Balaselvi, S. Kalavathi, G. L. N. Reddy, V. Sankara Sastry, Y. Haritharan and T. S. Radhakrishnan, *Physica* C **370**, 211 (2002)

[14] R. A. Ribeiro, S. L. Bud'ko, C. Petrovic and P. C. Canfield, *Physica* C **385**, 16 (2003)

[15] R. A. Ribeiro, S. L. Bud'ko, C. Petrovic and P. C. Canfield, *Physica* C **384**, 227 (2003)

[16] S. Lee, T. Masui, A. Yamamoto, H. Uchiyama and S. Takama *Physica* C **397**, 7–13 (2003)

[17] P. Samuely, Z. HoIanova, P. Szabo, J. Kacmarcık, R. A. Ribeiro, S. L. Bud'ko and P. C. Canfield, *Phys. Rev.* B **68**, 020505(R) (2003)

[18] H. Schmidt, K. E. Gray, D. G. Hinks, J. F. Zasadzinski, M. Avdeev, J. Jorgensen and J. C. Burley *Phys. Rev.* B **68**, 060508(R) (2003)

[19] M. Avdeev, J. D. Jorgensen, R. A. Ribeiro, S. L. Bud'ko and P. C. Canfield, *Physica* C **387**, 301 (2003).

[20] P .P. Singh, *Solid State Communications* **127**, 271-274 (2003)

[21] M. Pissas, D. Stamnopoulos, S. Lee and S. Tajima, *Phys. Rev.* B **70**, 134503-1 (2004)

[22] T. Masui, S. Lee and S. Tajima, *Phys. Rev.* B **70**, 024504-1 (2004)

[23] E. Ohmichi, T. Masui, S. Lee, S. Tajima and T. Osada, *Phys. Rev.* B **70**, 1-5 (2004)

[24] R. H. T. Wilke, S. L. Bud'ko, P. C. Canfield, D. K. Finnemore, R. J. Suplinskas and S. T. Hannahs, *Phys. Rev. Lett.* **92** 217003 (2004)

[25] R.A. Ribeiro, S. Bud'ko, C. Petrovic, P.C. Canfield, *Physica C* **382**, 166 (2002).

[26] S. Soltanian, J. Horvat, X. L. Wang, P. Munroe and S. X. Dou, *Physica C* **390**, 185 (2003).

[27] C.H. Cheng, H. Zhang, Y. Zhao, Y. Feng, X. F. Rui, P. Munroe, H. M. Zeng, N. Koshizuka and M. Murakami, *Appl. Phys. Lett.* **83** 2916 (2003).

[28] J. Wei, Y Li, C. Xu, B. Wei, and D. Wu, *Mater. Chem. Phys*. **78**, 785 (2003).

[29] S. X. Dou, V. Braccini, S. Soltanian, R. Klie, Y. Zhu, S. Li, X. L. Wang, D. Larbalestier, *J. of Appl. Phys.* **96** 7549 (2004)

[30] S. Soltanian, J. Horvat, X. L. Wang, P. R. Munroe and S. X. Dou, *Physica* C **390**, 185 (2003)

[31] J. Horvat, S. Soltanian, A. V. Pan and X. L. Wang, *J. Appl. Phys.* **96**, 8 (2004).

[32] J. M. Rowell, *Supercond. Sci. Technol.* **16**, R17 (2003)

Chapter 5: Effect of Carbon Nanotube Dimensions and Improving the Flux Pinning in MgB_2 by Ultrasonication

5.1 Introduction

The nanoparticles have to satisfy certain criteria to be acceptable as pinning centers. Their presence should not affect the formation of superconducting phase and they should disperse homogenously into the superconducting matrix. By creating centers for scattering of charge carriers via doping of MgB_2, the superconductor will be pushed to the dirty limit by shortening the mean free path of the charge carriers. In the case of carbon doping, it was shown that even with the $x = 0.2$ for $MgB_{1.8-x}C_x$, the two gap superconductivity has still been preserved [1].

It has been demonstrated that carbon nanotubes can be embedded in Bi-2212, thus offering a promising method for introduction of extended defects in superconductor [2]. The reason CNT is chosen is due to its special geometric ratio and mechanical properties. The magneto-optical image investigations have revealed that CNT's are functioning like columnar defects, enhancing J_c in the Bi-based superconductor [3]. However, the flux-pinning properties were improved only at low temperatures below 52 K [2].

As indicated in our previous chapter, carbon nanotube (CNT) doping can simultaneously address two different but related issues in MgB_2: H_{c2} and flux pinning. Carbon from a small fraction of CNT can substitute B in MgB_2, while the unreacted CNT can act as effective pinning centers due to their size. However, achieving homogeneity in the CNT doped MgB_2 remains a major challenge, as nanotubes tend to entangle, preventing their mixing with MgB_2 and dispersion. It remains unclear how the dimensions of CNT affect the J_c. We demonstrated that significant fraction of CNT can be successfully embedded into the MgB_2 matrix, as indicated by the TEM and J_c measurements. The TEM images showed that CNT's are still present after sintering at the temperature as high as 900^{o}C. The results also indicate that further improvement of CNT doped samples can be achieved by varying the sintering temperature and sintering time.

High intensity ultrasonic excitation can induce a wide range of effects. The high local temperatures and pressures during the ultrasonication provide extreme conditions for chemical reaction, enhancing the reactivity of the chemicals. Yu et al. [4] discovered that, entangled nanotube structure was broken into individual short bundles and tubes after 2 hours of high intensity ultrasonication. Shockwaves created by the ultrasound induce high velocity collisions among suspended solid particles, resulting in more completely grinded grains. The process is so aggressive that it overcomes usual surface limitations, and generates a uniform composite with nanoparticles in the slurry. Prozorov et al. have successfully modified the superconducting properties of MgB_2 [5] and $Bi_2Sr_2CaCu_2O_{8+x}$ superconductor [6] by high intensity ultrasonic irradiation.

In this chapter we study the effect of varying the diameter, length and the aspect ratio of CNT (table 5.1 and figure 5.1) on the J_c, T_c and unit cell structure of the doped MgB_2. It is also important to investigate issue of nanotube dispersion. In this case, low intensity ultrasonication technique was employed to prevent any undesirable reactions due to ultrasonication. Furthermore, acetone was used as medium of ultrasonication, which easily evaporated after ultrasonication.

Table 5.1 Outside diameter and length of carbon nanotubes used

Sample	CNT's' outside diameter (nm)	CNT's' average length (μm)
A	< 8	0.5-200
B	8-15	0.5-200
C	20-30	0.5-2
D	60-100	5-15

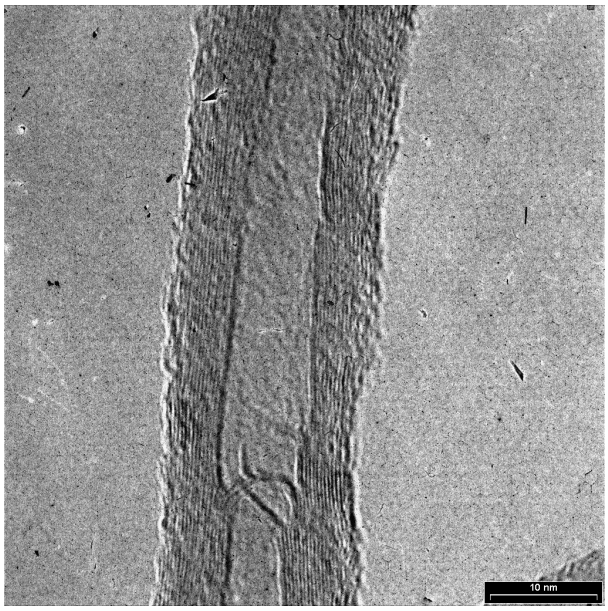

Figure 5.1 TEM images of carbon nanotube with 8-15nm diameter under high magnification

5.2 Experimental

MgB_2 pellets were prepared by conventional solid-state reaction. High purity powders of magnesium (99%), amorphous boron (99%) and multi-walled carbon nanotubes were weighed out according to the nominal atomic ratio $MgB_{1.8}C_{0.2}$ and well mixed through grinding. To disperse the CNT homogenously, the well-mixed powder was agitated by ultrasound. The ultrasonication was performed by Unisonic Ultrasonic Cleaner Model FXP 10 (60Hz) for 30 min with acetone as medium. The acetone was easily removed after the ultrasonication by heating up in the oven. All the samples were pressed into pellets of 13 mm in diameter and 1 mm thickness. The pellets were sealed in Fe tubes, then heat treated in flowing high purity Ar for 900^{o}C for 30 minutes, followed by a furnace cooling to room temperature. An undoped sample was also made under the same conditions for use as a reference sample.

A MAC Science MX03 diffractometer with Cu K_α radiation was used to determine the phase and crystal structure of all the samples. Si powder was used as an internal standard to calculate the lattice parameters. The magnetization was measured by a physical property measurement system (PPMS, Quantum Design). J_c was calculated from the height of the magnetization loop ΔM using the critical state model (refer chapter 3). Bar shaped samples with a size of $3 \times 1.5 \times 1$ mm^3 were cut from each pellet for magnetic measurements. T_c was obtained from the measurements of AC susceptibility. TEM was used to assess the homogeneity and the crystallinity over smaller length scales.

5.3 Results and Discussions

5.3.1 Comparison of CNT with different dimension

The XRD patterns for the three samples corresponding to different diameter of CNT's are shown in Fig. 5.2 with pure Si as reference. It can be seen from the XRD patterns that the major phase is MgB_2, with a minor phase of MgO, as reported in the previous studies [7, 8]. There is a shift of the (110) peaks to the higher angle that indicated a distortion of the lattice parameter *a*, although all the samples have the same nominal composition. This difference in the distortion of the MgB_2 lattice suggests that different level of substitution occurred, which may be due to the effect of CNT geometry or homogeneity of the mixing. However, the lattice parameter *c* remains the same.

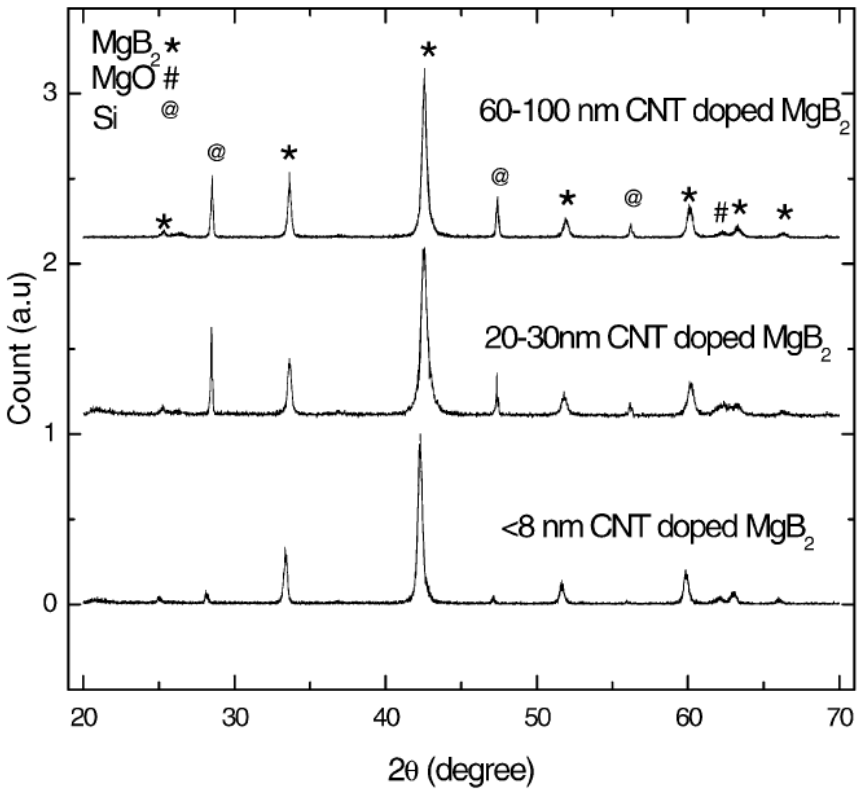

Figure 5.2 X-ray diffraction pattern of MgB_2 doped with carbon nanotubes of different diameter, processed at 900°C for 30 minutes.

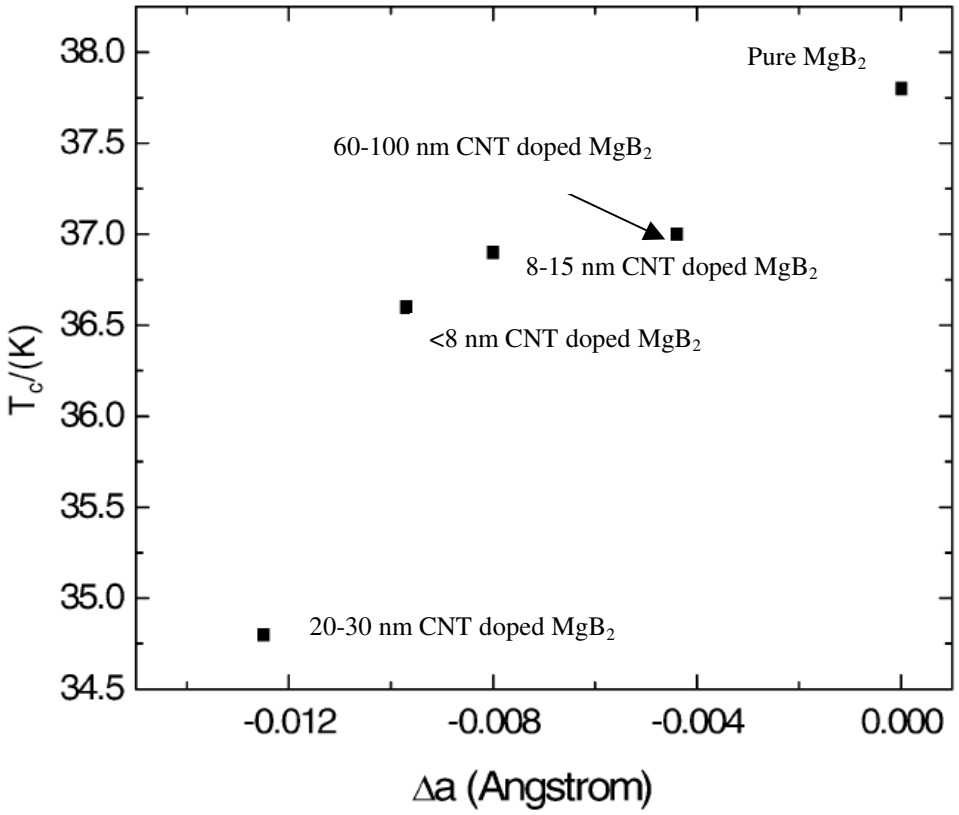

Figure 5.3 Critical temperature, T_c as a function of change of lattice parameter a. Reference sample is also included as comparison. All the samples were processed at 900^{o}C for 30min.

The T_c values, shown in Fig. 5.3 against the shift of lattice parameter a, were defined by the onset of superconducting screening in ac susceptibility measurements. The result for pure MgB_2 is included for comparison. The 20-30nm CNT doped MgB_2 showed the largest change in a, followed by < 8nm, 8-15nm and 60-100nm CNT doped MgB_2. The T_c decreased rapidly with the increase of distortion. T_c drops to 34.4 K with the change of Δa by 0.1252 Å for 20-30nm CNT doped MgB_2. For the sample of 60-100nm CNT doped MgB_2, T_c was 37 K with of a by 0.0044 Å . As suggested by Wilke et al., T_c may be used as an indicator of how much carbon is in MgB_2 [9].

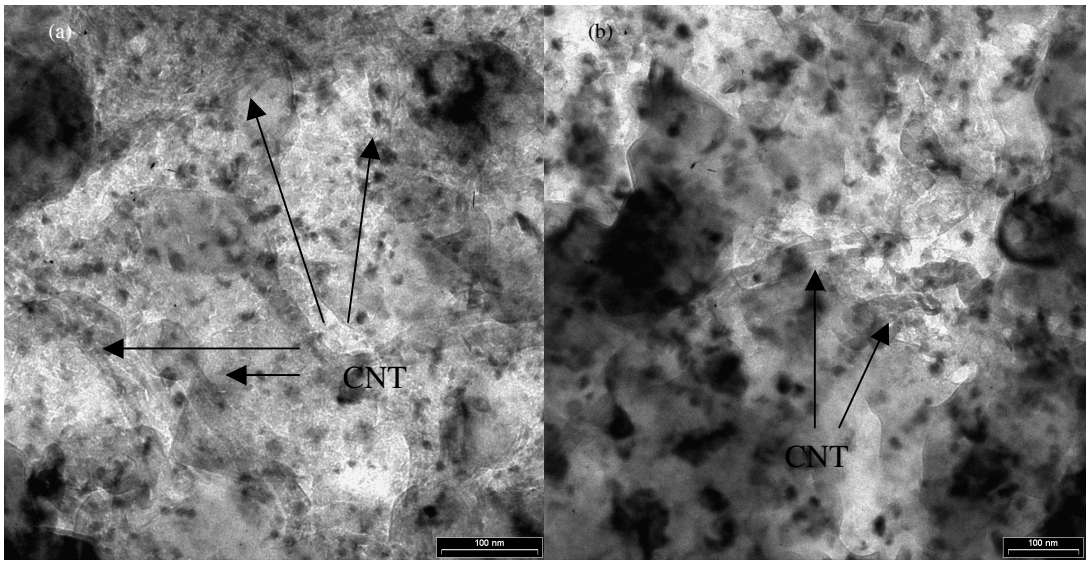

Figure 5.4 TEM image showing the carbon nanotubes embedded into the MgB_2 matrix for (a) carbon nanotube with diameter 8-15nm and (b) carbon nanotube with diameter 20-30nm.

Figure 5.4 shows the TEM image for MgB_2 doped with CNT of 8-15nm and 20-30nm in diameter. The picture shows that some CNT's are well embedded in the grains of MgB_2 for all diameters of CNT. The reacting temperature of MgB_2 that offered the possibility to encapsulate the nanotubes in the superconductor matrix was around 600^oC. This would suggest that the nanotubes could get embedded within the grains before the sintering temperature of 900^oC is reached. At the same time this encapsulation restricted the reaction of oxygen with CNT. This microstructure provides the samples with a good grain connection for the MgB_2 phase and high density of flux-pinning centers created by the CNT.

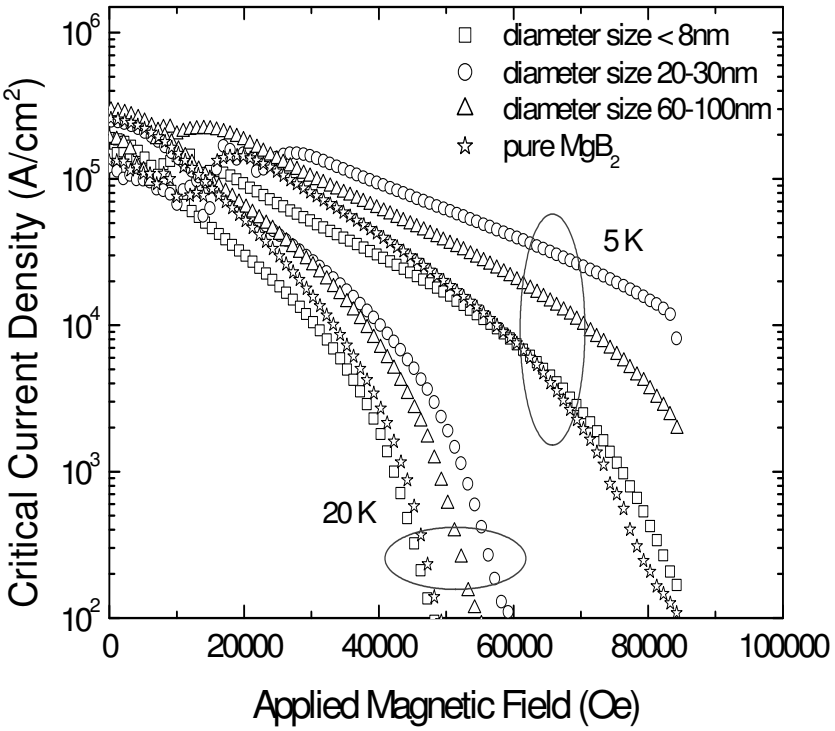

Figure 5.5 A comparison of magnetic J_c (H) at 5K and 20 K for all the carbon nanotube doped samples and the pure MgB_2.

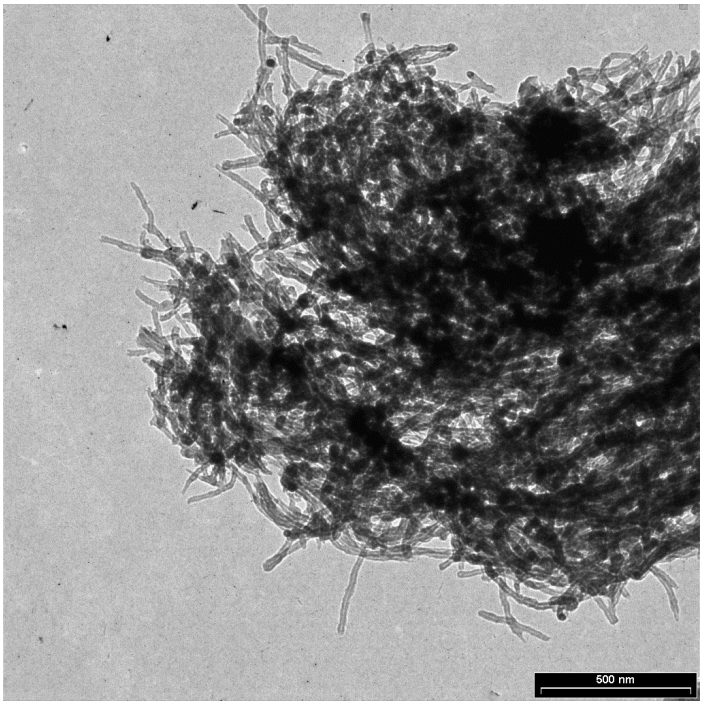

Figure 5.6 TEM image showing agglomeration of carbon nanotubes in MgB_2 with nanotube diameter 8-15nm.

However, longer CNT's tend to entangle and agglomerate, that makes the mixture inhomogeneous. CNT's with outside diameter <8nm and 8-15nm have the longest length of all the other nanotubes used. The J_c for samples doped with these nanotubes was the lowest, as shown in figure 5.5. It should be noted that the inhomogeneous mixing causes the J_c of sample to become lower than the pure MgB_2. TEM image in figure 5.6 showed that the unreacted CNT's were found in the CNT doped MgB_2. This also suggests that the pinning behaviour of the CNT doped MgB_2 depends on the density of the unreacted CNT's in the samples. We believe that the unreacted CNT's will block the transport of the current density and suppresses the $J_{c.}$ This also implies that most of the CNT doped MgB_2 samples are not homogenous and may not have an even distribution of nanotubes. The same problem was faced by Galvan et al. [10] when they embedded nanotubes in the Bi-based superconductor. This suggests that shorter length nanotube would be the solution for more homogenous mixing and substitution. TEM studies again confirmed that nanotube –like structures were present in the samples after full processing even at high temperature.

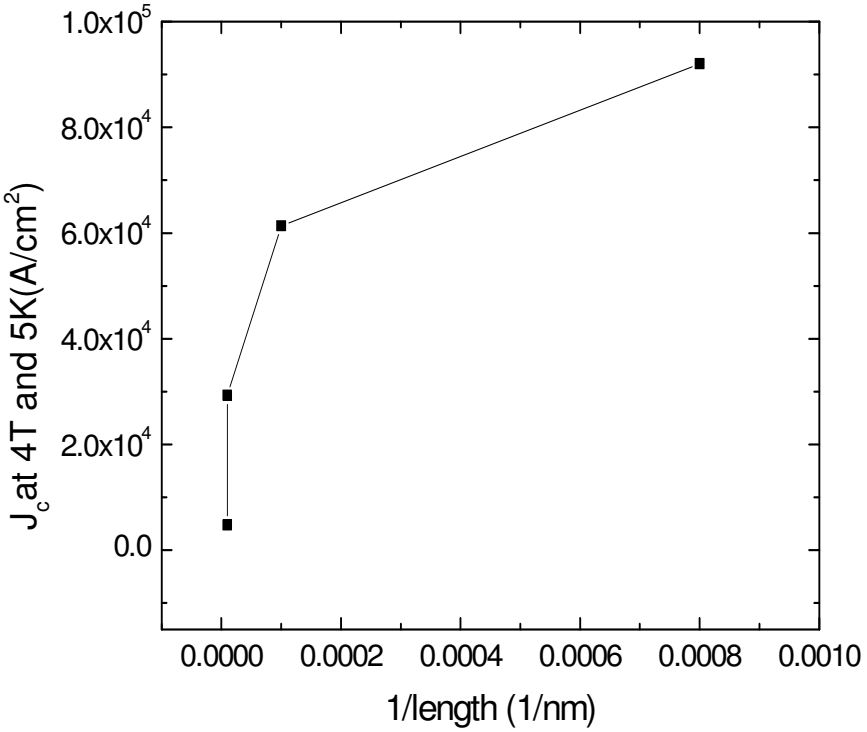

Figure 5.7: Dependence of J_c as a function of the average length of nanotubes incorporated into the MgB_2 matrix. The solid line through the points is guide to the eye.

Figure 5.7 shows that J_c changed with the length of the CNT. The graph indicates that shorter length of CNT will result in a higher density of CNT in the MgB_2, because longer CNT tend to agglomerate and entangle with each other. As a result, the main factor to successfully embed the CNT in the MgB_2 will be the length of nanotubes instead of their diameter. As a result, an improved preparation method has been designed to disperse the CNT homogenously in the MgB_2 matrix.

5.3.2 Dispersion of CNT's by Ultrasonication

Table 5.2 displays the T_c and sample density for normal grinding and with ultrasonication treatment after grinding for all CNT doped MgB_2. As reported in our previous chapter and section 5.3.1, for the sample doped nominally with 10 at. % CNT

the T_c decreased with increasing sintering temperature. However, it should be noted only a small portion of carbon from CNT actually replaces boron in MgB_2, depending on processing procedure. The extent of C substitution in MgB_2 increases with increasing sintering temperature. In this work we process all the samples at 900^{o}C, the only difference being the length and diameter of CNT's. The T_c for all four samples was further degraded by 0.5-2 K if the ultrasonication was used to disperse CNT's. This clearly indicates that ultrasonication promoted the reaction between CNT and MgB_2 as CNT's are better dispersed by ultrasonication. It is interesting to note that samples with CNT having OD 20-30nm show a noticeably lower T_c than others, which suggests that the short CNT's have higher reactivity than the long CNT's presumably because CNT's donate carbon from their ends**.** The ultrasonication also increases the density of the samples, which is believed to enhance the $J_c(H)$ in high field [11]. Figure 5.8 shows superconducting critical temperature versus unit cell volume for both ultrasonicated and normally prepared samples. It is apparent that T_c for normal and ultrasonicated samples shows the same monotonic decrease with the unit cell volume. However, the unit cell for the normally prepared sample is bigger than for the corresponding ultrasonicated sample. The contraction of unit cell and T_c for ultrasonicated samples indicates that more carbon substitution on boron sites takes place.

Table 5.2: Variation of outside diameter, length of CNT, critical temperature and density of the sample for the CNT doped MgB_2 prepared by normal grinding and ultrasonication

Sample	CNTs' outside diameter (nm)	Normal grinding		Grinding and Sonication	
		T_c(K)	Density (mg/mm^3)	T_c(K)	Density (mg/mm^3)
A	< 8	36.40	1.137	35.56	1.302
B	8-15	36.93	0.866	35.44	1.109
C	20-30	34.51	1.180	34.03	1.204
D	60-100	37.09	1.112	35.05	1.340

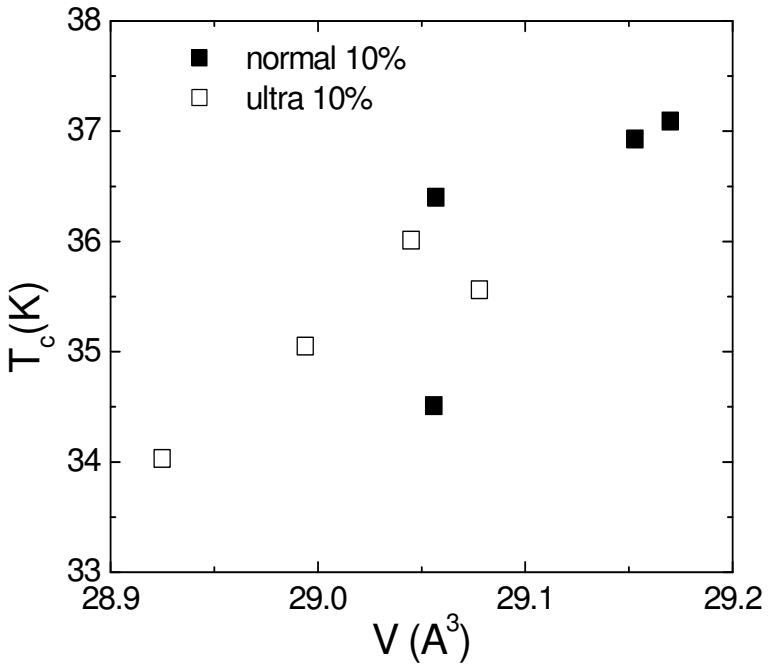

Figure 5.8: Variation of critical temperature with the unit cell volume of CNT doped $MgB_{1.8}C_{0.2}$.

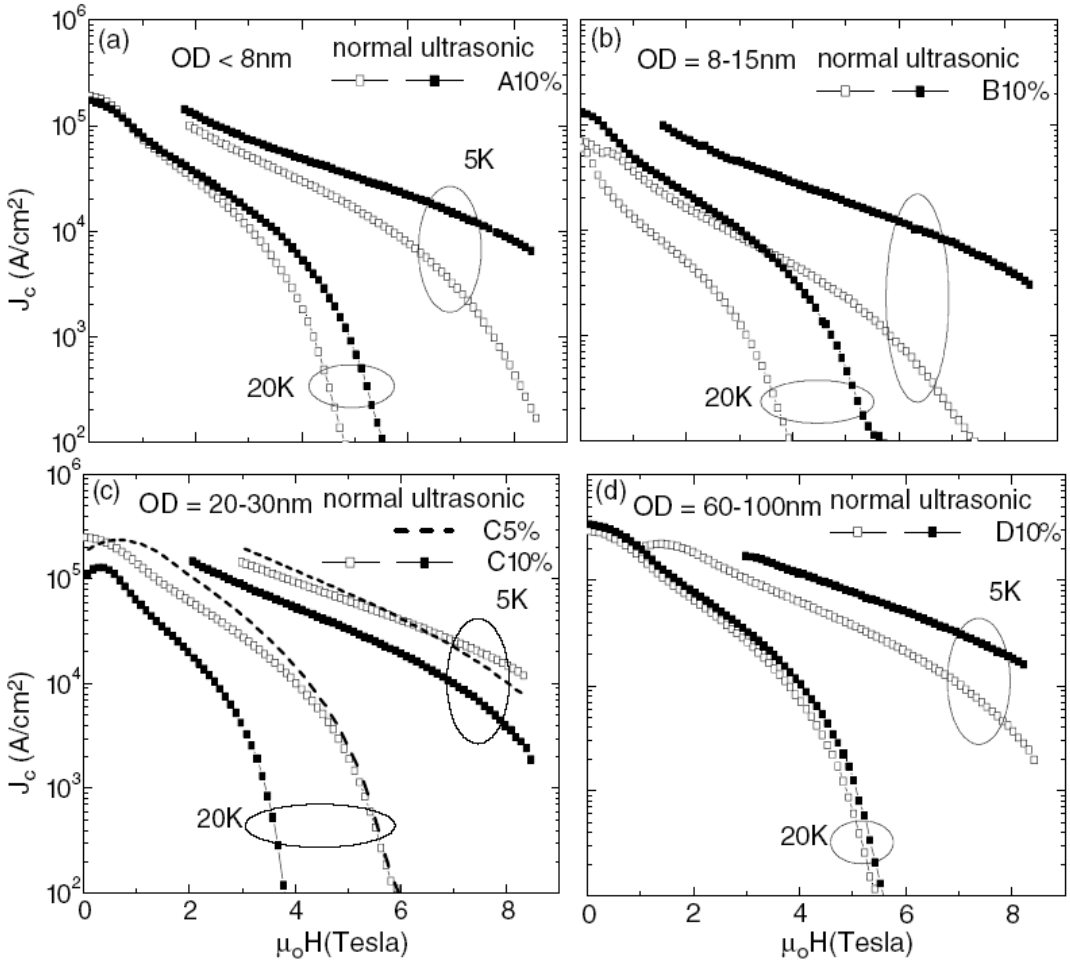

Figure 5.9: Critical current density as a function of applied magnetic field at 5 K and 20 K for both normal grinding and ultrasonicated after grinding MgB_2, doped (a) 10at. % of OD < 8nm CNT, (b) 10at. % of OD 8-15 nm CNT, (c)CNT 10% and at. 5% of OD 20-30 nm CNT and (d) 10at. % of OD 60-100 nm

Figure 5.9 shows a comparison of $J_c(H)$ curves at 5 and 20 K for samples A, B, C and D with and without ultrasonication. The critical current density is enhanced for all of the samples after the ultrasonic treatment except for sample C at the 10% doping level. The most significant enhancement was observed for samples A and B, which contain long CNT's (0.5–200 μm). The improvement of $J_c(H)$ for the ultrasonicated samples, as compared to $J_c(H)$ for the normal grinding method, may be attributable to the following factors: homogeneous mixing of the precursor powders with CNT's, shortening of CNT's resulting in more open-ended CNT's and improved reaction between the dopant

and MgB_2 matrix due to more intimate mixing of CNT with precursors. It should be noted that both A and B samples, that shared similar dimensions of CNT, showed almost the same $J_c(H)$ at 5 and 20 K after ultrasonication, which is indicative of the effect of homogenous mixing. In fact, samples D prepared by the sonication process exhibited $J_c(H)$ as high as the normal C at 5 K, which is the highest $J_c(H)$ achieved so far in the CNT-doped MgB_2 sample. We believe that the poor J_c of sample C at the 10% CNT doping level occurred because of over-doping, which is evidenced by the decrease in T_c and the unit cell volume as shown in figure 8 and table 2. This is because these nanotubes are much shorter than the others and availability of carbon from the ends of nanotubes for the substitution of boron in MgB_2 was much better, resulting in over-doping. For comparison, a 5 at% of ultrasonicated sample C was prepared. The enhancement of J_c with the corresponding CNT doped MgB_2 at 5 at. wt% after ultrasonication supports the previous assumption (see figure 5.9 c).

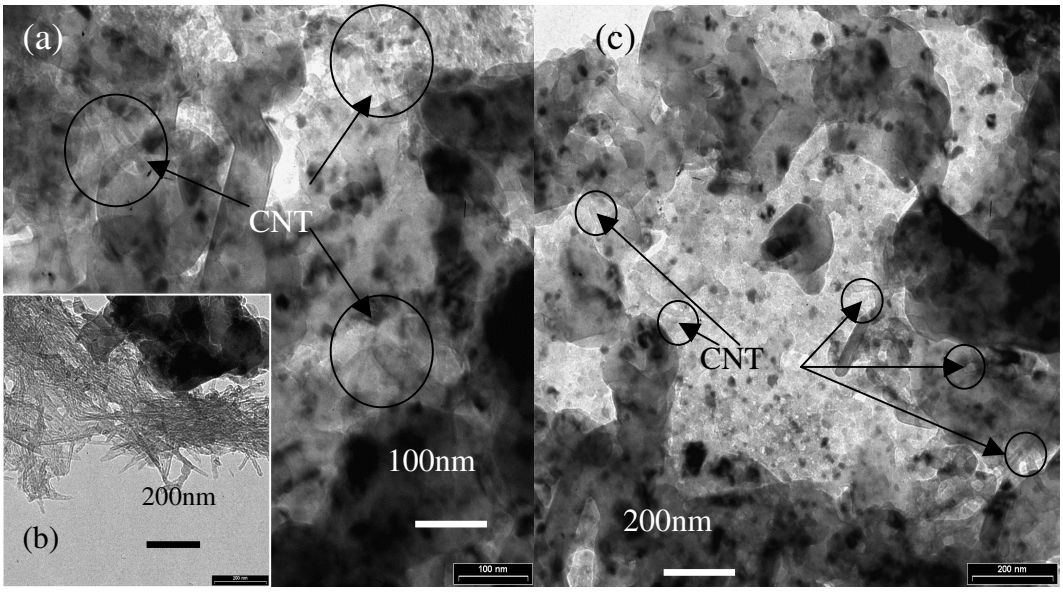

Figure 5.10: TEM image showing the carbon nanotube embedded into the MgB_2 matrix for carbon nanotube in (a) & (b) the normal grinding samples with the circles show agglomeration of carbon nanotubes (b) the normal grinding and ultrasonication sample with circles showing a good dispersion of carbon nanotubes

Figure 5.10 shows the TEM images for $MgB_{1.8}C_{0.2}$, prepared with normal grinding (a) and (b) and ultrasonicated after grinding (c). Both the samples showed similar structures, with some CNT's well embedded in the grains of MgB_2. This structure consisted of a number of fine grains about 100nm in diameter, though grains in 3(c) appeared a little larger than in the 3(a). Within these grains a very large number of fine particles, a few tens of nm in size, can be seen. It is assumed that these finer particles derive from the inclusion of CNT, which may act as nano pinning centers. The circles in the images show a few of regions that suggest the presence of CNT. In some areas (Fig.3b), large clumps of unreacted CNT were observed, as reported in the previous section. The incomplete mixing of the precursor materials suggests that the pinning behaviour of the CNT doped MgB_2 depends on the density of the unreacted and well dispersed CNT in the samples. We believe that the unreacted clumped CNT's will block the transport of the current density and suppress the J_c. However, no separate clumps of CNT were observed in 3c), which suggests better mixing with ultrasonication.

The $J_c(H)$ results are in agreement with TEM examinations. Samples prepared under the normal grinding method have some proportion of CNT appearing as agglomerates due to the inhomogeneous dispersion of CNT under the normal grinding. By introducing the ultrasonication, entangled CNT's are broken into individual short bundles. High velocity of collision between B, Mg and CNT promote a more complete mixing, thus inducing the change of the surface morphology [12]. Surface transformation in the ultrasonicated sample improved grain coupling between each superconducting crystal, as a result of densification.

Cavitations and the shockwaves generated by the ultrasonication will substantially enhance the reactivity of the nano size particles like CNT. Extent of the C substitution reaction increases with ultrasonication process, resulting in T_c depression, which is consistent with the contraction of the unit cell**.** We believe that the degree of carbon substitution in the CNT doped MgB_2 highly depends on the dimensions of CNT's as short CNT's are more reactive than the long ones. The low T_c and large contraction of the unit cell in the 20-30nm 10 % CNT is a good example of over-doping. Nevertheless, for the samples not having yet the optimal J_c, ultrasonication is another way to improve the J_c, instead of sintering at higher temperature to encourage better reaction between the dopant and MgB_2. Sintering at higher temperatures involves a risk of creation of a second compound, while ultrasonication may have less secondary effects like these.

5.4 Conclusion

As the conclusion, nanotubes are seen to adhere to the MgB_2 matrix for all the samples, with some proportion of them appearing as agglomerates. Magnetization measurements of J_c imply a change in the critical current density with the length of nanotube and not with its outside diameter. This implies that longer nanotubes tend to entangle, preventing their homogenous mixing with MgB_2 and dispersion. This suggests that an extra care should be taken with the sample preparation method if dealing with nanotube doping particles.

Homogeneous distribution of CNT's in MgB_2 matrix has been achieved by an ultrasonic method. Ultrasonication leads to significant enhancement of $J_c(H)$ due to the homogenous adherence of CNT in MgB_2 matrix and better connectivity between grains.

We also demonstrate that by controlling the processing parameters, an optimized $J_c(H)$ performance can be achieved in the CNT doped samples. Ultrasonication process is very effective in dispersing long CNT's and enhancing the reactivity and mixing, while avoiding the side-effects that would occur at higher sintering temperatures.

5.5 References

[1] P. Samuely, Z. Holanove, P. Szabo, J. Kacmarcik, R. A. Ribeiro, S. L. Bud'ko and P. C. Canfield, *Phys. Rev. B*, **68**, 020505(R) (2003)

[2] K. Fossheim, E. D. Tuset, T. W. Ebbesen, M. M. J. Treacy and J. Schwartz, *Physica C*, **248**, 195, (1995).

[3] S. Huang, M. R. Koblischka, K. Fossheim, T. W. Ebbesen and T. H. Johansen *Physica C*, **311**, 172, (1999).

[4] Z. Yu and L. Brus, *J. Phys. Chem. B*, **105**, 1123 (2001).

[5] T. Prozorov, R. Prozorov, A. Snezhko, and K. S. Suslick, *Appl. Phys. Lett*., **83**, 2019 (2003).

[6] T. Prozorov, B. McCarty, Z. Cai, R. Prozorov, and K. S. Suslick, *Appl. Phys. Lett*., **85**, 3513 (2004).

[7] S. X. Dou, W. K. Yeoh, J. Horvat and M. Ionescu, *Appl. Phys. Lett*., **83**, 4996 (2003).

[8] W. K. Yeoh, J. Horvat1, S. X. Dou and V. Keast, *Supercond. Sci. Technol*., **17**, S572–S577, (2004).

[9] R. H. T. Wilke, S. L. Bud'ko, P. C. Canfield, D. K. Finnemore, R. J. Suplinskas and S. T. Hannahs, *Phys. Rev. Lett.*, **92**, 217003, (2004).

[10] D.H. Galvan, S. Li, W. M. Yuhasz, J. H. Kim, M. B. Maple and E. Adem, *Physica C*, **403**, 145 (2004)

[11] J. Horvat, S. Soltanian, A. V. Pan, and X. L. Wang, *J. of Appl. Phys*., **96**, 4342 (2004).

[12] S. J. Doktycz and k. S. Suslick, *Science*, **247**, 1067 (1990)

Chapter 6: Enhanced Performance of MgB_2/Fe Superconducting Wires prepared by In-situ Method with Carbon Nanotube inclusion

6.1 Introduction

The rapid progress in developing MgB_2 superconductors since its relatively recent discovery [1] has made this material a strong competitor to other low- and high-temperature superconductor (HTS) materials for technological applications, especially in niche markets such as magnetic resonance imaging (MRI). High in-field J_c of MgB_2 superconductors is a major requirement for large-scale applications. In addition to this, MgB_2 wires need to exhibit good mechanical properties and thermal stability. The additives studied so far have mainly been used to improve $J_c(H)$ by introducing effective pinning sites in *bulk* MgB_2. Not much attention has been focused on the mechanical and thermal properties of the MgB_2 *wire* core. CNT doping has a potential to improve the mechanical and thermal properties of the MgB_2 wires, in addition to improvement of the field dependence of J_c. Namely, CNT's have been used as reinforcing components in a number of different composites [2, 3]. It is widely known that the CNT have good electrical, thermal, and mechanical properties, although they exhibit some peculiarities because of their high aspect ratio and nanometer scale diameters. Many properties of CNT are directly influenced by the way of the graphite sheets are wrapped around.

Fossheim et al. have reported an enhanced flux pinning in $Bi_2Sr_2CaCu_2O_{8+x}$ superconductors with embedded CNT's [4]. Yang et al. have discovered a significant enhancement in $J_c(H)$ for HTSs by introducing nanorods as columnar pinning centers in the composites [5, 6, 7]. We previously reported that CNT doping enhanced J_c under magnetic fields for bulk MgB_2 [8, 9]. In addition, the effect of heating rates and the processing temperature and period on the properties of MgB_2 wires has to be investigated to produce high-performance and economically-viable MgB_2 wires. Variation in the J_c of MgB_2 is often reported worldwide, which can be attributed in part to different thermo-mechanical processing, and not just differences between the precursor powders [10-12]. Sintering temperatures and durations have a strong effect on critical current density [13, 14]. Because of the lack of substantial reaction between Fe and MgB_2, the importance of heating rates in Fe-sheathed wires is often underestimated [15]. The importance of heating rates for the well-established A15 conductors used in MRI and NMR magnet applications has been clearly established, and it has prompted the development of *in situ* optimization techniques [16].

Inspired by the previous reports, we demonstrate that CNT enhances the flux pinning in MgB_2 *wires*, too. We also report a systematic study of the influence of heating rates on the superconducting properties of *in situ* MgB_2/Fe wires.

6.2 Experimental

The starting powders were magnesium (99 %, -325 mesh), amorphous boron (99 %, 1-2 μm) and multi-walled carbon nanotubes (>94 %, OD 20-30 nm, length 0.5-2 μm). Two types of wires were prepared with powders of nominal composition

MgB_2 and $MgB_{1.8}C_{0.2}$ respectively, using the standard powder-in-tube (PIT) method. The powders were packed into Fe tubes and then drawn to about 1.4 mm in diameter. Short samples (~ 5 cm each) were cut from the wires and heat treated in a tube furnace which was being constantly pumped down to vacuum (10^{-6} Torr) during the heat treatments. Two heating rates of 100 °C/h and 900 °C/h were used, followed by isothermal processing at 650 °C or 850 °C for 30 min, and then furnace cooling to room temperature.

The microstructure of the wires was evaluated by Focused-Ion Beam Scanning Electron Microscope (FIB-SEM), transmission electron microscope (TEM), and x-ray diffraction (XRD). Magnetization and ac susceptibility were measured by a physical property measurement system (PPMS, Quantum Design) and dc SQUID magnetometer. The magnetic critical current density (J_c) was derived from the height of the magnetization loop using critical state model (refer chapter 3). X-ray diffractometry (XRD) was conducted using Cu-K□ radiation in the Bragg-Brentano configuration to determine the phase composition of the samples.

6.3 Results and Discussions

Fig. 6.1 shows the magnetic J_c calculated from magnetization hysteresis loops with magnetic field, H, applied both parallel to and perpendicular to the wire sample axis, *a,* for both undoped and CNT doped MgB_2 wires. It is noted that for the undoped MgB_2 wire there is only a small difference in $J_c(H)$ in relation to the measuring field direction due to the wire drawing process. In contrast, the $J_c(H$) for the CNT doped wires shows

two distinguished features: a strong anisotropy in relation to the measuring field direction and a clear enhancement of flux pinning in high field region compared to that of the undoped sample. The anisotropy in J_c at 5 K is stronger than that at 20 K and the extent of the anisotropy in J_c increases with magnetic field H, ranging from a factor of 2-3 in low fields up to more than one order of magnitude in high fields. The enhancement in $J_c(H)$ performance due to CNT doping is more significant at low temperatures and higher fields. For example, in the applied field, H, perpendicular to the wire axis, a, the J_c $(H \perp a)$ increases by a factor of 37 at 5 K and 7 T, as a result of CNT doping. What is more striking is that the enhancement in J_c of the CNT doped MgB_2 occurs in both directions of applied field H in respect to the wire axis. $J_c(H \perp a)$ shows more significant enhancement than $J_c(H//a)$ compared to that of undoped MgB_2 wire.

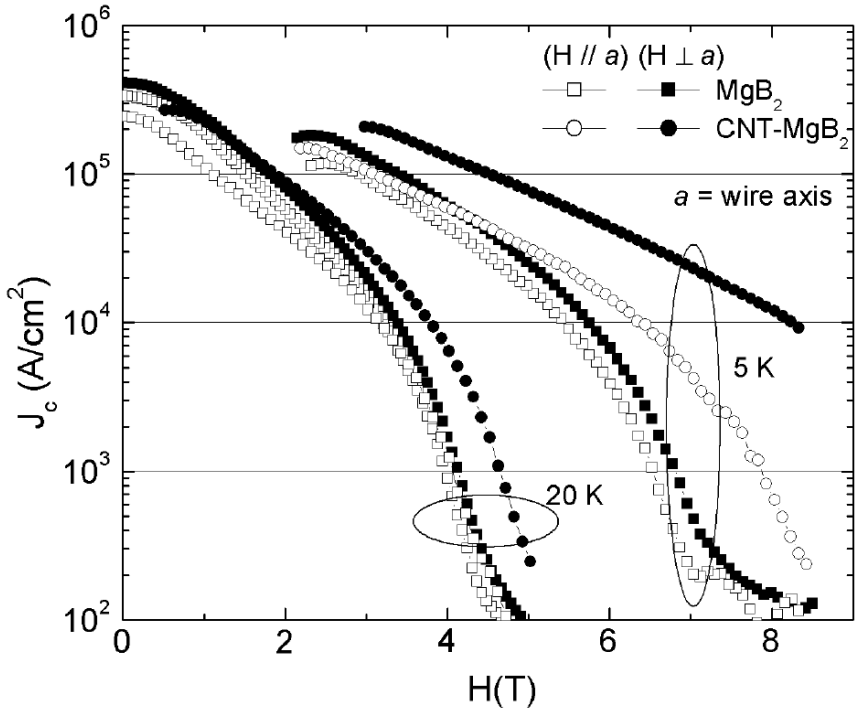

Fig. 6.1 Critical current density as a function of applied magnetic field at 5 K and 20 K for the undoped and CNT doped MgB_2 wires processed at 800°C for 30 min. All the samples made for magnetic measurement have the same dimension of 0.7mm OD and 2.7mm in length. The measurement field H was applied perpendicular and parallel to the wire axis, a, during the measurement of M-H loops.

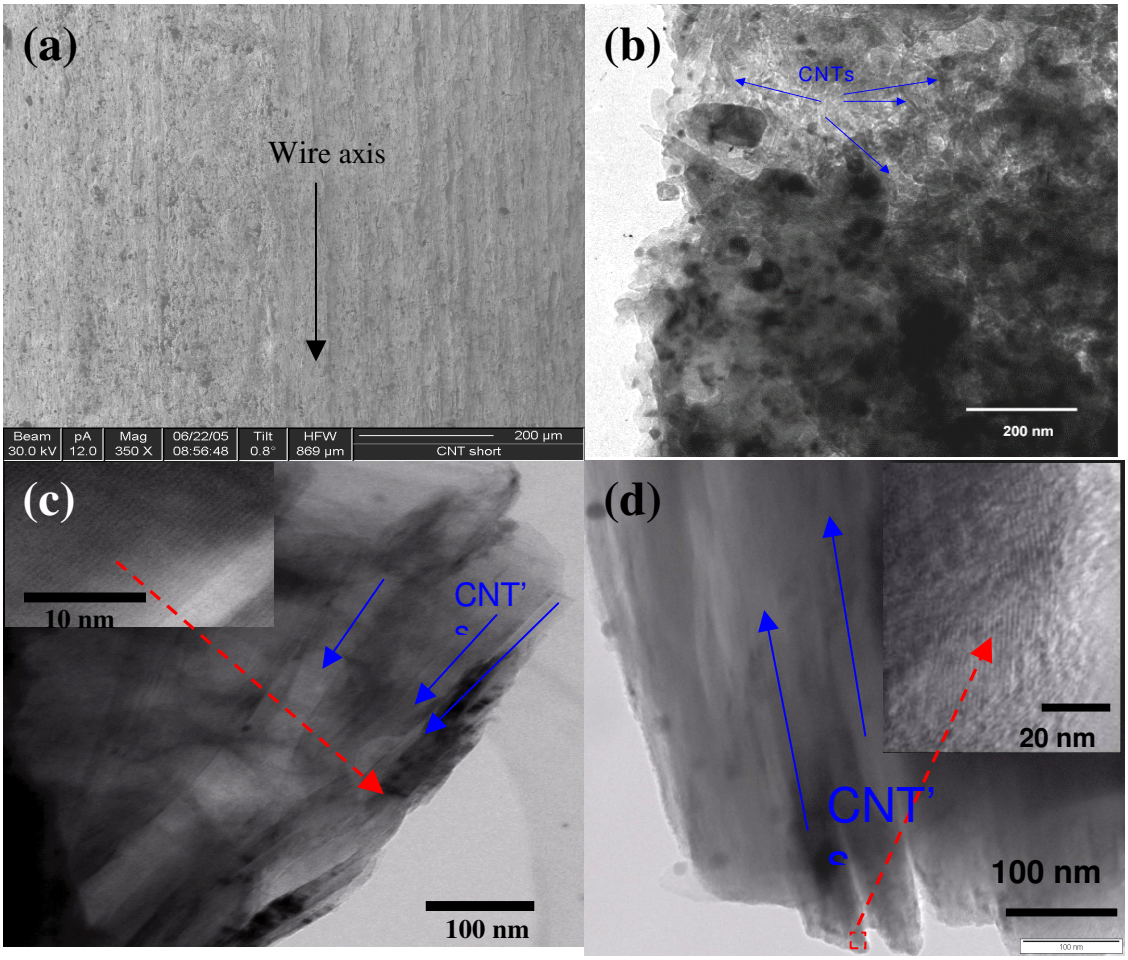

Fig. 6.2 (a) FIB-SEM micrographs of the CNT doped MgB_2 wire core processed at 800°C for 30 min, showing the elongated macrostructure along the wire axis, (b) Transmission electron micrographs (TEM) for the CNT doped MgB_2 pellet processed at 800°C for 30 minutes, showing the entangled CNT's randomly distributed in the MgB_2 matrix, (c) TEM image for the CNT doped MgB_2 wire processed at 800°C for 30 minutes, showing bundled CNT's in the one direction in the MgB_2 matrix. The inset in Fig 2 (c) is the high resolution image of CNT, and (d) TEM image for several parallel CNT's embedded in MgB_2. The inset in Fig 2 (d) is the high resolution lattice image of one of CNT's.

For the reason of anisotropy in J_c, both XRD and electron diffraction patterns show no evidence for the crystalline orientation of MgB_2 grains in the wire core in both longitudinal and transverse direction to the wire axis, because the formation MgB_2 crystals is accomplished through reaction *in situ* process in which there is no driving

force for the MgB_2 crystalline alignment. Thus, the anisotropy is not due to the MgB_2 crystalline alignment. Fig. 6.2 (a) shows scanning electron micrographs for the CNT doped MgB_2 wire. A strong elongated macrostructure along wire axis is clearly evident. In the CNT doped bulk materials the CNT's are randomly dispersed in the MgB_2 matrix and most CNT are highly entangled, as shown in Fig. 6.2 (b). In contrast, for the PIT process, the mixture of Mg and B powder and the CNT additives flows along the wire axis upon mechanical deformation into wires, as a result of continuing drawing and reduction process. Fig. 6.2 (c) shows a TEM image of the embedded CNT's in the same direction in the MgB_2 wire core. The inset shows the high resolution image of the CNT lattice. The inset in Fig 6.2 (d) is the high resolution lattice image of one of CNT's. We believe that the anisotropy in J_c originates from the elongation of CNT in MgB_2 upon drawing the powder filled tubes into wires. The CNT induced anisotropy in J_c may be attributable to two factors: high axial conductivity [17, 18] and large aspect ratio of CNT's. The CNT's along the core axis will improve the connectivity between grains by bridging poorly connected regions, which are common problem for the reaction in situ process because the density of MgB_2 can only reach about 50% of theoretical density in this process.

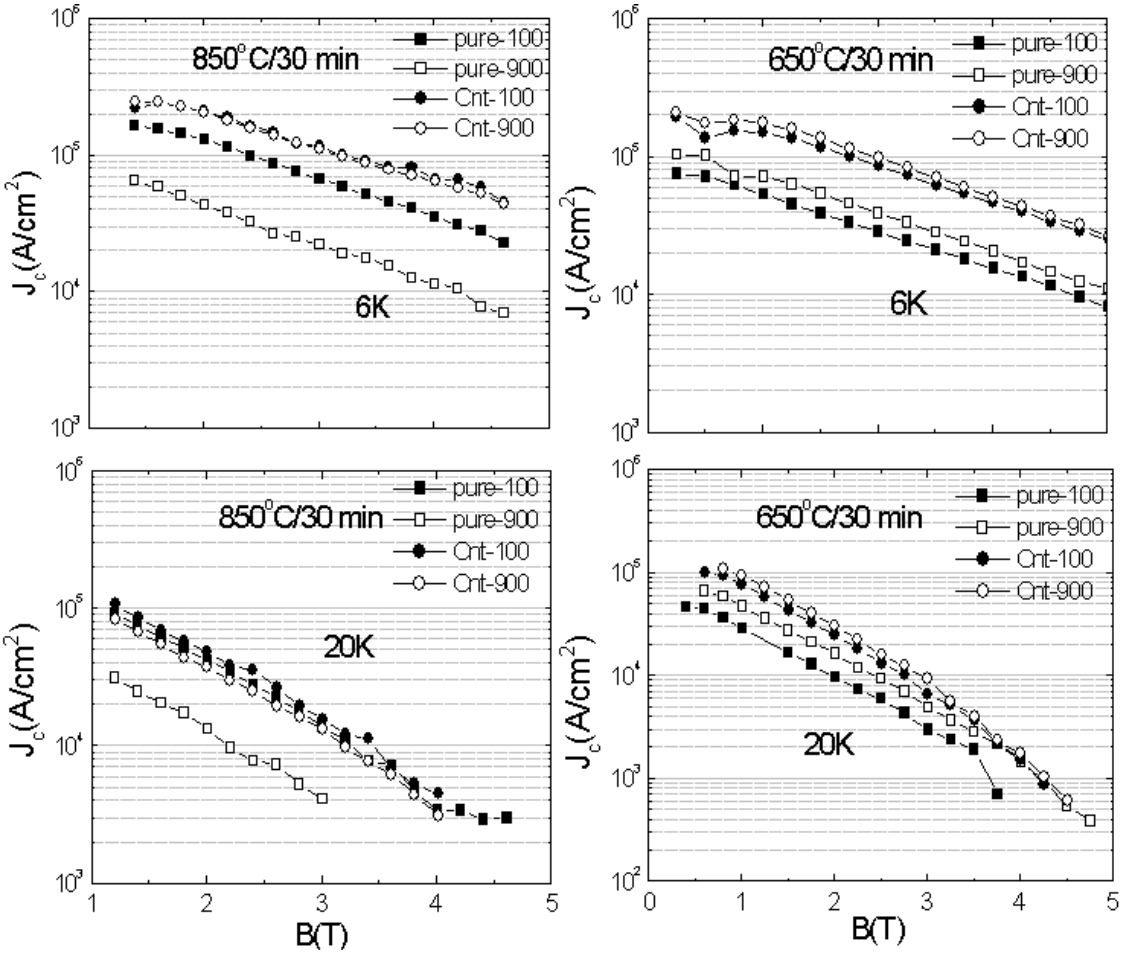

Figure 6.3 Critical current density, J_c as a function of magnetic field at 6 and 20K for pure and CNT doped MgB_2/Fe wires annealed at 650 °C or 850 °C for 30 min with two different heating rates of 100 °C/h and 900 °C/h.

Furthermore, the CNT's have a strong effect on heat transfer during materials processing due to their high thermal conductivity. The effect of heating rates and annealing temperatures on J_c of each type of MgB_2/Fe wires are presented in figure 6.3. It shows that the J_c of *pure* MgB_2 is strongly influenced by heating rate, in addition to the differences caused by annealing temperature; for either annealing temperature, better J_c is obtained on slow heating. This is because the slower heating rate ensured a more homogeneous temperature in the samples just below the melting point of Mg, allowing more MgB_2 to form through solid state diffusion and hence minimizing the

amount of free Mg on attaining the melting temperature of 650 °C. In contrast, the Mg loss by evaporation becomes more significant when heated at fast rates and to high temperatures, hence causing Mg deficiency in the sample.

For CNT-doped samples, the J_c is insensitive to the heating rate. Fig. 6.3 shows that all CNT doped wires heated at 850 °C have similar J_c, and a higher J_c than samples heated at 650 °C, regardless of heating rates. A high annealing temperature promotes the C substitution reaction for B, thus enhancing flux pinning in MgB_2. As can be seen from Fig. 6.3, the high-field J_c is improved in the samples heat treated at higher temperature. Occupation of an intragranular site by an intact CNT and the unique geometry of the CNT are responsible for effective pinning, and the resulting J_c enhancement dominates over any negative effects of magnesium loss during rapid heating.

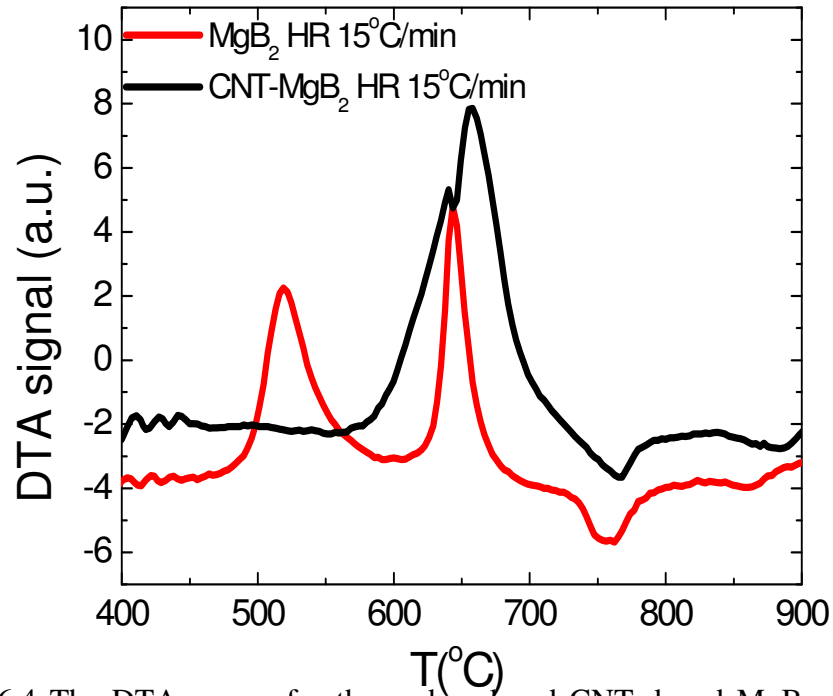

Figure 6.4 The DTA curves for the undoped and CNT doped MgB_2 wires processed with heating rate of 15°C/min.

We interpret our results by CNT's delaying the solid state reactions until the temperatures close to the melting point of Mg, above which the liquid phase reaction takes place, leading to a stronger matrix of MgB_2 wire. This is due to good thermal conductivity of CNT's, thereby homogenizing the sample temperature and preventing any undesirable chemical reactions in localized volume with higher temperature. As Mg melts in whole of the sample at the same time, MgB_2 is quickly formed and other compounds are not likely to occur. This interpretation is further verified by the curves of differential thermal analysis (DTA) for the Fe sheathed pure MgB_2 and 10% CNT doped MgB_2 wires with heating rate at 15^oC/min as shown in Fig. 6.4. There are two exothermic peaks for pure MgB_2 wire, while for CNT doped MgB_2 there is only one broad peak. The first peak is due to the reaction between Mg and B_2O_3, while the second peak is attributable to the formation of MgB_2 [19]. CNT's, because of their high aspect ratio and high heat conductivity, are desirable nucleation centers for triggering and propagating of MgB_2 formation along their entire length. Since the CNT's have a high thermal conductivity, heat is transferred along the CNT's to the adjacent regions. Thus, the MgB_2 formation reaction takes place with the CNT's as the nucleation centers and propagates along the length of the CNT's. The high thermal conductivity and desirable elongated geometry of the CNT's is responsible for the insensitivity of CNT-doped MgB_2 wires to the heating rate, which is convenient and advantageous for the manufacture of practical conductors.

6.4 Conclusion

In summary, the elongated CNT doped MgB_2 wire shows an enhancement of J_c by more than an order of magnitude in high field region. The CNT's induce anisotropy in J_c in relation to the direction of applied field and significantly improve heat transfer and dissipation during materials processing. We note that the heating rate has no effect on $J_c(H)$ for the CNT doped MgB_2 wire, while $J_c(H)$ for the pure MgB_2 wire processed at a rapid heating rate of 15 °C min^{-1} is lower than that at a slow heating rate of 1.7 °C min^{-1} by a factor of three. In addition to the benefits of electrical and thermal conductivity of CNT doping, the elongated CNT's in the wire axis direction will take full advantage of their unusual axial strength to enhance the mechanical properties such as tensile strength and flexibility. Studies on these properties are underway.

6.5 References

[1] J. Nagamatsu, N. Nakagawa, T. Muranaka, Y. Zenitani, J. Akimitsu, *Nature* **410**, 63 (2001).

[2] Y. Li, I. A. Kinloch, A. H. Windle, *Science* **304**, 276 (2004).

[3] E. S. Choi, J. S. Brooks, D. L. Eaton, M. S. Al-Haik, M. Y. Hussaini, H. Garmestani, D. Li, K. Dahmen, *J. Appl. Phys.* **94**, 6034 (2003).

[4] K. Fossheim, E. D. Tuset, T. W. Ebbesen, M. M. J. Treacy, J. Schwartz, *Phys. C (Amsterdam, Neth.)* **248**, 195 (1995).

[5] P. Yang, C. M. Lieber, *Science* **273**, 1836 (1996).

[6] P. Yang, C. M. Lieber, *Appl. Phys. Lett.*, **70**, 3158 (1997).

[7] P. Yang, C. M. Lieber, *J. Mater. Res.*, **12**, 2981 (1997).

[8] S. X. Dou, W. K. Yeoh, J. Horvat, M. Ionescu, *Appl. Phys. Lett.* **83**, 4996 (2003).

[9] W. K. Yeoh, J. Horvat, S. X. Dou, V. Keast, *Supercond. Sci. Technol.* **17**, S572 (2004).

[10] C. Buzea and T. Yamashita, *Supercond. Sci. Technol*. **14**, R115 (2001).

[11] R. Flukiger, H. L. Suo, N. Musolino, C. Beneduce, P. Toulemonde, and P. Lezza, *Physica C* **385**, 286 (2003).

[12] S. H. Zhou, A. V. Pan, J. Horvat, M. J. Qin, and H. K. Liu, *Supercond. Sci. Technol.* **17**, S528 (2004).

[13] X. L. Wang, S. Soltanian, J. Horvat, A. H. Liu, M. J. Qin, H. K. Liu, and S. X. Dou, *Physica C* **361**, 149 (2001).

[14] M. Bhatia, M. D. Sumption, M. Tomsic, and E. W. Collings, *Physica C* **407**, 153 (2004).

[15] C. R. M. Grovenor, L. Goodsir, C. J. Salter, P. Kovac, and I. Husek, *Supercond.5Sci. Technol.* **17**, 479 (2004).

[16] K. S. Tan, S. C. Hopkins, and B. A. Glowacki, *Physica C* **415**, 179 (2004).

[17] B. Q. Wei, R. Vajtai, P. M. Ajayan, *Appl. Phys. Lett.* **79**, 1172 (2001).

[18] S. Frank, P. Poncharal, Z. L. Wang, W. A. de Heer, *Science*, **280**, 1744 (1998).

[19] W. Goldacker, S. I. Schlachter, B. Obst, and M. Eisterer, *Supercond. Sci. Technol*. **17**, S490 (2004)

Chapter 7: Control of Nano Carbon Substitution for Enhancing the Critical Current Density in MgB_2

7.1 Introduction

The effects of carbon doping have been investigated by several groups [1-12]. In fact, all the carbon substitutions resulted in much higher J_c values of MgB_2 than those reported for the pure material. Recently, the J_c enhancement due to carbon substitution has been confirmed with different carbon sources such as diamond [13], graphite [14], and carbon "nanohorns" [15]. Besides that, carbon-containing compounds, such as SiC [16-18] and B_4C [19], have been reported to be effective for improving J_c in MgB_2. The previous chapters describe systematic studies of the effects of CNT doping of MgB_2 in bulk and wire form [20-26]. Enhancement of J_c by two orders of magnitude at 8T and 5K and 7T and 10K was observed in the CNT doped MgB_2 compared to the pure material. In fact, the short CNT's are believed to have an effect that is similar to that of amorphous carbon due to their low aspect ratio [26].

This chapter presents the effects of amorphous carbon nanoparticle substitution in MgB_2 in the bulk form. It is shown that by controlling the extent of carbon substitution, an enhancement of flux pinning and critical current density by two orders of magnitude in high magnetic fields can be achieved in bulk samples. Both bulk and wire of the CNT and nano C doped MgB_2 will be evaluated by focusing on the optimum doping level and effect of carbon substitution on the J_c.

7.2. Experiment

Powders of magnesium (99%, -325 mesh), amorphous boron (99%, 1-2 μm), MWCNT (>95%, outside diameter 20-30nm, average length 0.5-200) and amorphous carbon (particle size < 20nm) with the nominal atomic ratio of $MgB_{2-x}C_x$ where x = 0, 0.05, 0.1, 0.2 and 0.3 was prepared by an *in situ* reaction method. MgB_2/Fe monofilament wires were prepared by an *in-situ* reaction process, using the powder-in-tube method. The mixture was mixed through grinding and mixed powders were packed into Fe tubes with a length of 140 mm, an outer diameter (O.D) of 10 mm, and an inner diameter (I.D) of 8 mm and subsequently drawn to wire 1.4 mm in diameter (refer chapter for the detail of processing). All the samples were sealed in Fe tubes or Zr foil, then heat treated with a heating rate of 5^{o}C/min in flowing high purity Ar at 800 and 900 ^{o}C for 30 minutes, followed by a furnace cooling to room temperature.

The phase and crystal structure of all the samples were investigated using a MAC Science MX03 diffractometer with Cu Kα radiation. The lattice parameters and unit cell volumes were estimated from the (002) and the (100) peaks. The magnetization was measured by a Physical Property Measurement System (PPMS, Quantum Design) up to 8.7 T. Magnetic J_c values were determined from the magnetization hysteresis loops using the appropriate critical state model (see chapter 3 for calculation). Bar-shaped samples with a size of 3 × 1.5 × 1 mm^3 were cut from each wire core for magnetic measurements. The grain morphology and microstructure were examined by transmission electron microscopy.

7.3 Results and Discussions

Fig 7.1(a) shows the XRD pattern for the samples of $MgB_{2-x}C_x$, where x = 0, 0.05, 0.1, 0.2 and 0.3 are the nominal values for C content. The nano-C precursor powder is also included as a reference and comparison. It can be seen that all the doped samples exhibit well-developed MgB_2 phase, with only a small amount of MgO present, even at high sintering temperature of 1000°C. No other impurity phases, such as Mg_2C_3 or MgB_2C_2, can be detected. Figure 7.1 (b) shows the shift of lattice parameter *a* for various carbon doped bulk samples. As the doping level increases, the lattice parameter *a* shrinks monotonically, while the lattice parameter *c* varies very little with the different C doping. The decrease in value of *a* is an indication of the boron substitution for carbon, as the carbon substitution is more pronounced at higher doping levels of C.

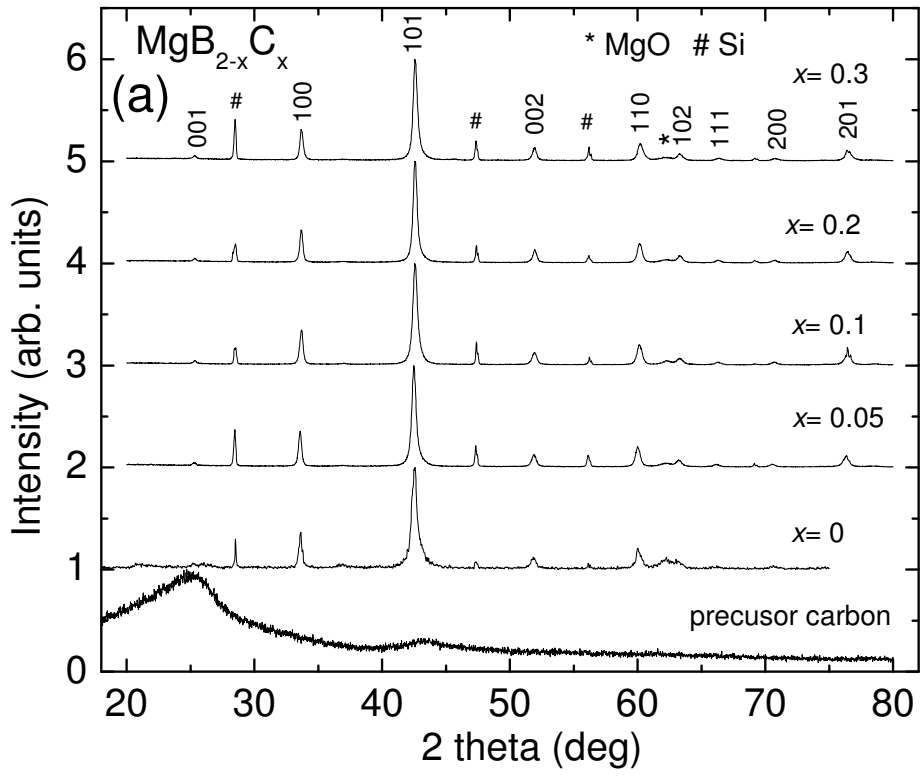

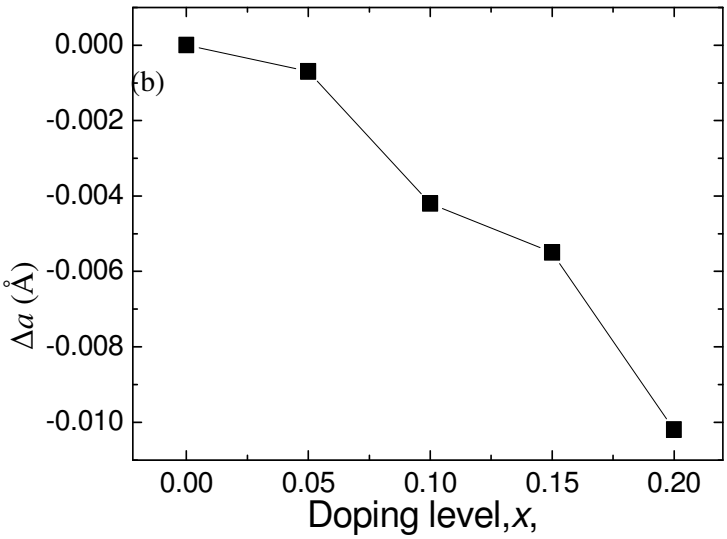

Figure 7.1 (a) XRD data for various carbon doped bulk samples sintered at 900°C for 30min. (b)Variation of lattice parameters *a* for various carbon doping levels in bulk MgB_2.

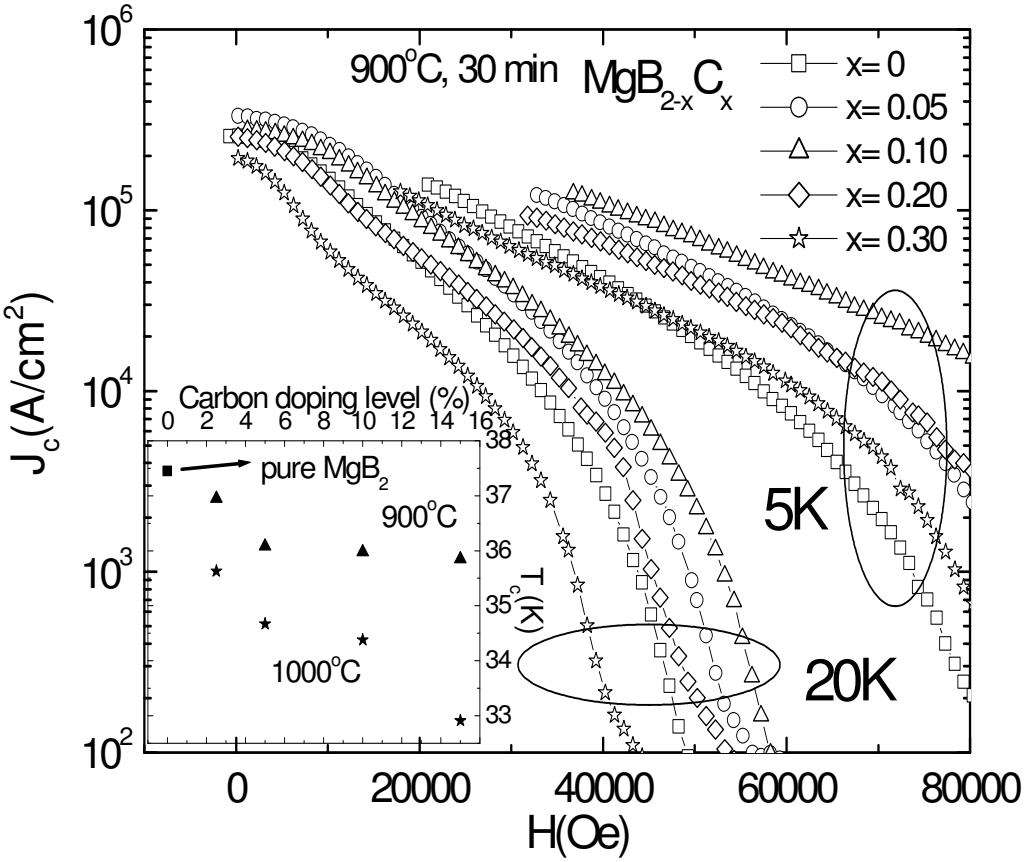

Figure 7.2: The magnetic $J_c(H)$ curves at 5K and 20K for the samples of bulk $MgB_{2-x}C_x$, where x = 0, 0.05, 0.1, 0.2 and 0.3. Inset shows the critical temperature (T_c) for the samples with 2.5-15 at% C that was sintered at 900 and 1000°C for 30 min.

Fig. 7.2 shows the magnetic $J_c(H)$ curves at 5K and 20K for the bulk samples of $MgB_{2-x}C_x$, where x = 0, 0.05, 0.1, 0.2 and 0.3 are the nominal values for C content, with all the samples sintered at 900°C for 30 min. All the $J_c(H)$ curves for doped samples have a higher J_c than the non-doped sample at high fields above 5T at 5K and all the fields at 20K except at 15 at% C (x=0.3). Similar to the CNT doped MgB_2, $J_c(H)$ at self field and 20K showed minor improvement for the low carbon content samples. The sample doped with 5 at% carbon (x = 0.1) gives the best J_c at high field with J_c increasing by two orders of magnitude at 5K for a field of 8T, and by a factor of 33 at 20K for a field of 5T, as compared to the non-doped sample. The enhancement was also observed in the low field region at 20K for samples with 2.5 and 5 at% carbon substitution. This suggests that by controlling the extent of the carbon substitution we can achieve a significant enhancement in the critical current density and flux pinning in magnetic field, which demonstrates that the $MgB_{2-x}C_x$ composition can be a promising candidate for practical applications at 20K. The inset in Figure 7.2 shows the critical temperature (T_c) for the bulk samples with 2.5-15 at% C, which was sintered at 900 and 1000°C for 30 min. The T_c of samples sintered at 900°C undergoes a sharp drop from 2.5 to 5 at% C followed by an insignificant decrease in T_c, even as the carbon content increased from 5 up to 15 at%. However, at 1000°C the T_c degrades monotonically with increasing carbon content from 35.6 K for 2.5 at% to 32.91 for 15 at% of carbon doped MgB_2. This indicates that the extent of the C substitution reaction increases with increasing sintering temperature, resulting in T_c depression, which is consistent with a recent report [20].

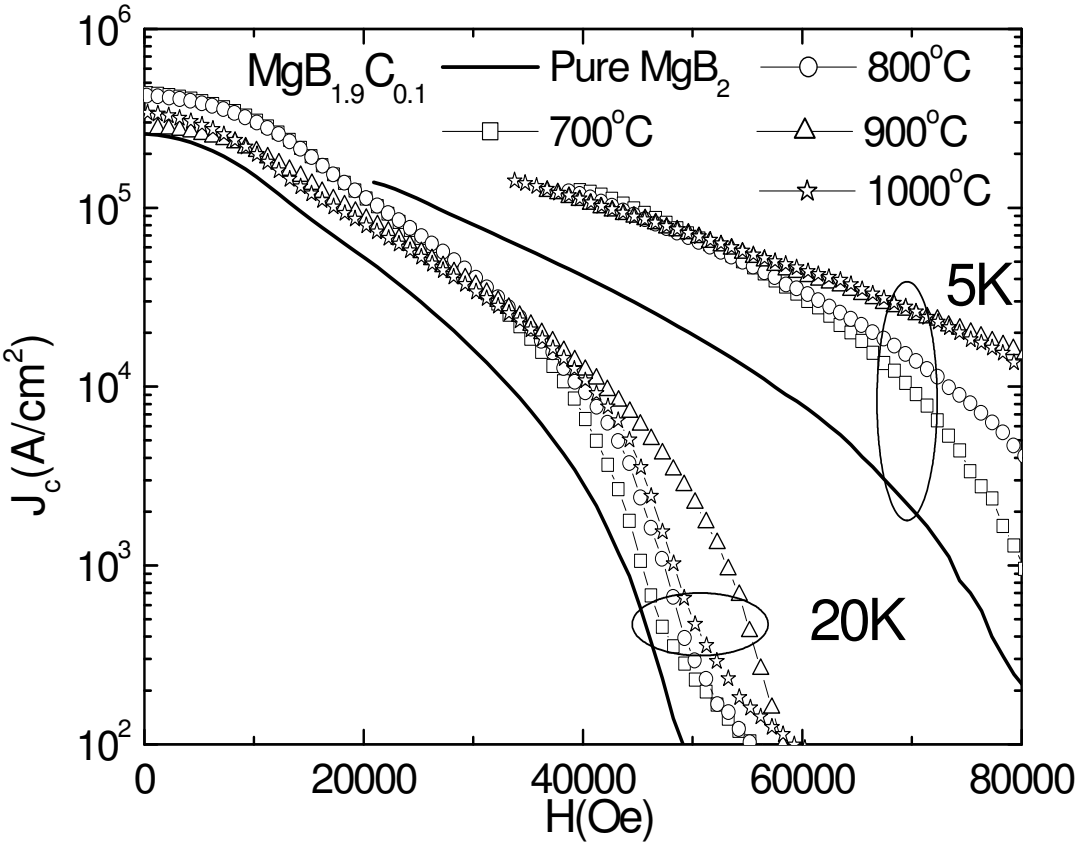

Figure 7.3: Magnetic $J_c(H)$ for bulk $MgB_{1.9}C_{0.1}$ samples with various sintering temperature.

Magnetic $J_c(H)$ for $MgB_{1.9}C_{0.1}$ bulk samples with various sintering temperatures is shown in Figure 7.3. All the $J_c(H)$ values of 5 at% C doped MgB_2 are higher than for the pure MgB_2 sample even at a sintering temperature as high as 1000°C. In fact, the samples sintered at both 900°C and 1000°C show the highest $J_c(H)$. These results are consistent with those previously reported [20, 21] on CNT doped MgB_2, where high temperature is preferable for higher $J_c(H)$. A higher sintering temperature promotes better carbon substitution, resulting in enhancement of $J_c(H)$. We also believe that even at a temperature as high as 1000°C, full carbon substitution is not achieved, as C may appear as excess nano-particle or react with B or Mg to form BC [27] and MgC_3[12] at low temperature as the sample heats up. Nevertheless, nano-C doped MgB_2 has proved

to be one of the most promising dopants for MgB_2 superconductor with high J_c, besides SiC and CNT.

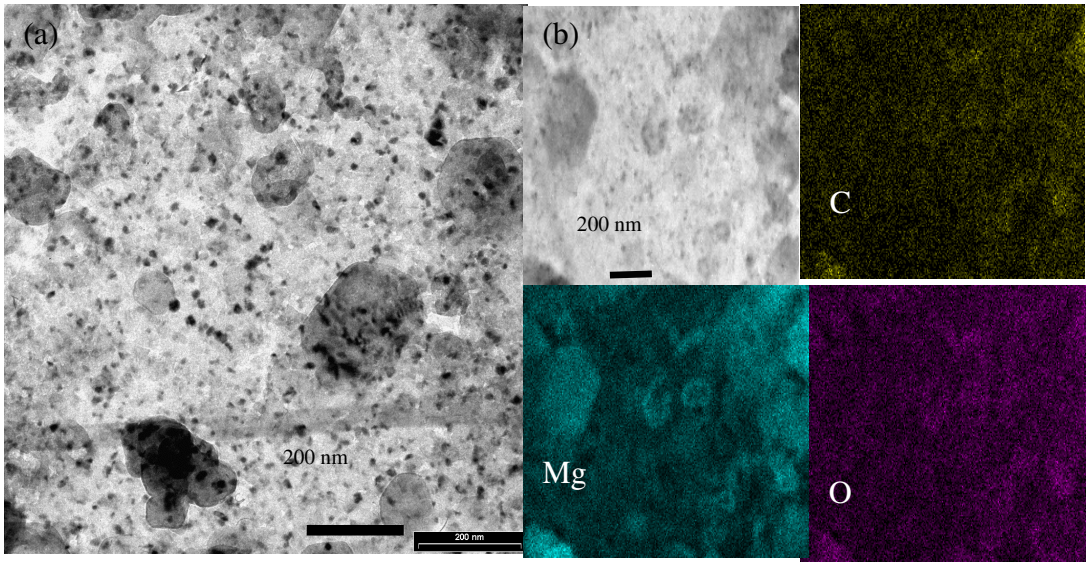

Figure 7.4: (a) TEM image and (b) the EDX elemental mapping for carbon doped bulk MgB_2. Grey image is the original TEM image with brighter area indicates higher concentration for Mg, O and C, respectively.

A typical TEM image and the Energy Dispersive X-ray, (EDX) elemental mapping for carbon doped MgB_2 are shown in Figure 7.4. The carbon doped MgB_2 appeared to be homogenous and well consolidated, with a grain size of 50-200nm. The microstructure exhibits noticeable nanoparticles with sizes around 10-20nm. Dark field images using MgB_2 reflections and Energy Dispersive Spectrometry (EDS) spectra from both the MgB_2 matrix and the nanoparticles are essentially the same, indicating that the nanoparticles are also essentially MgB_2[28]. This morphology of the MgB_2 crystal is similar to that of CNT doped MgB_2, but is different from that of pure MgB_2. The chemical maps showed no evidence of unreacted nano-C particles, but did show a homogenous distribution of O in the MgB_2 matrix. However, it should be noted that some of the areas show a higher C or Mg concentration and some of these areas

overlapped with each other. Therefore, it is believed that the sample might contain pure MgB_2 phase, MgO phase, Mg $(B, C)_2$ phase, or un-reacted Mg phase.

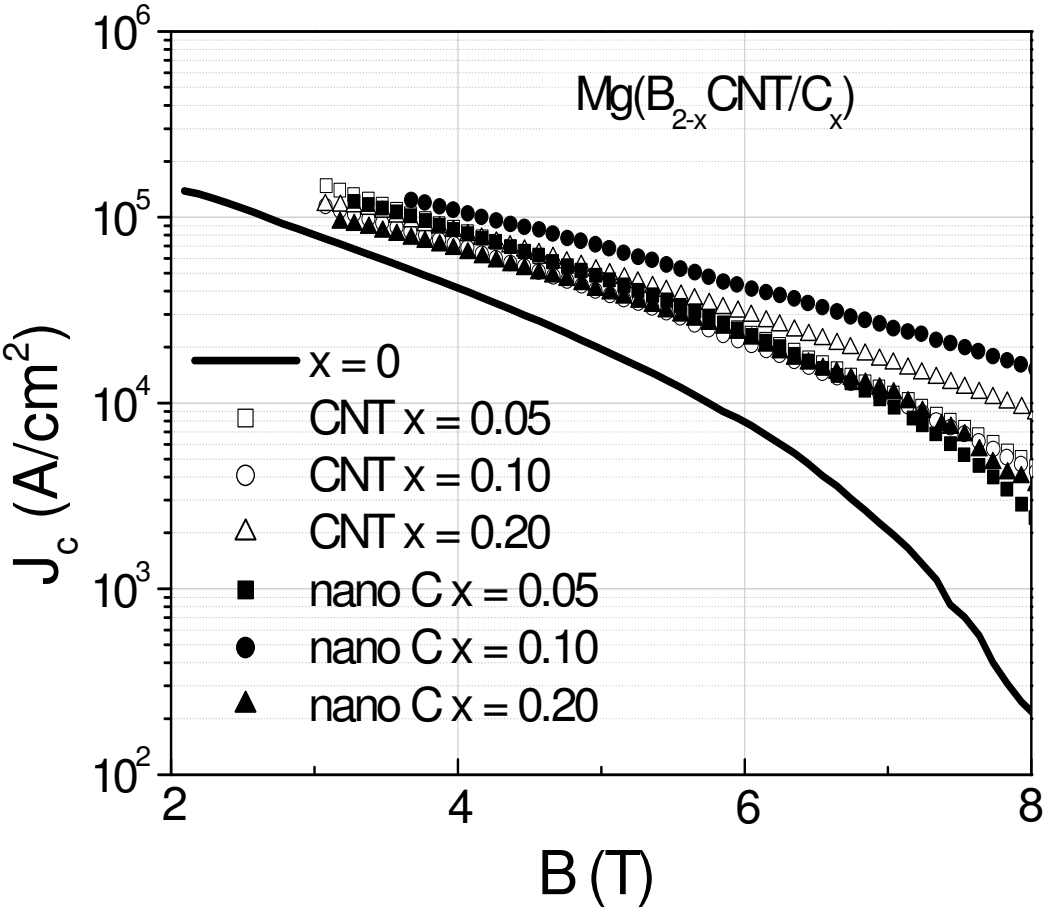

Figure 7.5: Comparison of magnetic $J_c(H)$ for bulk nano carbon and CNT samples sintered at 900°C for 30 min.

In order the to clarify the effect of the carbon role in the CNT and nano C doping samples, the magnetic $J_c(H)$ of CNT doped and nano-C doped MgB_2 sintered at the 900°C for 30 min are plotted in the figure 7.5. All the $J_c(H)$ curves for doped samples have a higher J_c than the non-doped sample at high fields above 5T at 5K. This implies that MgB_2 has a high tolerance to the carbon impurities since only small part of added carbon actually substitutes into the boron site. In fact, both samples showed two different optimum doping levels under the same processing condition with the optimum

doping level of nano-C and CNT sample being $x = 0.10$ and $x = 0.20$, respectively. As mentioned above, the reactivity of the carbon source plays an important role to determine the carbon substitution in the MgB_2. The form of carbon source can substantially enhance the reactivity of the C and the MgB_2 as shown by the B_4C [5, 29] Approach for carbon substitution by using B_4C of MgB_2 was suggested by Mickelson *et al.* to overcome the diffusion problem by using C as starting material to achieve better mixing of B and C atoms [5]. As a result, we believe the variation of J_c shown by the two optimum doping levels for nano-C and CNT as carbon sources is most likely due to the reactivity of different carbon sources requiring different kinetic energy for carbon substitution. However, the nano-C doping showed a better J_c performance in high field compared to the CNT sample. For example, the $J_c(H)$ for CNT, nano-C and pure MgB_2 samples was 8624 A/cm^2, 15418 A/cm^2 and 215 A/cm^2 at 8T and 5K. This means that $J_c(H)$ was enhanced by a factor of 1.8 for nano-C doped MgB_2 , as compared to CNT doped sample.

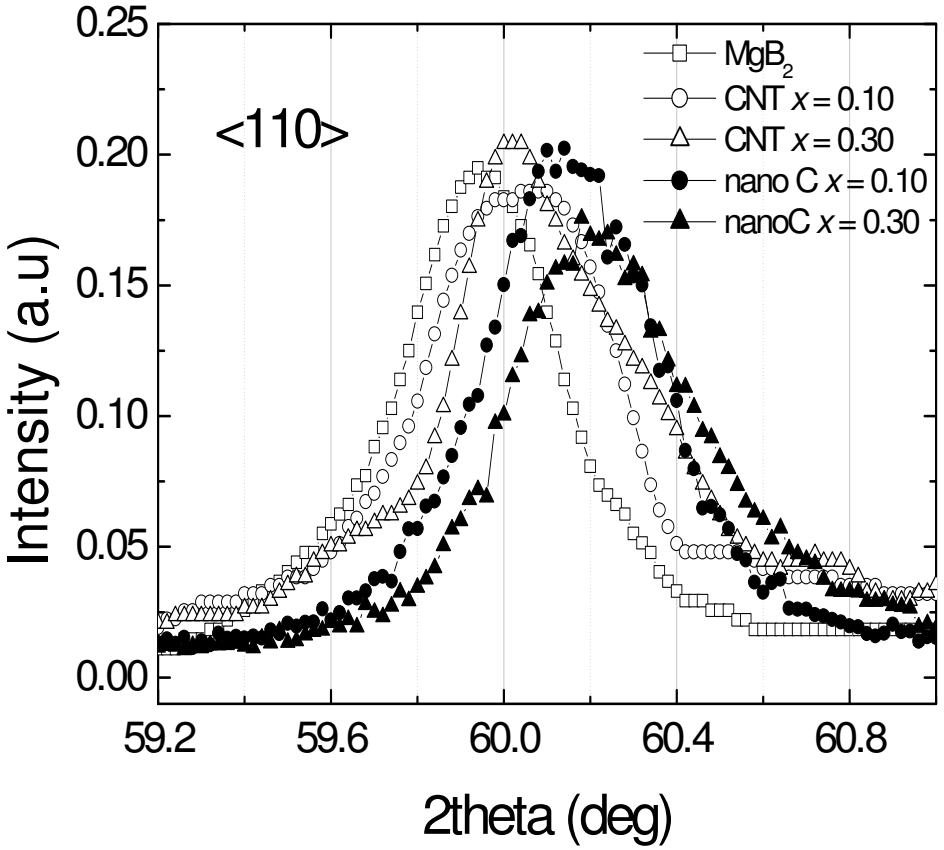

Figure 7.6 <110> peak of the XRD pattern for nano C and CNT samples.

This assumption of carbon substitution has been further verified by the <110> peak from the XRD patterns for nano-C and CNT samples. In the orthorhombic structure like MgB_2, <110> peak that corresponding to lattice parameter *a*, shifted to the higher angle as doping level of the carbon source increased for both nano-C and CNT doping. This lead to the shrinkage of the lattice parameter *a* and the lattice distortion which is due to the partial substitution of carbon into the boron sites. It should be pointed out that the shift of <110> peak in CNT doped samples was smaller than for nano-C doped samples. This indicates that under the same doping level and processing condition, carbon substitution is more pronounced for the nano-C doped samples than for the CNT doped

samples. Since the carbon in the CNT needs to break out from the carbon sheet of CNT before it can take part in the carbon substitution, the carbon substitution with the CNT consumed more energy than with the nano-C doping and indirectly reduced the opportunity of carbon substitution under the same condition. Previous study showed that nanotubes tend to entangle, preventing their homogenous mixing with MgB_2 and dispersion. As a result, this will also suppress the reactivity of the CNT and the Mg and B powders.

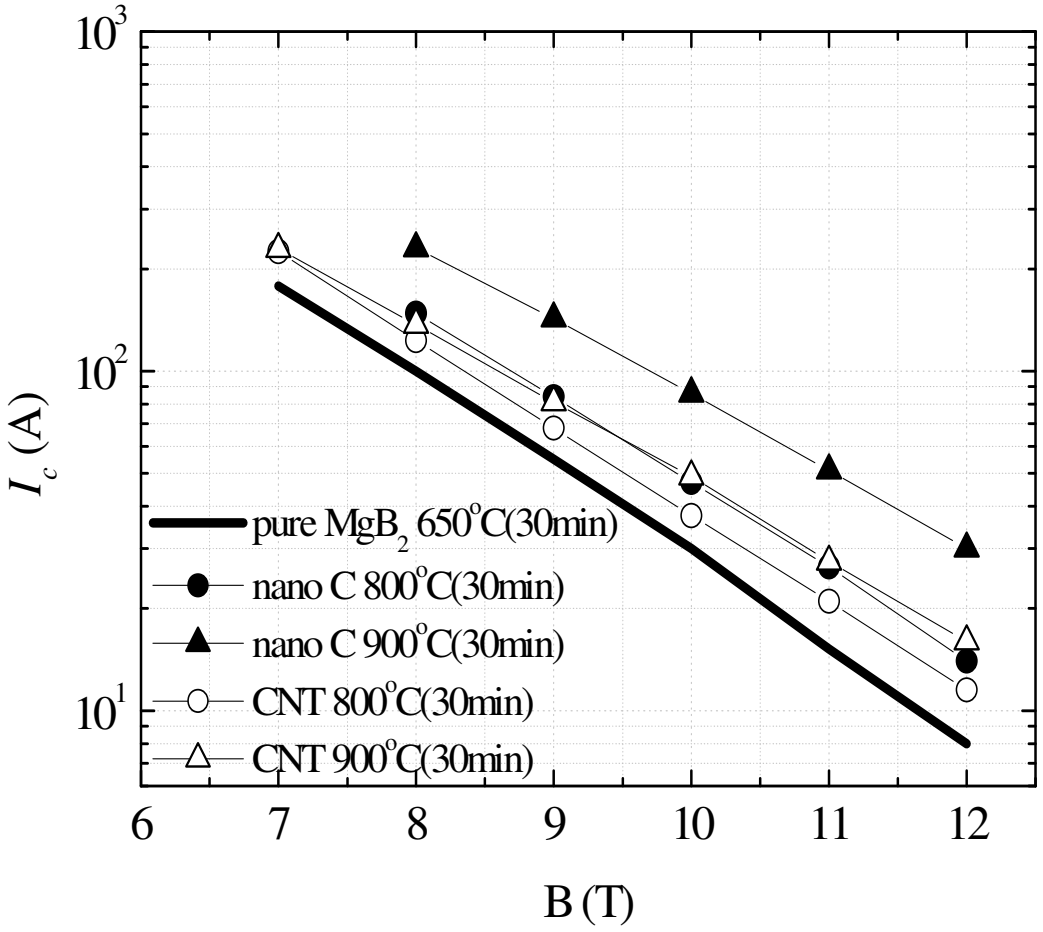

Figure 7.7 transport I_c for nano-C and CNT at 4 K under various sintering temperature

Figure 7.7 shows the transport critical current at 4.2 K at fields up to 12 T for $MgB_{1.9}C_{0.1}$ and $MgB_{1.8}CNT_{0.2}$ wire produced at various sintering temperatures. The composition was chosen based on the optimum doping level from the previous results. The $I_c(H)$ was improved systematically as the sintering temperature was increased from 800°C to 900°C with the slope of the $I_c(H)$ becoming smaller with increasing of sintering temperature. The flux pinning in the both samples was enhanced as processing temperature increased and the best $I_c(H)$ was observed at 900°C processing temperature. This result indicates that flux pinning at high processing temperature was enhanced by a large amount of carbon substitution. The best I_c was estimated to be 30A and 14A at 12 T and 4.2 K for nano C and CNT sample, respectively. This in contrast with the SiC doped MgB_2 where low sintering temperature was the optimum temperature for the good J_c. The higher I_c shown by the nano C sample again indicated a better reactivity of C and B and more homogenous mixing compared to the CNT sample.

7.4 Conclusion

As conclusion, nano-C doped MgB_2 resulted in better improvement in magnetic and transport $J_c(H)$ compared to CNT doped MgB_2. Due to carbon substitution effect, both substitutions exhibited excellent J_c at high temperature (900°C). It was found that the lattice distortion and optimum doping level is different in the CNT and nano-C samples which is due to different reactivity of carbon sources, as carbon substitution is more direct process with the nano-C doping than with CNT doping. However this still does not mean nano-C doping would provide better MgB_2 wires than CNT doping. This is

because CNT doped MgB_2 can provide extra thermal stability, heat dissipation, and mechanical support of MgB_2 superconductor wire compared to other doping samples.

References

[1] T. Takenobu, T. Ito, D.H. Chi, K. Prassides, and Y. Iwasa, *Phys. Rev. B* **64**, 134513 (2001).

[2] A. Bharathi, S. Jemima Balaselvi, S. Kalavathi, G. L. N. Reddy, V. Sankara Sastry, Y. Hariharan and T. S. Radhakrishnan, *Physica C* **370**, 211 (2002).

[3] Z. H. Cheng, B. G. Shen, J. Zhang, S. Y. Zhang, T. Y. Zhao, and H. W. Zhao, *J. Appl. Phys*. **91**, 7125 (2002).

[4] M. Paranthaman, J.R. Thompson, and D.K. Christen, *Physica C* **355**, 1. (2001)

[5] W. Mickelson, J. Cumings, W.Q. Han, and A. Zettl, *Phys. Rev. B* **65**, 052505 (2002).

[6] I. Maurin, S. Margadonna, K. Prassides, T. Takenobu, T. Ito, D. H. Chi, Y. Iwasa and A. Fitch, *Physica B* **318**, 392 (2002).

[7] K. Papagelis, J. Arvanitidis, S. Margadonna, Y. Iwasa, T. Takenobu, M. Pissas and K. Prassides, *J. Phys.: Condens. Matter* **14**, 7363 (2002).

[8] R.A. Ribeiro, S.L. Bud'ko, C. Petrovic, and P.C. Canfield, *Physica C* **384**, 227. (2003)

[9] H. L. Xu, Y. Feng, Z. Xu, G. Yan, L.Z. Cao and X.G. Li Xiao, *Chin. Phys. Lett.* **21**, 2511 (2004)

[10] S. Soltanian, J. Horvat, X.L. Wang, P. Munroe, S.X. Dou, *Physica C* **390**, 185–190 (2003)

[11] B. J. Senlowocz, J. E. Giencke, S. Patnaik, C. B. Eom, E. E. Hellstrom, and D. C. Larbalestier, *Appl. Phys. Lett*. **86**, 202502 (2005)

[12] Y. Ma, X. Zhang, G. Nishijima, K. Watanabe, and X. Bai, *Appl. Phys. Lett*. **88**, 072502 (2006)

[13] Y. Zhao, C. H. Cheng, X. F. Rui, H. Zhang, P. Munroe, H. M. Zeng, N. Koshizuka and M. Murakami, *Appl. Phys. Lett*. **83**, 2916 (2003).

[14] H. L. Xu, Y. Feng, Z. Xu, G. Yan, L. Z. Cao and X. G. Li, *Chin. Phys. Lett*. 21, 2511 (2004).

[15] E. Ban, R. Sakaguchi, Y. Matsuoka, T. Goto, K. Watanabe, and G. Nishijima *Physica C* **426–431**, 1249–1253 (2005).

[16] S. X. Dou, S. Soltanian, J. Horvat, X. L. Wang, S. H. Zhou, M. Ionescu, H. K. Liu, P. Munroe and M. Tomsic, *Appl. Phys. Lett*. **81**, 3419 (2002).

[17] H. Kumakura, H. Kitaguchi, A. Matsumoto, and H. Hatakeyama, *Appl. Phys. Lett*. **84**, 3669-3671 (2004)

[18] M. D. Sumption, M. Bhatia, S. X. Dou, M. Rindfliesch, M. Tomsic, L. Arda, M. Ozdemir, Y. Hascicek and E. W. Collings, *Supercond. Sci. Technol*. **17**, 1180–1184 (2004)

[19] A. Yamamoto, J. Shimoyama, S. Ueda, Y. Katsura, S. Horii, and K. Kishio, *IEEE Trans on Appl. Supercond*. **15**, 3292 (2005).

[20] S. X. Dou, W. K. Yeoh, J. Horvat and M. Ionescu, *Appl. Phys. Lett.* **83**, 4996. (2003).

[21] W. K. Yeoh, J. Horvat J, S. X. Dou and V. Keast, *Supercond. Sci. Technol.* **17**, S572 (2004).

[22] W. K. Yeoh, J. Horvat J, S. X. Dou and P. Munroe, *IEEE Trans on Appl. Supercond*. **15**, 3284 (2005).

[23] S. K. Chen, K. S. Tan, B. A. Glowacki, W. K. Yeoh, S. Soltanian, J. Horvat and S. X. Dou, *Appl. Phys. Lett.* **87**, 182504 (2005).

[24] W. K. Yeoh, J. H. Kim, J. Horvat, S. X. Dou and P. Munroe, *Supercond. Sci. Technol*. **19**, L5–L8 (2006).

[25] S. X. Dou, W. K. Yeoh, O. Shcherbakova, D. Wexler, Y. Li, Z. M. Ren, P. Munroe, S. K. Chen, K. S. Tan, B. A. Glowacki and J. L. MacManus-Driscoll, *Advanced Materials* **18**, 785-788 (2006).

[26] J. H. Kim, W. K. Yeoh, M. J. Qin, X. Xu and S. X. Dou, accepted by *J. of Appl. Phys.*

[27] S. X. Dou, V. Braccini, S. Soltanian, R. Klie, Y. Zhu, S. Li, X. L. Wang, and D. Larbalestier, *J. of Appl. Phys*. **96** 7549 (2004).

[28] S. Li, T. White, K. Laursen, T. T. Tan, C. Q. Sun, Z. L. Dong, Y. Li, S. H. Zho, J. Horvat, and S. X. Dou, *Appl. Phys. Lett.* **83**, 314 (2003)

[29] M. Avdeev M, Jorgensen J D, Ribeiro R A, Bud'ko S L and Canfield P C *Physica* C **387**, 301 (2003).

Chapter 8 Conclusions

The carbon substitution from CNT to boron sites was found to enhance J_c in magnetic fields but depress T_c. The depression of T_c, which is caused by the boron substitution for carbon, increases with increasing the doping level, sintering temperature and duration. By controlling the extent of the substitution and addition of carbon nanotubes, the optimal improvement on critical current density and flux pinning in magnetic fields was achieved while maintaining the minimum reduction in T_c. Under these conditions, J_c was enhanced by two orders of magnitude at 8T and 5K and 7T and 10K. J_c was more than 10,000A/cm^2 at 20K and 4T and 5K and 8.5T, respectively. As predicted by the two bands theory of, enhancement of H_{c2} and H_{irr} shown by CNT doped samples was observed at high sintering temperature. Carbon nanotube inclusions and B substitution for C are proposed to be responsible for the enhancement of flux pinning, upper critical field and the irreversibility field.

Under the Electron microscopy studies, nanotubes are seen to adhere to the MgB_2 matrix for all the samples, with some proportion of them appearing as agglomerates. In contrast, magnetization measurements indicate a change in the critical current density with the length of nanotube and not with its outside diameter. This is due to longer nanotubes tending to entangle, preventing their homogenous mixing with MgB_2 and dispersion. As a result, the main factor to successfully embed the CNT in the MgB_2 will be the length of nanotubes instead of their diameter.

Low intensity ultrasonication as a method of dispersion of CNT's into precursor magnesium and boron powder has improved homogenous mixing of CNT's with the MgB_2 matrix. Cavitations and the shockwaves generated by the ultrasonication will substantially enhance the reactivity of nano-size particles, like CNT's. The extent of the C substitution reaction increases with the ultrasonication process, resulting in T_c depression, which is consistent with the contraction of the unit cell. We believe that the degree of carbon substitution in the CNT-doped MgB_2 highly depends on the dimensions of CNT's as short CNT's are more reactive than the long ones. Ultrasonication of CNT doped MgB_2 resulted in a significant enhancement in the field dependence of critical current density, while avoiding the side-effects that would occur at higher sintering temperatures.

The elongated CNT's induce anisotropy in J_c in relation to the direction of applied field. It was found the J_c of the carbon nanotube-doped wire to be insensitive to heating rates. In addition to the benefits of electrical and thermal conductivity of CNT doping, the elongated CNT's in the wire axis direction will take full advantage of their unusual axial strength to enhance the mechanical properties such as tensile strength and flexibility. Studies on these properties are underway.

Due to carbon substitution effect, both nano-C and CNT substitution exhibited excellent J_c at high temperature (900^oC). However, nano-C doped MgB_2 resulted in better improvement of magnetic and transport $J_c(H)$, as compared to CNT doped MgB_2. Magnetic J_c was enhanced by the factor of 1.8 at 5K in the bulk sample, while transport I_c showed an enhancement by a factor of 1.9 at 12 T and 4.2 K for nano C sample, as

compared to CNT doped MgB_2. It was found that the variation in the lattice distortion and optimum doping level for CNT and nano-C samples, can be explained by the reactivity of carbon source. Carbon substitution is more direct process in the nano-C precursor while carbon substitution only occurred after break out of carbon atoms from CNT. However, CNT doped MgB_2 showed a much better thermal stability, heat dissipation, and mechanical support of MgB_2 superconductor wire which have not been observed for other doping procedures so far.

Publications

J. H. Kim, *__W. K. Yeoh__, M. J. Qin, X. Xu, and S. X. Dou, P. Munroe, H. Kumakura, T. Nakane, C. H. Jiang "Enhancement of *in-field* J_c in MgB_2/Fe wire using single and multi-walled nanotubes" accepted by *Appl. Phys. Lett.*

J. Horvat, *__W. K. Yeoh__, J. H. Kim, S. Soltanian and S. X. Dou "Transport and Magnetic J_c for MgB_2 Superconductor" Wagga-Wagga Conference 2006 Australia

J. H. Kim, *__W. K. Yeoh,__ M. J. Qin, X. Xu and S. X. Dou "The doping effect of multiwall carbon nanotube on MgB_2/Fe superconductor wire" *J. of Appl. Phys.* **100**, 013908- (2006)

*__W. K. Yeoh__, J. H. Kim, J. Horvat, X. Xu, M. J. Qin, S. X. Dou, C. H. Jiang, T. Nakane, H. Kumakura and P. Munroe "Control of Nano Carbon Substitution for Enhancing the Critical Current Density in MgB_2" *Supercond. Sci. Technol.* **19** 596-599 (2006).

X. Xu, M. J. Qin, K. Konstantinov, Dayse I dos Santos, *__W. K. Yeoh__, J. H. Kim and S. X. Dou "Effect of boron powder purity on superconducting properties of MgB_2" Supercond. Sci. Technol. **19** 466–469 (2006)

S. X. Dou, *__W. K. Yeoh__, O. Shcherbakova, Y. Li, Z. M. Ren, D. Wexler, P. Munroe, S. K. Chen, K. S. Tan, B. A. Glowacki and J. L. MacManus-Driscoll "Alignment of carbon nanotube additives for enhancing the magnesium diboride superconductors' performance" *Advanced Materials* **18**, 785-788 (2006).

*__W. K. Yeoh,__ J. H. Kim, J. Horvat, S. X. Dou and P. Munroe "Improving Flux Pinning of MgB_2 by carbon nanotube doping and ultrasonication" *Supercond. Sci. Technol*. **19** L5–L8 (2006)

S. K. Chen, K. S. Tan, B. A. Glowacki, *__W. K. Yeoh__, S. Soltanian, J. Horvat and S. X. Dou, "Effect of heating rates on superconducting properties of pure MgB_2, carbon nanotube- and nano-SiC-doped in situ MgB2/Fe wires" *Appl. Phys. Lett.*, **87**, 182504 (2005)

J. Horvat, *__W. K. Yeoh__ and L M Miller "Interaction between superconductor and ferromagnetic domains in iron sheath: Peak effect in MgB2/Fe wires" *Appl. Phys. Lett.* **87**, 102503 (2005)

S. X. Dou, S. Soltanian *__W. K. Yeoh__ and Y. Zhang, "Effect of nano-particle doping on the upper critical field and flux pinning in MgB_2" *IEEE Transactions on Applied Superconductivity*, **15,** 3219 (2005)

*W. K. Yeoh, J. Horvat, S. X. Dou and P. Munroe, "Effect of carbon nanotube size on superconductivity properties of MgB_2" *IEEE Transactions on Applied Superconductivity*, **15,** 3284 (2005)

J. Horvat, S. Soltanian and ***W. K. Yeoh**, "The relevance of the self-field for the 'peak effect' in the transport $J_c(H)$ of iron-sheathed MgB_2 wires" *Supercond. Sci. Technol*., **18**, 682 (2005)

***W.K. Yeoh** J. Horvat S. X. Dou and V. Keast, "Strong pinning and high critical current density in carbon nanotube doped MgB_2", *Supercond. Sci. Technol*., **17**, S572 (2004)

S. X. Dou, ***W. K. Yeoh**, J. Horvat and M. Ionescu, "Effect of carbon nanotube doping on critical current density of MgB_2 superconductor", *Appl. Phys. Lett.* **83**, 4996 (2003)